

DTP/98/90
INLO-PUB 11/98

**RADIATIVE CORRECTIONS TO PAIR PRODUCTION
OF UNSTABLE PARTICLES: RESULTS FOR $E^+E^- \rightarrow 4$ FERMIONS**

W. Beenakker^{*)}

Physics Department, University of Durham, Durham DH1 3LE, England

F.A. Berends and A.P. Chapovsky^{†)}

Instituut–Lorentz, University of Leiden, The Netherlands

ABSTRACT

Radiative corrections to processes that involve the production and subsequent decay of unstable particles are complex due to various theoretical and practical problems. The so-called double-pole approximation offers a way out of these problems. This method is applied to the reaction $e^+e^- \rightarrow W^+W^- \rightarrow 4$ fermions, which allows us to address all the key issues of dealing with unstable particles, like gauge invariance, interactions between different stages of the reaction, and overlapping resonances. Within the double-pole approximation the complete $\mathcal{O}(\alpha)$ electroweak corrections are evaluated for this off-shell W -pair production process. Examples of the effect of these corrections on a number of distributions are presented. These comprise mass and angular distributions as well as the photon-energy spectrum.

November 1998

^{*)}Research supported by a PPARC Research Fellowship.

^{†)}Research supported by the Stichting FOM.

1 Introduction

In order to test the Standard Model (SM) of electroweak interactions, millions of Z bosons have been produced and studied at LEP1 [1]. High-precision measurements of the Z -boson parameters have been performed by measuring

$$e^+e^- \rightarrow Z \rightarrow \bar{f}f \quad (1)$$

and comparing the results with the theoretical predictions. This requires theoretical precision calculations for the reaction

$$e^+e^- \rightarrow \bar{f}f, \quad (2)$$

involving *all* lowest-order diagrams and the radiative corrections (RC) to them [2].

Measuring the parameters of the W boson provides further tests of the SM. In particular, the accuracy of the W -boson mass (M_W) has to be improved, since it can give indirect information on the Higgs sector and on physics beyond the SM. At LEP2, W bosons can be studied in the W -pair production reaction

$$e^+e^- \rightarrow W^+W^- \rightarrow 4 \text{ fermions}. \quad (3)$$

Besides the mass M_W also the Yang–Mills form of the triple gauge-boson couplings (TGC) ZW^+W^- and γW^+W^- can be tested in reaction (3), where they directly manifest themselves in the lowest-order cross-section. Deviations from the SM Yang–Mills couplings can be searched for most effectively by a detailed investigation of angular distributions [3].

Just like in the case of the Z boson, the precise determination of the W -boson parameters requires both accurate experiments and accurate theoretical predictions. Since the statistics at LEP2 is much smaller than at LEP1, the theoretical calculations do not have to be as precise as those for LEP1. However, just the Born prediction for process (3), involving only three diagrams, is not sufficient [4]. Therefore, one would like to have an idea how the cross-sections for the four-fermion process

$$e^+e^- \rightarrow 4 \text{ fermions} \quad (4)$$

are affected by the inclusion of the remaining lowest-order diagrams and the RC to the *complete* set of lowest-order diagrams.

The question of the complete lowest-order calculation of process (4) has been studied in the literature [4, 5]. Roughly speaking, those diagrams that contain a single W boson are a factor of $\mathcal{O}(\Gamma_W/M_W)$ smaller than those for the W -pair production process (3). Diagrams that do not contain a W boson at all are down by $\mathcal{O}(\Gamma_W^2/M_W^2)$. Note, however, that some diagrams that do not contain two W bosons can nevertheless be large, e.g. as a result of the exchange of almost real photons. Besides such special cases, the lowest-order “background” diagrams in (4), i.e. the non- W -pair diagrams, will give at most a correction of $\mathcal{O}(\Gamma_W/M_W)$ to the Born cross-section of process (3).

The RC to process (3) are a priori of $\mathcal{O}(\alpha)$, i.e. they are generically of the same order as the lowest-order background diagrams. In analogy to the lowest-order case, the RC to the background diagrams are at most of $\mathcal{O}(\alpha\Gamma_W/M_W)$.

In view of the above estimates, the most relevant corrections to the Born cross-section of process (3) are divided into two classes:

1. $\mathcal{O}(\alpha)$ RC to the W -pair process (3).
2. $\mathcal{O}(\Gamma_W/M_W)$ lowest-order background contributions from the full four-fermion process (4).

At present the first class of corrections has not been fully studied in the literature. What has been discussed quantitatively and qualitatively is merely a subset of $\mathcal{O}(\alpha)$ effects:

- 1.1. Initial-state radiation (ISR). Since ISR corrections are enhanced by collinear-photon effects, they are large and even higher-order contributions should be taken into account [4]–[6].
- 1.2. Final-state radiation (FSR). Similarly FSR can be sizeable, in particular for distributions in the fermion-pair invariant masses. This QED effect has recently been pointed out in the literature [7]. Again higher-order corrections are non-negligible for these W line-shape distributions.
- 1.3. Whereas the effects 1.1 and 1.2 are enhanced by logarithms originating from collinear photons, also non-enhanced $\mathcal{O}(\alpha)$ effects have been studied. One of those belongs to the class of the so-called non-factorizable corrections [8]–[10], i.e. corrections that at first sight do not seem to have two overall W propagators as factors. As such one would expect these corrections to be suppressed by additional powers of Γ_W/M_W . In the special case of semi-soft photonic corrections, however, the suppression does not take place and an $\mathcal{O}(\alpha)$ correction survives. This $\mathcal{O}(\alpha)$ correction has been calculated and turns out to be relatively small. In the vicinity of the W -pair threshold also the Coulomb interaction between the unstable W bosons has been studied in great detail [11]. The corrections are relatively large, but higher orders are not required.
- 1.4. The effects 1.1–1.3 are all of QED origin. Complete electroweak RC to process (3) have not been applied yet, but some attempts have been made to take into account the dominant effects. An overall effect of electroweak corrections has been considered by using G_μ as coupling constant instead of α . From other calculations it is known that a G_μ parametrization of the lowest-order term reduces the size of the one-loop non-photonic RC considerably. In addition to this overall effect, the full electroweak RC to stable W -pair production [12]–[14] and on-shell W decay [15] are already known for quite some time.

The purpose of this paper is twofold. In the first place we will present a complete quantitative evaluation of $\mathcal{O}(\alpha)$ electroweak RC to W -pair-mediated four-fermion production. To this end we calculate all $\mathcal{O}(\alpha)$ factorizable corrections and add them to our previous results on non-factorizable corrections. In this way the gap in the above list of corrections 1.1–1.4 will be filled, and the exact size of all $\mathcal{O}(\alpha)$ corrections to reaction (3) will be known. In the light of the physics motivation given above, this practical result is clearly wanted.

Secondly, this paper discusses in detail the so-called pole scheme. This scheme offers a way to avoid theoretical problems associated with the gauge-invariant treatment of reactions that involve the production and subsequent decay of unstable particles. The study of the W -pair case serves as a relevant example of this method and can be used as a guideline for other cases. Since there are more unstable-particle production processes to be studied at future accelerators, the relevance of the presented study goes beyond the W -pair case.

The outline of the paper is as follows. In Sect. 2 various gauge-invariance issues will be discussed. In Sect. 3 the pole-scheme treatment is described, with special emphasis on the so-called double-pole approximation (DPA), since it is the basic ingredient for our calculation of the $\mathcal{O}(\alpha)$ RC. The comparison with the exact lowest-order evaluation in Sect. 4 gives an estimate of the accuracy of this approximation. The discussion of the RC in the DPA for the W -pair production process (3) is presented in Sect. 5, whereas the corresponding numerical results can be found in Sect. 6. In Sect. 7 we give the conclusions of our study.

2 Gauge-invariant treatment of unstable gauge bosons

2.1 Lowest order

The above-described processes, with or without RC, all involve fermions in the initial and final state and unstable gauge bosons as intermediate particles. Sometimes a photon is also present in the final state. If complete sets of graphs contributing to a given process are taken into account, the associated matrix elements are in principle gauge-invariant, i.e. they are independent of gauge fixing and respect Ward identities. This is, however, not guaranteed for incomplete sets of graphs like the ones corresponding to the off-shell W -pair production process (3). Indeed this process was found to violate the $SU(2)$ Ward identities [6].

In addition, the unstable gauge bosons that appear as intermediate particles can give rise to poles $1/(p^2 - M^2)$ in physical observables if they are treated as stable particles. This can be cured by introducing the finite decay widths for these gauge bosons. In field theory, such widths arise naturally from the imaginary parts of higher-order diagrams describing the gauge-boson self-energies, resummed to all orders. However, in doing a Dyson summation of self-energy graphs, we are singling out only a very limited subset of all possible higher-order diagrams. It is therefore not surprising that one often ends up with a result that violates Ward identities and/or retains some gauge dependence resulting from incomplete higher-order contributions.

Since the latter gauge breaking is caused by the finite decay width and is, as such, in principle suppressed by powers of Γ/M , one might think that it is of academic nature. For LEP1 observables we indeed know that gauge breaking can be negligible for all practical purposes. However, the presence of small scales can amplify the gauge-breaking terms. This is for instance the case for almost real space-like photons [16, 17] or longitudinal gauge bosons (V_L) at high energies [18], involving scales of $\mathcal{O}(p_B^2/E_B^2)$ for $B = \gamma, V_L$. The former plays an important role in TGC studies in the reaction $e^+e^- \rightarrow e^-\bar{\nu}_e u\bar{d}$, where the electron may emit a virtual photon

with an invariant mass p_γ^2 as small as m_e^2 . The latter determines the high-energy behaviour of the generic reaction $e^+e^- \rightarrow 4$ fermions. In these situations the external current coupled to the photon or to the longitudinal gauge boson becomes approximately proportional to p_B . Sensible theoretical predictions, with a proper dependence on p_γ^2 and a proper high-energy behaviour, are only possible if the amplitudes with external currents replaced by the corresponding gauge-boson momenta fulfil appropriate Ward identities.

So, how should one go about including the finite decay widths? The simplest approach is the so-called “fixed-width scheme”, involving the systematic replacement $1/(p_V^2 - M_V^2) \rightarrow 1/(p_V^2 - M_V^2 + iM_V\Gamma_V)$, where Γ_V denotes the physical width of the gauge boson V with mass M_V and momentum p_V . Since in perturbation theory the propagator for space-like momenta does not develop an imaginary part, the introduction of a finite width also for $p_V^2 < 0$ has no physical motivation and in fact violates unitarity, i.e. the cutting equations. This can be cured by using a running width $iM_V\Gamma_V(p_V^2)$ instead of the constant one $iM_V\Gamma_V$ (“running-width scheme”). However, as in general the resonant diagrams are not gauge-invariant by themselves, the introduction of a constant or running width destroys gauge invariance.

A truly gauge-invariant scheme evidently has to be a bit more sophisticated than this. It should be stressed, however, that any such scheme is arbitrary to a greater or lesser extent: since the Dyson summation must necessarily be taken to all orders of perturbation theory, and we are not able to compute the complete set of *all* Feynman diagrams to *all* orders, the various schemes differ even if they lead to formally gauge-invariant results. Bearing this in mind, we need besides gauge invariance some physical motivation for choosing a particular scheme. In this context two options can be mentioned. The first option is the so-called “pole scheme” [19]. In this scheme one decomposes the complete amplitude by expanding around the poles. As the physically observable residues of the poles are gauge-invariant, gauge invariance is not broken if the finite width is taken into account in the pole terms $\propto 1/(p_V^2 - M_V^2)$. Note that the leading terms in such an expansion play a special role in view of their close relation to on-shell production and decay of the unstable particles. This point will be explained in more detail in the following sections.

The second option is based on the philosophy of trying to determine and include the minimal set of Feynman diagrams that is necessary for compensating the gauge violation caused by the self-energy graphs. This is obviously the theoretically most satisfying solution, but it may cause an increase in the complexity of the matrix elements and consequently a slowing down of the numerical calculations. For the gauge bosons we are guided by the observation that the lowest-order decay widths are exclusively given by the imaginary parts of the fermion loops in the one-loop self-energies. It is therefore natural to perform a Dyson summation of these fermionic one-loop self-energies and to include the other possible one-particle-irreducible fermionic one-loop corrections (“fermion-loop scheme”) [17, 18]. For the LEP2 process $e^+e^- \rightarrow 4$ fermions this amounts to adding the fermionic corrections to the triple gauge-boson vertex. The complete set of fermionic contributions forms a gauge-independent subset and obeys all Ward identities exactly, even with resummed propagators [18].

The above arguments, although general, apply in particular to tree diagrams. Therefore an

additional discussion for RC is required.

2.2 Radiative corrections

The next question that should be addressed involves the interplay between RC and gauge invariance. After all, the RC are indispensable for coming up with reliable theoretical predictions for the LEP2 process $e^+e^- \rightarrow 4 \text{ fermions}$.

As far as real-photon corrections are concerned, not much changes as compared to the lowest-order case. Still both the pole scheme and fermion-loop scheme yield gauge-invariant results. However, in the fermion-loop-scheme treatment of the process $e^+e^- \rightarrow 4f\gamma$ the full set of fermionic corrections to the quartic gauge-boson vertex emerges. This evidently is too much complexity for a tree-level calculation. The pole-scheme, with its close relation to on-shell subprocesses, remains relatively simple. As we shall see later on, some subtleties arise when photons are radiated from a virtual W boson, because this W boson may give rise to two poles.

The implementation of the one-loop RC adds an additional level of complexity by the sheer number of contributions ($10^3 - 10^4$) that have to be evaluated. By employing a gauge-invariant lowest-order finite-width scheme it is possible to cover the most important electroweak effects, like running couplings and leading QED corrections (see previous section), which are controlled by factorization theorems. However, there is still the question about the remaining corrections, which can be large, especially at high energies [4, 6, 20].

In order to include these corrections one might attempt to extend the fermion-loop scheme. At present this solution is not yet workable in view of the fact that a gauge-invariant inclusion of the one-loop corrections to the decay width in turn requires the inclusion of (the imaginary parts of) some two-loop corrections. Moreover, the number of one-loop contributions that have to be evaluated remains large.

As a more appealing and economic strategy we discuss in the next section how the RC can be calculated in an approximated pole-scheme expansion.

3 The pole scheme in double-pole approximation

As mentioned above, the pole scheme consists in decomposing the complete amplitude by expanding around the poles of the unstable particles. The residues in this expansion are physically observable and therefore gauge-invariant. The pole-scheme expansion can be viewed as a gauge-invariant prescription for performing an expansion in powers of Γ_V/M_V . It should be noted that there is no unique definition of the residues. Their calculation involves a mapping of off-shell matrix elements with off-shell kinematics on on-resonance matrix elements with restricted kinematics. This mapping, however, is not unambiguously fixed. After all, it involves more than just the invariant masses of the unstable particles and one thus has to specify the variables that have to be kept fixed in the mapping. The resulting implementation dependence manifests

itself in differences of subleading nature, e.g. $\mathcal{O}(\Gamma_V/M_V)$ suppressed deviations in the leading pole-scheme residue. In special regions of phase space, where the matrix elements vary rapidly, the implementation dependence can take noticeable proportions. This happens in particular near phase-space boundaries, like thresholds.

In order to make these statements a bit more transparent, we sketch the pole-scheme method for a single unstable particle. In this case the Dyson resummed lowest-order matrix element is given by

$$\begin{aligned}\mathcal{M}^\infty &= \frac{W(p_V^2, \omega)}{p_V^2 - \tilde{M}_V^2} \sum_{n=0}^{\infty} \left(\frac{-\tilde{\Sigma}_V(p_V^2)}{p_V^2 - \tilde{M}_V^2} \right)^n = \frac{W(p_V^2, \omega)}{p_V^2 - \tilde{M}_V^2 + \tilde{\Sigma}_V(p_V^2)} \\ &= \frac{W(M^2, \omega)}{p_V^2 - M^2} \frac{1}{Z(M^2)} + \left[\frac{W(p_V^2, \omega)}{p_V^2 - \tilde{M}_V^2 + \tilde{\Sigma}_V(p_V^2)} - \frac{W(M^2, \omega)}{p_V^2 - M^2} \frac{1}{Z(M^2)} \right],\end{aligned}\quad (5)$$

where $\tilde{\Sigma}_V(p_V^2)$ is the unrenormalized self-energy of the unstable particle V with momentum p_V and unrenormalized mass \tilde{M}_V . The renormalized quantity M^2 is the pole in the complex p_V^2 plane, whereas $Z(M^2)$ denotes the wave-function factor:

$$M^2 - \tilde{M}_V^2 + \tilde{\Sigma}_V(M^2) = 0, \quad Z(M^2) = 1 + \tilde{\Sigma}'_V(M^2). \quad (6)$$

The first term in the last expression of Eq. (5) represents the single-pole residue, which is closely related to on-shell production and decay of the unstable particle. The second term between the square brackets has no pole and can be expanded in powers of $p_V^2 - M^2$. The argument ω denotes the dependence on the other variables, i.e. the implementation dependence. After all, the unstable particle is always accompanied by other particles in the production and decay stages. For instance, consider the LEP1 reaction $e^+e^- \rightarrow \bar{f}f$. In the mapping $p_Z^2 \rightarrow M^2$ one can either keep $t = (p_{e^-} - p_f)^2 = -p_Z^2(1 - \cos\theta)/2$ fixed or $\cos\theta$. In the former mapping $\cos\theta_{\text{pole}}$ is obtained from the on-shell relation $\cos\theta_{\text{pole}} = 1 + 2t/M^2$, whereas in the latter mapping $t_{\text{pole}} = -M^2(1 - \cos\theta)/2$. It may be that a particular mapping leads to an unphysical point in the ‘on-shell’ phase space. In the present example t_{pole} will always be physical when $\cos\theta$ is kept fixed in the mapping. However, since $|\cos\theta_{\text{pole}}| > 1$ for $t < -\text{Re } M^2$, it is clear that mappings with fixed Mandelstam variables harbour the potential risk of producing such unphysical phase-space points.¹ This can have repercussions on the convergence of the pole-scheme expansion. Therefore we choose in our calculations only implementations that are free of unphysical on-shell phase-space points.

It should be noted that the mass and width of the W and Z bosons are usually defined in the so-called on-shell scheme:

$$M_V^2 - \tilde{M}_V^2 + \text{Re } \tilde{\Sigma}_V(M_V^2) = 0, \quad Z_{\text{OS}}(M_V^2) = 1 + \text{Re } \tilde{\Sigma}'_V(M_V^2), \quad M_V \Gamma_V = \frac{\text{Im } \tilde{\Sigma}_V(M_V^2)}{Z_{\text{OS}}(M_V^2)}. \quad (7)$$

Both schemes can be related according to (see e.g. Ref. [18]):

$$M^2 = (M_V^2 - iM_V \Gamma_V) \left[1 - \frac{\Gamma_V^2}{M_V^2} + \mathcal{O}\left(\frac{\Gamma_V^3}{M_V^3}\right) \right],$$

¹In the resonance region, $|p_Z^2 - M^2| \ll |M^2|$, the unphysical ‘on-shell’ phase-space points occur near the edge of the off-shell phase space, since $t < -\text{Re } M^2$ requires $\cos\theta \approx -1$.

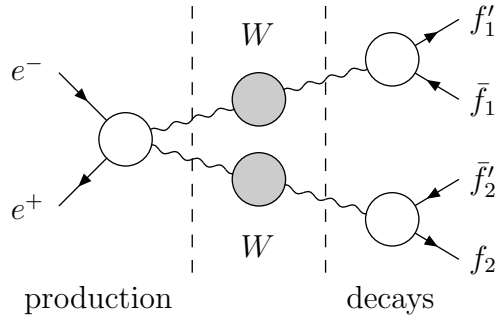


Figure 1: The generic structure of the factorizable W -pair contributions. The shaded circles indicate the Breit–Wigner resonances, whereas the open circles denote the Green functions for the production and decay subprocesses up to $\mathcal{O}(\alpha)$ precision.

$$(p_V^2 - M^2) Z(M^2) = \left(p_V^2 - M_V^2 + i p_V^2 \frac{\Gamma_V}{M_V} \right) \left[Z_{\text{os}}(M_V^2) + \mathcal{O}(\alpha^2) \right]. \quad (8)$$

As we are aiming for $\mathcal{O}(\alpha)$ precision in our study, the differences between both schemes can be ignored. For the same reason $i p_V^2 \Gamma_V / M_V$ can be replaced by $i M_V \Gamma_V$, since the difference only induces $\mathcal{O}(\alpha^2)$ corrections to the cross-sections.

The at present only workable approach for evaluating the RC to resonance-pair-production processes, like W -pair production, involves the so-called double-pole approximation (DPA). This approximation restricts the complete pole-scheme expansion to the term with the highest degree of resonance. In the case of W -pair production only the double-pole residues are hence considered. The intrinsic error associated with this procedure is $\alpha \Gamma_W / (\pi M_W) \lesssim 0.1\%$, except far off resonance, where the pole-scheme expansion cannot be viewed as an effective expansion in powers of Γ_V / M_V , and close to phase-space boundaries, where the DPA cannot be trusted to produce the dominant contributions. In the latter situations also the implementation dependence of the double-pole residues can lead to enhanced errors. Close to the nominal (on-shell) W -pair threshold, for instance, the intrinsic error is effectively enhanced by a factor $M_W / (\sqrt{s} - 2M_W)$. In view of this it is wise to apply the DPA only if the energy is several Γ_W above the threshold.

In the DPA one can identify two types of contributions. One type comprises all diagrams that are strictly reducible at both unstable W -boson lines (see Fig. 1). These corrections are therefore called factorizable and can be attributed unambiguously either to the production of the W -boson pair or to one of the subsequent decays. The second type consists of all diagrams in which the production and/or decay subprocesses are not independent and which therefore do not seem to have two overall W propagators as factors (see Fig. 2). We refer to these effects as non-factorizable corrections.² In the DPA the non-factorizable corrections arise exclusively from the exchange or emission of photons with $E_\gamma \lesssim \mathcal{O}(\Gamma_W)$. Hard photons as

²It should be noted that the exact split-up between factorizable and non-factorizable radiative corrections requires a precise (gauge-invariant) definition. We will come back to this point in Sect. 5.

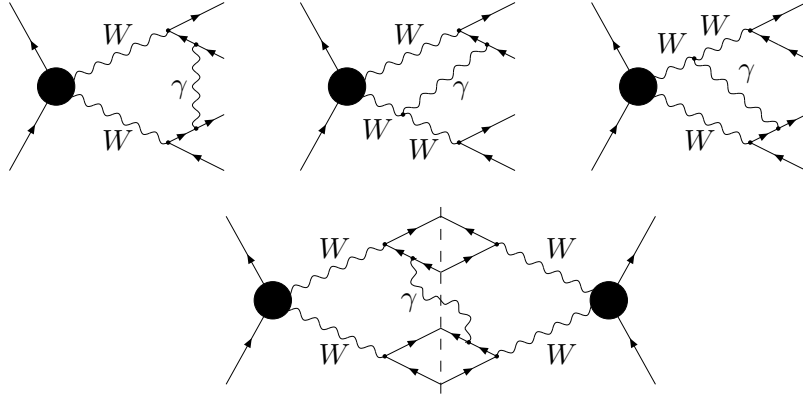


Figure 2: Examples for virtual (top) and real (bottom) non-factorizable corrections to W -pair production. The black circles denote the lowest-order Green functions for the production of the virtual W -boson pair.

well as massive-particle exchanges do not lead to double-resonant contributions. The physical picture behind all of this is that in the DPA the W -pair process can be viewed as consisting of several subprocesses: the production of the W -boson pair, the propagation of the W bosons, and the subsequent decay of the unstable W bosons. The production and decay are “hard” subprocesses, which occur on a relatively short time interval, $\mathcal{O}(1/M_W)$. They are in general distinguishable as they are well separated by a relatively big propagation interval, $\mathcal{O}(1/\Gamma_W)$. Consequently, the corresponding amplitudes have certain factorization properties. The same holds for the RC to the subprocesses. The only way the various stages can be interconnected is via the radiation of soft photons with energy of $\mathcal{O}(\Gamma_W)$. These photons induce relatively long range interactions and thereby allow the various subprocesses to communicate with each other.

Within the DPA the generic form of the virtual and soft-photonic $\mathcal{O}(\alpha)$ RC to off-shell W -pair production can now be cast in the following gauge-invariant form:

$$d\sigma_{\text{DPA}} = d\sigma_{\text{DPA}}^0(1 + \delta_{\text{DPA}}), \quad (9)$$

where $d\sigma_{\text{DPA}}^0$ is the lowest-order differential cross-section in DPA. The hard-photon effects in DPA are added separately, in view of their dependence on the phase-space of the hard photons. Their contribution strongly depends on the distribution that is studied, i.e. on the integrations that have to be performed. More details will be given in Sect. 5. Since one also knows the exact Born cross-sections for off-shell W -pair production [$d\sigma_{WW}^0$] and for the background diagrams contained in the four-fermion process (4) [$d\sigma_{\text{bkg}}^0$], one can also add those to the above expression. The final gauge-invariant result up to $\mathcal{O}(\alpha)$ or, equivalently, $\mathcal{O}(\Gamma_W/M_W)$ precision reads

$$d\sigma = d\sigma_{\text{DPA}}^0(1 + \delta_{\text{DPA}}) + (d\sigma_{WW}^0 - d\sigma_{\text{DPA}}^0) + d\sigma_{\text{bkg}}^0. \quad (10)$$

The purpose of this paper is to give a detailed discussion of δ_{DPA} , i.e. the $\mathcal{O}(\alpha)$ corrections to $d\sigma_{\text{DPA}}^0$. In order to make contact with experimental cross-sections the other terms, $d\sigma_{WW}^0 - d\sigma_{\text{DPA}}^0$ and $d\sigma_{\text{bkg}}^0$, are also relevant. The full gauge-invariant Born term, including all diagrams,

has been discussed in the literature [5]. It has also been compared with the non-gauge-invariant cross-section $d\sigma_{WW}^0$, calculated in the unitary gauge. In many cases $d\sigma_{WW}^0$ gives numerically a good approximation to the complete Born cross-section. Moreover, in practice it is often extracted from the data in the experimental analyses. Therefore it is useful to present a numerical comparison between $d\sigma_{WW}^0$ and $d\sigma_{DPA}^0$. This will be done in Sect. 4.

3.1 The double-pole approximation: conventions and an example

As is clear from the above-given discussion of the DPA, a specific prescription has to be given for the calculation of the DPA residues. Or, in other words, we have to fix the implementation of the mapping of the full off-shell phase space on the kinematically restricted (on-resonance) one. We have opted to always extract *pure double-pole residues*. This means in particular that after the integration over decay kinematics and invariant masses has been performed the on-shell cross-section should be recovered.

In the rest of this subsection we will explain our method in more detail by applying it to the lowest-order reaction

$$e^+(q_1) e^-(q_2) \rightarrow W^+(p_1) W^-(p_2) \rightarrow \bar{f}_1(k_1) f'_1(k'_1) f_2(k_2) \bar{f}'_2(k'_2), \quad (11)$$

involving only those diagrams that contain as factors the Breit–Wigner propagators for the W^+ and W^- bosons. Here \bar{f}_1 and f'_1 are the decay products of the W^+ boson, and f_2 and \bar{f}'_2 those of the W^- boson. It should be noted that a large part of the RC in DPA to this reaction can be treated in a way similar to the lowest-order case, which is therefore a good starting point. The amplitude for process (11) takes the form

$$\mathcal{M} = \sum_{\lambda_1, \lambda_2} \Pi_{\lambda_1 \lambda_2}(M_1, M_2) \frac{\Delta_{\lambda_1}^{(+)}(M_1)}{D_1} \frac{\Delta_{\lambda_2}^{(-)}(M_2)}{D_2}, \quad (12)$$

where any dependence on the helicities of the initial- and final-state fermions has been suppressed, and

$$D_i = M_i^2 - M_W^2 + i M_W \Gamma_W, \quad M_i^2 = (k_i + k'_i)^2. \quad (13)$$

The quantities $\Delta_{\lambda_1}^{(+)}(M_1)$ and $\Delta_{\lambda_2}^{(-)}(M_2)$ are the off-shell W -decay amplitudes for specific spin-polarization states λ_1 (for the W^+) and λ_2 (for the W^-), with $\lambda_i = (-1, 0, +1)$. The off-shell W -pair production amplitude $\Pi_{\lambda_1 \lambda_2}(M_1, M_2)$ depends on the invariant fermion-pair masses M_i and on the polarizations λ_i of the virtual W bosons. In the limit $M_i \rightarrow M_W$ the amplitudes Π and $\Delta^{(\pm)}$ go over into the on-shell production and decay amplitudes.

The choice of the polarization states labelled by λ_i is in principle free. The amplitude \mathcal{M} is obtained by summing over the polarizations and is therefore independent of such a specific choice. As it turns out, it will be convenient to use different choices in different parts of the RC calculation (see Apps. A and B).

In the cross-section the above factorization leads to

$$\sum_{\text{fermion helicities}} |\mathcal{M}|^2 = \sum_{\lambda_1, \lambda_2, \lambda'_1, \lambda'_2} \mathcal{P}_{[\lambda_1 \lambda_2][\lambda'_1 \lambda'_2]}(M_1, M_2) \frac{\mathcal{D}_{\lambda_1 \lambda'_1}(M_1)}{|D_1|^2} \frac{\mathcal{D}_{\lambda_2 \lambda'_2}(M_2)}{|D_2|^2}. \quad (14)$$

In Eq. (14) the production part is given by a 9×9 density matrix

$$\mathcal{P}_{[\lambda_1 \lambda_2][\lambda'_1 \lambda'_2]}(M_1, M_2) = \sum_{e^\pm \text{ helicities}} \Pi_{\lambda_1 \lambda_2}(M_1, M_2) \Pi_{\lambda'_1 \lambda'_2}^*(M_1, M_2). \quad (15)$$

Similarly the decay part is governed by 3×3 density matrices

$$\mathcal{D}_{\lambda_i \lambda'_i}(M_i) = \sum_{\text{fermion helicities}} \Delta_{\lambda_i}(M_i) \Delta_{\lambda'_i}^*(M_i), \quad (16)$$

where the summation is performed over the helicities of the final-state fermions.

It is clear that Eq. (15) is closely related to the absolute square of the matrix element for stable unpolarized W -pair production. In that case the cross-section contains the trace of the above density matrix

$$\mathbf{Tr} \mathcal{P}(M_W, M_W) = \sum_{\lambda_1, \lambda_2} \mathcal{P}_{[\lambda_1 \lambda_2][\lambda_1 \lambda_2]}(M_W, M_W) = \sum_{\text{all polarizations}} |\Pi_{\lambda_1 \lambda_2}(M_W, M_W)|^2. \quad (17)$$

The decay of an unpolarized on-shell W boson is determined by

$$\mathbf{Tr} \mathcal{D}(M_W) = \sum_{\lambda_i} \mathcal{D}_{\lambda_i \lambda_i}(M_W) = \sum_{\text{all polarizations}} |\Delta_{\lambda_i}(M_W)|^2. \quad (18)$$

Note, however, that also the off-diagonal elements of $\mathcal{P}(M_W, M_W)$ and $\mathcal{D}(M_W)$ are required for determining Eq. (14) in the limit $M_i \rightarrow M_W$.

As a next step it is useful to describe the kinematics of process (11) in a factorized way, i.e. using the invariant masses M_1 and M_2 of the fermion pairs. The differential cross-section takes the form

$$d\sigma = \frac{1}{2s} \sum |\mathcal{M}|^2 d\Gamma_{4f} = \frac{1}{2s} \sum |\mathcal{M}|^2 d\Gamma_{\text{pr}} \cdot d\Gamma_{\text{dec}}^+ \cdot d\Gamma_{\text{dec}}^- \cdot \frac{dM_1^2}{2\pi} \cdot \frac{dM_2^2}{2\pi}, \quad (19)$$

where $d\Gamma_{4f}$ indicates the complete four-fermion phase-space factor and $s = (q_1 + q_2)^2$ the centre-of-mass energy squared. The phase-space factors for the production and decay subprocesses, $d\Gamma_{\text{pr}}$ and $d\Gamma_{\text{dec}}^\pm$, read

$$\begin{aligned} d\Gamma_{\text{pr}} &= \frac{1}{(2\pi)^2} \delta(q_1 + q_2 - p_1 - p_2) \frac{d\vec{p}_1}{2p_{10}} \frac{d\vec{p}_2}{2p_{20}}, \\ d\Gamma_{\text{dec}}^+ &= \frac{1}{(2\pi)^2} \delta(p_1 - k_1 - k'_1) \frac{d\vec{k}_1}{2k_{10}} \frac{d\vec{k}'_1}{2k'_{10}}, \\ d\Gamma_{\text{dec}}^- &= \frac{1}{(2\pi)^2} \delta(p_2 - k_2 - k'_2) \frac{d\vec{k}_2}{2k_{20}} \frac{d\vec{k}'_2}{2k'_{20}}. \end{aligned} \quad (20)$$

When the factorized form for $\sum |\mathcal{M}|^2$ is inserted one obtains

$$\begin{aligned} d\sigma &= \frac{1}{2s} \sum_{\lambda_1, \lambda_2, \lambda'_1, \lambda'_2} \mathcal{P}_{[\lambda_1 \lambda_2][\lambda'_1 \lambda'_2]}(M_1, M_2) d\Gamma_{\text{pr}} \times \mathcal{D}_{\lambda_1 \lambda'_1}(M_1) d\Gamma_{\text{dec}}^+ \times \mathcal{D}_{\lambda_2 \lambda'_2}(M_2) d\Gamma_{\text{dec}}^- \times \\ &\quad \times \frac{1}{2\pi} \frac{dM_1^2}{|D_1|^2} \times \frac{1}{2\pi} \frac{dM_2^2}{|D_2|^2}. \end{aligned} \quad (21)$$

As mentioned before, the definition of the DPA residues is not unique. To define them we first organize the four-fermion kinematics in a special way. In the laboratory (LAB) frame we write the four-fermion phase space in terms of a solid production angle for the W^+ boson and solid decay angles for two of the final-state fermions, one originating from the W^+ boson and one from the W^- boson. These angles will be kept fixed at any time during the process of defining the DPA residues. For later use we explicitly write down our conventions for the momenta, invariants, and phase-space factors. The momenta read

$$\begin{aligned} q_1 &= E(1, \sin \theta, 0, \cos \theta), & q_2 &= E(1, -\sin \theta, 0, -\cos \theta), \\ p_1 &= E_1(1, 0, 0, \frac{p}{E_1}), & p_2 &= E_2(1, 0, 0, -\frac{p}{E_2}), \\ k_1 &= E_3(1, \sin \theta_3 \cos \phi_3, \sin \theta_3 \sin \phi_3, \cos \theta_3), & k_2 &= E_4(1, \sin \theta_4 \cos \phi_4, \sin \theta_4 \sin \phi_4, -\cos \theta_4), \end{aligned} \quad (22)$$

with

$$\begin{aligned} E &= \frac{1}{2} \sqrt{s}, & E_{1,2} &= \frac{1}{2\sqrt{s}}(s + M_{1,2}^2 - M_{2,1}^2), & E_{3,4} &= \frac{1}{2} \frac{M_{1,2}^2}{E_{1,2} - p \cos \theta_{3,4}}, \\ p &= \frac{1}{2\sqrt{s}} \lambda^{1/2}(\sqrt{s}, M_1, M_2), & \lambda(\sqrt{s}, M_1, M_2) &= [s - (M_1 + M_2)^2][s - (M_1 - M_2)^2]. \end{aligned} \quad (23)$$

The momenta of the other final-state particles follow from $k'_i = p_i - k_i$. The masses of the fermions are neglected whenever possible. This, hence, excludes situations in which the fermion masses are needed to regularize singularities from the radiation of collinear photons. The Mandelstam invariants are defined as

$$s = (q_1 + q_2)^2, \quad t = (p_1 - q_1)^2, \quad u = (p_2 - q_1)^2 = M_1^2 + M_2^2 - s - t. \quad (24)$$

From all this it should be clear that the invariant masses M_i only appear explicitly in the energies and velocities of the W bosons and their decay products.

In this notation the production phase-space factor reads

$$d\Gamma_{\text{pr}} = \frac{1}{8\pi} \frac{p}{E} \frac{d\Omega}{4\pi}, \quad (25)$$

with $d\Omega$ denoting the solid angle between the W^+ boson and the positron. The decay phase-space factors are given by

$$d\Gamma_{\text{dec}}^+ = \frac{1}{8\pi} \frac{M_1^2}{(E_1 - p \cos \theta_3)^2} \frac{d\Omega_3}{4\pi} \quad (26)$$

and a similar expression for $d\Gamma_{\text{dec}}^-$. Here $d\Omega_3$ denotes the solid decay angle between the W^+ boson and \bar{f}_1 .

Our choice of the DPA residues amounts to a two-step procedure for fixing the invariant masses M_1 and M_2 , appearing in the four-fermion kinematics and the amplitudes $\Pi(M_1, M_2)$, $\Delta^{(+)}(M_1)$, and $\Delta^{(-)}(M_2)$. The first step is the replacement

$$M_i^2 \rightarrow M_W^2 - i M_W \Gamma_W, \quad (27)$$

i.e. the residue is taken at the Breit–Wigner poles [see discussion below Eq. (8)]. Note that this replacement, of course, does not apply to the Breit–Wigner resonances themselves. The phase-space conventions displayed above fix our choice for the implementation. The solid angles are kept fixed, whereas the energies and velocities become complex [as can be seen from Eq. (23)]. Note that the so-obtained set of momenta preserves momentum conservation. This protects the DPA residues against effectively crossing the four-fermion phase-space boundaries, which might lead to a reduced quality of the DPA.

For practical purposes, however, it is messy to evaluate the $\mathcal{O}(\alpha)$ RC to the amplitudes $\Pi(M_1, M_2)$, $\Delta^{(+)}(M_1)$, and $\Delta^{(-)}(M_2)$ at the complex Breit–Wigner poles. This would require the analytic continuation of the one-loop expressions to the second Riemann sheet. As such we approximate the DPA residues by using

$$M_i = M_W. \quad (28)$$

The error introduced by the *on-shell* approximation (28) is of order $\mathcal{O}(\Gamma_W/M_W)$. When this error comes on top of the $\mathcal{O}(\alpha)$ RC it can be neglected, since terms of $\mathcal{O}(\alpha\Gamma_W/M_W)$ are neglected anyhow in the DPA approach. By having fixed the solid angles in the mapping, the on-shell phase-space points defined with Eq. (28) remain physical. From this point of view it is a sound implementation procedure. A procedure that fixes Mandelstam variables in the mapping involves phase-space regions where it may be regarded as being unsound, as has been indicated in the example below Eq. (6). In such cases it is preferable to set the cross-section to zero rather than evaluating it for unphysical values.

The thus-obtained amplitudes become (gauge-invariant) on-shell ones, whereas the four-fermion phase space is reduced to the phase space of two fermion pairs with invariant masses M_W . Since the DPA forces us to only consider collider energies that are several Γ_W above the on-shell W -pair threshold, the W -boson velocities stay well defined in our approximation. The only place where the invariant masses M_i still show up is in the Breit–Wigner resonances D_i , which can be pulled out as overall factors. The integration over the Breit–Wigner resonances need not be restricted to the physical region $M_i > 0$, $M_1 + M_2 < \sqrt{s}$. Since the DPA is anyhow not valid far off resonance, we can just as well integrate over the full range of the distributions, $(-\infty, +\infty)$, which guarantees that the on-shell results are recovered when the decay kinematics and invariant masses are integrated out. This means that the following integral will be used:

$$\frac{1}{2\pi} \int_{-\infty}^{\infty} dM_i^2 \frac{1}{|D_i|^2} = \frac{1}{2M_W\Gamma_W}. \quad (29)$$

So far we have explained how to calculate the canonical multidifferential cross-section $d\sigma/(d\Omega d\Omega_3 d\Omega_4 dM_1^2 dM_2^2)$ in the DPA. In case one needs a multidifferential cross-section in other variables one should relate that cross-section to the canonical one by means of a Jacobian. In order to obtain this Jacobian the off-shell kinematical relations (22) and (23) should be used.

4 A numerical comparison of different Born cross-sections

In order to have an idea of the differences between the exact Born cross-section $d\sigma_{WW}^0$, corresponding to process (3), and its DPA limit $d\sigma_{DPA}^0$, we now present a brief numerical comparison.

First we discuss the set of parameters used to produce the plots throughout this paper. To facilitate cross-checks with the results presented in the literature, we adopt the LEP2 input-parameter scheme advocated in Ref. [4]. In this scheme the Fermi constant G_μ , the fine-structure constant α , and the masses of the light fermions³ and W, Z bosons are the independent input parameters. The mass of the top quark, m_t , follows from the Standard Model prediction for muon decay

$$G_\mu = \frac{\alpha\pi}{\sqrt{2}M_W^2(1 - M_W^2/M_Z^2)} \frac{1}{1 - \Delta r}. \quad (30)$$

The quantity Δr denotes the loop corrections to muon decay. It is zero at tree level, but when loop corrections are included it depends on the input parameters as well as on m_t , the Higgs-boson mass M_H , and the strong coupling α_S .⁴

In analogy to Ref. [4] we use in our numerical evaluations the following set of (slightly outdated) input parameters:

$$\begin{aligned} \alpha &= 1/137.0359895, & G_\mu &= 1.16639 \times 10^{-5} \text{ GeV}^{-2}, \\ M_Z &= 91.1884 \text{ GeV}, & M_W &= 80.26 \text{ GeV}, \\ m_e &= 0.51099906 \text{ MeV}, & m_\mu &= 105.658389 \text{ MeV}, & m_\tau &= 1.7771 \text{ GeV}, \\ m_u &= 47 \text{ MeV}, & m_d &= 47 \text{ MeV}, \\ m_s &= 150 \text{ MeV}, & m_c &= 1.55 \text{ GeV}, \\ m_b &= 4.7 \text{ GeV}, \end{aligned} \quad (31)$$

and choose

$$M_H = 300 \text{ GeV}, \quad \alpha_S(M_Z^2) = 0.123. \quad (32)$$

The solution of Eq. (30), using a calculation of Δr that contains all the known higher-order effects, gives the value for the top-quark mass [4]

$$m_t = 165.26 \text{ GeV}. \quad (33)$$

As was already mentioned in Sect. 1, the use of G_μ instead of α in the lowest-order cross-sections very often reduces the size of the one-loop non-photonic RC considerably. This so-called G_μ -parametrization consists in the replacement

$$d\sigma = d\sigma^0(1 + \delta^{1\text{-loop}}) \rightarrow \frac{d\sigma^0}{(1 - \Delta r)^n} (1 + \delta^{1\text{-loop}} - n\Delta r^{1\text{-loop}}) \equiv d\bar{\sigma}^0(1 + \bar{\delta}^{1\text{-loop}}), \quad (34)$$

³The masses of the light quarks are adjusted in such a way that the experimentally measured hadronic vacuum polarization is reproduced.

⁴The so-obtained top-quark mass will become α_S - and M_H -dependent. It can be confronted with the direct measurements at Fermilab and the indirect ones from LEP in order to obtain indirect information on M_H .

where $d\sigma^0 \propto \alpha^n$ and according to Eq. (30) $d\bar{\sigma}^0 \propto G_\mu^n$. The results presented in this paper are all calculated in this parametrization.

Another important parameter featuring in our calculations is the width of the W boson. As explained below Eq. (8), we will use the calculated on-shell width. Since we want the Breit–Wigner resonances to be as close to reality as possible, we will always use the $\mathcal{O}(\alpha)$ - and $\mathcal{O}(\alpha_S)$ -corrected width Γ_W , regardless of the fact that we sometimes consider lowest-order distributions. Using the above set of input parameters we find in the G_μ -parametrization

$$\Gamma_W = 2.08174 \text{ GeV.} \quad (35)$$

For future use we note that the lowest-order W -boson width in this parametrization reads $\Gamma_W^0 = 2.03540 \text{ GeV}$. It is also relevant to stress that the $\mathcal{O}(\alpha)$ corrections to the leptonic partial widths $\Gamma_{W \rightarrow \ell \nu_\ell}$ are small and negative ($\sim -0.3\%$). The $\mathcal{O}(\alpha_S)$ corrections to the hadronic partial widths are positive, leading to the positive overall correction to the total W -boson width.

Having fixed the input, we now compare $d\sigma_{WW}^0$ and $d\sigma_{DPA}^0$ for the total cross-section σ_{tot} (in Fig. 3) and the differential cross-section $d\sigma/d\cos\theta$ (in Fig. 4), where θ is the polar angle between the W^+ boson and the positron in the LAB frame [see Eq. (22)]. The latter distribution is given for $2E = 184 \text{ GeV}$, whereas σ_{tot} is presented for a range of LEP2 energies. We select one particular purely leptonic final state, $\mu^+ \nu_\mu \tau^- \bar{\nu}_\tau$. In view of the massless treatment of the final-state fermions and the universal lowest-order interaction between the fermions and the W bosons, the results for the various final states can be obtained by multiplying the purely leptonic result by a factor $N_C^{f_1} |V_{f'_1 f_1}|^2 N_C^{f_2} |V_{f'_2 f_2}|^2$. Here $V_{f'_i f_i}$ is the mixing matrix and $N_C^{f_i}$ the colour factor. For leptons only $V_{\nu_\ell \ell} = 1$ is non-vanishing and $N_C^\ell = 1$.

We consider the following four cases:

- i) The calculation for stable W bosons, multiplied by the branching ratio $(\Gamma_{W \rightarrow \ell \nu_\ell}^0 / \Gamma_W^0)^2$.
- ii) The DPA calculation, where in Eq. (21) the on-shell approximation is applied to both the matrix elements and the four-fermion phase space. The M_i^2 integrations over the Breit–Wigner resonances are extended to the full range $(-\infty, +\infty)$, i.e. Eq. (29) is used.
- iii) The calculation where the matrix element (12) is on-shell, but the four-fermion phase space in Eq. (21) is not. The M_i^2 integrations are performed in the physical region.
- iv) The off-shell calculation according to Eq. (21), with the M_i^2 integrations performed in the physical region. This corresponds to $d\sigma_{WW}^0$.

In cases ii), iii), and iv) the W -boson propagators contain the width Γ_W , as given in Eq. (35). The matrix element in case iv) is not gauge-invariant, it is calculated in the unitary gauge.

For the total cross-section (see Fig. 3) cases i) and ii) differ by a fixed overall factor, as was to be expected from the Breit–Wigner integrals. The overall factor is determined by $(\Gamma_W / \Gamma_W^0)^2 = 1.04605$ and is found to be 1.04609. The agreement with this overall factor is a

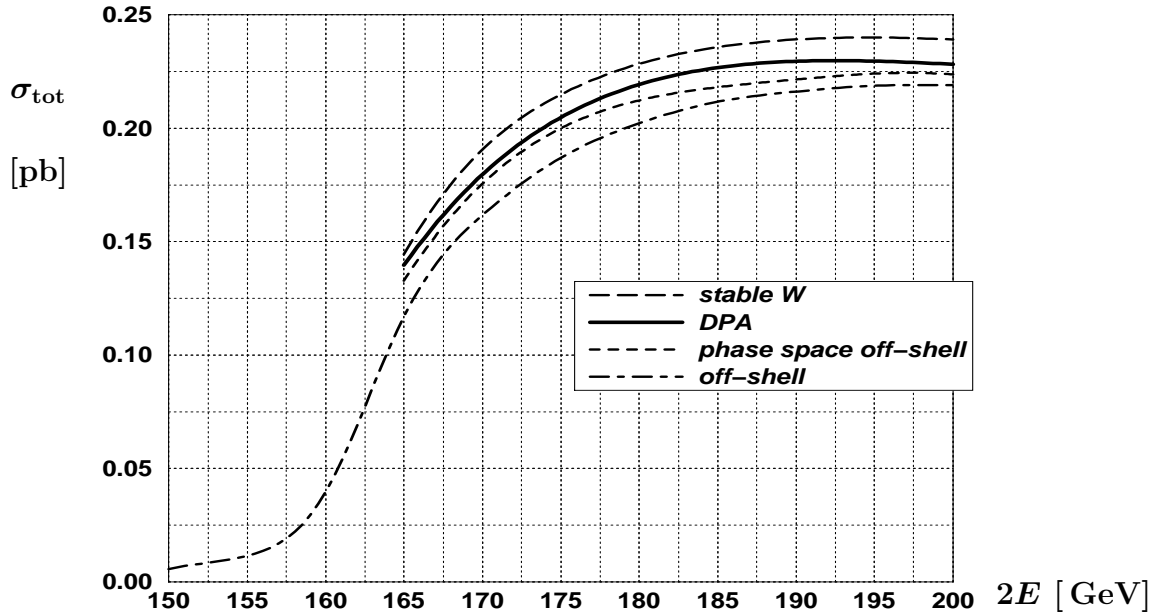


Figure 3: Comparison of different Born approximations for the total cross-section σ_{tot} as a function of the accelerator energy. The four curves correspond to the cases i)–iv) introduced in the text.

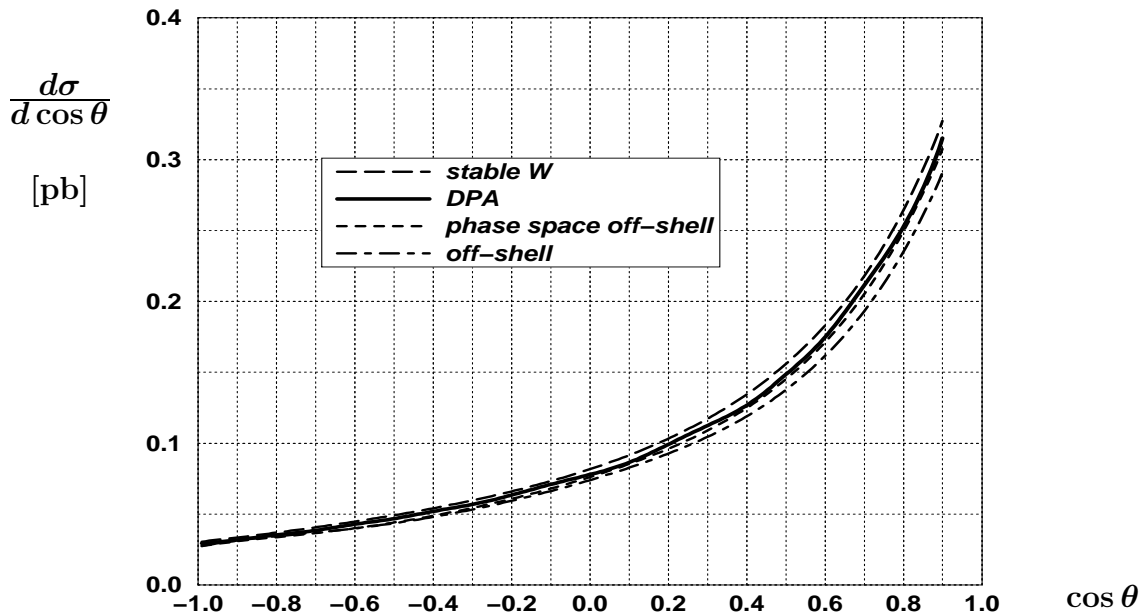


Figure 4: The same curves as in the previous plot, this time for the lowest-order production-angle distribution $d\sigma/d\cos\theta$ at $2E = 184$ GeV.

check on the numerical integration over the decay angles. For the production-angle distribution (see Fig. 4) the same overall factor is observed.

One of the ingredients of Eq. (10) is the difference $d\sigma_{WW}^0 - d\sigma_{\text{DPA}}^0$. By comparing cases ii) and iv) in Fig. 3 one observes that this difference varies between 18% and 5%, when going from 165 GeV to 200 GeV. This is in good agreement with the expected $\mathcal{O}(\Gamma_W/\Delta E)$ precision of the DPA limit, where ΔE is defined as the distance in energy to the W -pair threshold, $\Delta E = \sqrt{s} - 2M_W$. Larger differences arise when the comparison between σ_{WW}^0 and σ_{DPA}^0 is carried out at much higher energies. The reason is that σ_{WW}^0 is not $SU(2)$ gauge-invariant and does not fall off sufficiently fast. By properly combining σ_{WW}^0 and the background contributions σ_{bkg}^0 the $SU(2)$ gauge invariance can be restored and σ_{DPA}^0 again turns out to be a good approximation to the total (four-fermion) cross-section.

5 Radiative corrections in the double-pole approximation

In this section we discuss the complete $\mathcal{O}(\alpha)$ RC to process (11) in the context of the DPA. As mentioned in Sect. 3, the most economic way of calculating the RC up to $\mathcal{O}(\alpha)$ precision involves the DPA. In this approximation all virtual corrections can be classified into two groups: factorizable and non-factorizable corrections. The factorizable corrections are directly linked to the electroweak one-loop RC to the on-shell production and on-shell decay of the W bosons. The remaining non-factorizable virtual corrections can be viewed as describing interactions between different stages of the off-shell process. They will only originate from certain photonic loop diagrams, as stated in Sect. 3. The real-photon corrections can also be classified in factorizable and non-factorizable corrections, although the various regimes for the photon energy require some special attention.

In the following we will describe the calculation of all these corrections in more detail and comment on the accuracy and applicability of the results. At this point we remind the reader that throughout the calculations of the RC in the DPA two additional approximations are used. First, whenever possible we consider the initial- and final-state fermions to be massless, i.e. excluding the cases in which the fermion masses are needed to regularize singularities from the radiation of collinear photons. The error of this approximation is at most $\mathcal{O}(\alpha m_\tau/M_W)$ or $\mathcal{O}(\alpha |V_{cb}| m_b/M_W)$, which is beyond the accuracy of our calculation. Second, we assume that the accelerator energy is sufficiently far (read: several Γ_W) above the threshold for on-shell W -pair production. Close to threshold the DPA cannot be trusted to produce the dominant contributions and therefore our approach breaks down. The accuracy of this “far-from-threshold” approximation is $\mathcal{O}(\alpha \Gamma_W/\Delta E)$, where ΔE is the distance in energy to the W -pair threshold, $\Delta E = \sqrt{s} - 2M_W$.

5.1 Virtual corrections

As a first step we discuss how to separate the virtual corrections into a sum of factorizable and non-factorizable virtual corrections. The diagrammatic split-up according to reducible and irreducible W -boson lines is an illustrative way of understanding the different nature of the two classes of corrections, but since the double-resonant diagrams are not gauge-invariant by themselves the precise split-up needs to be defined properly.

We can make use of the fact that there are effectively two scales in the problem: M_W and Γ_W . Let us now consider virtual corrections coming from photons with different energies:

- soft photons, $E_\gamma \ll \Gamma_W$,
- semi-soft photons, $E_\gamma = \mathcal{O}(\Gamma_W)$,
- hard photons, $\Gamma_W \ll E_\gamma = \mathcal{O}(M_W)$.

Only soft and semi-soft photons contribute to both factorizable and non-factorizable corrections. The latter being defined to describe interactions between different stages of the off-shell process. The reason for this is that only these photons can induce relatively long-range interactions and thereby allow the various subprocesses, which are separated by a propagation interval of $\mathcal{O}(1/\Gamma_W)$, to communicate with each other. Virtual corrections involving the exchange of hard photons or massive particles contribute exclusively to the factorizable corrections. In view of the short range of the interactions induced by these particles, their contribution to the non-factorizable corrections are suppressed by at least $\mathcal{O}(\Gamma_W/M_W)$.

As hard photons contribute to the factorizable corrections only, we only need to define a split-up for soft and semi-soft photons. It is impossible to do this in a consistent gauge-invariant way on the basis of diagrams. As we will see, it might happen that only part of some particular diagram should be attributed to the non-factorizable corrections, the rest being of factorizable nature.

The matrix element for soft and semi-soft photons can be written as a product of the lowest-order matrix element in DPA ($\mathcal{M}_{\text{DPA}}^0$) and conserved (semi)soft-photon currents. These currents can be decomposed into production and decay currents with the help of a partial-fraction decomposition for virtual-photon emission from a W -boson line:

$$\begin{aligned} \frac{1}{[p^2 - M^2][p^2 + 2pk - M^2 + io]} &= \frac{1}{2pk + io} \left(\frac{1}{p^2 - M^2} - \frac{1}{p^2 + 2pk - M^2 + io} \right) \\ &= \frac{1}{2pk + io} \left(\frac{1}{D} - \frac{1}{D + 2pk + io} \right). \end{aligned} \quad (36)$$

Here $M^2 = M_W^2 - iM_W\Gamma_W$, k is the loop momentum of the exchanged photon, $p + k$ is the momentum of the W boson inside the integral, and p is the momentum of the W boson outside the integral. The infinitesimal imaginary part $+io$ is needed to ensure a proper incorporation

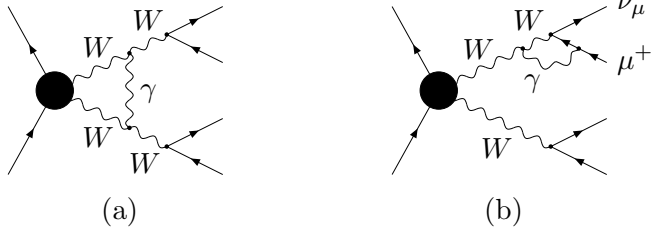


Figure 5: Examples of one-loop diagrams that contribute to both factorizable and non-factorizable corrections.

of causality. In this way one obtains a sum of two resonant W -boson propagators multiplied by an ordinary on-shell eikonal factor. This decomposition allows a gauge-invariant split-up of the matrix element in terms of one contribution where the photon is effectively emitted from the production part, and two others where the photon is effectively emitted from one of the two decay parts. The squares of the three contributions can be identified as factorizable corrections, whereas the interference terms are of non-factorizable nature.

In order to illustrate our method, we explicitly apply it to two special one-loop contributions (see Fig. 5). The first one [diagram (a)] is the so-called Coulomb graph, involving photon exchange between the two W bosons. The corresponding semi-soft matrix element reads

$$\begin{aligned}
 \mathcal{M}_a &= ie^2 \mathcal{M}_{\text{DPA}}^0 \int \frac{d^4 k}{(2\pi)^4 [k^2 + io]} \frac{4p_1 p_2}{[D_1 + 2kp_1 + io][D_2 - 2kp_2 + io]} \\
 &= ie^2 \mathcal{M}_{\text{DPA}}^0 \int \frac{d^4 k}{(2\pi)^4 [k^2 + io]} \frac{4p_1 p_2}{[2kp_1 + io][-2kp_2 + io]} \left\{ 1 - \frac{D_1}{D_1 + 2kp_1 + io} \right. \\
 &\quad \left. - \frac{D_2}{D_2 - 2kp_2 + io} + \frac{D_1 D_2}{[D_1 + 2kp_1 + io][D_2 - 2kp_2 + io]} \right\}. \tag{37}
 \end{aligned}$$

The first term in the last expression gives rise to a factorizable (on-shell) contribution to the production stage, whereas the other three terms are counted as non-factorizable contributions. These three terms are classified as $(\text{prod} \times \text{dec}^+)$, $(\text{prod} \times \text{dec}^-)$, and $(\text{dec}^+ \times \text{dec}^-)$, respectively. In other words, the Coulomb graph contributes both to the usual Coulomb effect in on-shell W -pair production and to a non-factorizable part. For the photonic interaction between the W^+ boson and its μ^+ decay product [diagram (b)] we obtain

$$\begin{aligned}
 \mathcal{M}_b &= -ie^2 \mathcal{M}_{\text{DPA}}^0 \int \frac{d^4 k}{(2\pi)^4 [k^2 + io]} \frac{4p_1 k_1}{[2kk_1 + io][D_1 + 2kp_1 + io]} \\
 &= -ie^2 \mathcal{M}_{\text{DPA}}^0 \int \frac{d^4 k}{(2\pi)^4 [k^2 + io]} \frac{4p_1 k_1}{[2kp_1 + io][2kk_1 + io]} \left\{ 1 - \frac{D_1}{D_1 + 2kp_1 + io} \right\}. \tag{38}
 \end{aligned}$$

Again the first term is a factorizable contribution, belonging to the W^+ decay stage, whereas the second term is a non-factorizable contribution of the type $(\text{prod} \times \text{dec}^+)$. As is clear from these examples, the non-factorizable contributions always involve the Breit–Wigner ratios $D_i/(D_i \pm 2kp_i)$, which effectively remove the overall W propagator $1/D_i$. The more energetic

the exchanged photon is, the more suppressed such a ratio will be in the vicinity of the M_i^2 resonance. In fact, for $k_0 > \Lambda$ the non-factorizable contributions are suppressed by $\mathcal{O}(M_W \Gamma_W / [E\Lambda])$ (see App. C).

Every one-loop diagram with a semi-soft photon can be treated in this way. By collecting all terms that contain the ratios $D_i/[D_i \pm 2kp_i]$ the formula for non-factorizable corrections is obtained. As one can see explicitly below, this expression is gauge-invariant. Since the expression contains those diagrams where irreducible W -boson lines are present, it can be viewed as a gauge-invariant extension of the set of W -irreducible diagrams.

The so-defined non-factorizable corrections read

$$\mathcal{M}_{\text{nf}}^{\text{virt}} = i\mathcal{M}_{\text{DPA}}^0 \int \frac{d^4k}{(2\pi)^4[k^2 + io]} \left[(\mathcal{J}_0^\mu + \mathcal{J}_\oplus^\mu) \mathcal{J}_{+, \mu} + (\mathcal{J}_0^\mu + \mathcal{J}_\ominus^\mu) \mathcal{J}_{-, \mu} + \mathcal{J}_+^\mu \mathcal{J}_{-, \mu} \right]. \quad (39)$$

The currents are given by

$$\begin{aligned} \mathcal{J}_0^\mu &= e \left[\frac{p_1^\mu}{kp_1 + io} + \frac{p_2^\mu}{-kp_2 + io} \right], \\ \mathcal{J}_\oplus^\mu &= -e \left[\frac{q_1^\mu}{kq_1 + io} - \frac{q_2^\mu}{kq_2 + io} \right], \quad \mathcal{J}_\ominus^\mu = +e \left[\frac{q_1^\mu}{-kq_1 + io} - \frac{q_2^\mu}{-kq_2 + io} \right] \end{aligned} \quad (40)$$

for photon emission from the production stage of the process, and

$$\begin{aligned} \mathcal{J}_+^\mu &= -e \left[\frac{p_1^\mu}{kp_1 + io} + Q_{f_1} \frac{k_1^\mu}{kk_1 + io} - Q_{f'_1} \frac{k'_1{}^\mu}{kk'_1 + io} \right] \frac{D_1}{D_1 + 2kp_1}, \\ \mathcal{J}_-^\mu &= -e \left[\frac{p_2^\mu}{-kp_2 + io} + Q_{f_2} \frac{k_2^\mu}{-kk_2 + io} - Q_{f'_2} \frac{k'_2{}^\mu}{-kk'_2 + io} \right] \frac{D_2}{D_2 - 2kp_2} \end{aligned} \quad (41)$$

for photon emission from the decay stages of the process. Here Q_f stands for the charge of fermion f in units of e . After having defined the gauge-invariant currents, the $+io$ terms can be dropped from $D_1 + 2kp_1$ and $D_2 - 2kp_2$, since $\text{Im } D_i > 0$. Note the difference in the sign of the io parts appearing in the currents \mathcal{J}_\ominus and \mathcal{J}_\oplus . These signs actually determine which interference terms give rise to a non-vanishing non-factorizable contribution after virtual and real-photon corrections have been added. As can be seen from Eq. (38), in the upper hemisphere of the complex k_0 plane there is only one pole: the so-called ‘photon pole’, originating from the photon propagator $1/[k^2 + io]$. When virtual and real-photon corrections are combined, such a non-factorizable contribution will vanish [21]. For the Coulomb graph, Eq. (37), this is not the case, as also poles from the other propagators are present in both hemispheres. As a result of such considerations only a very limited subset of ‘final-state’ interferences survives [9, 10]: the virtual corrections corresponding to Figs. 2 and 5(a) as well as the associated real-photon corrections.

The virtual factorizable corrections consist of all hard contributions and the above-indicated part of the semi-soft ones. The so-defined factorizable corrections have the nice feature that they can be expressed in terms of corrections to on-shell subprocesses, i.e. the production of

two on-shell W bosons and their subsequent on-shell decays. The corresponding matrix element can be expressed in the same way as described in Sect. 3:

$$\mathcal{M}_{\text{fact}}^{\text{virt}} = \sum_{\lambda_1, \lambda_2} \Pi_{\lambda_1 \lambda_2}(M_1, M_2) \frac{\Delta_{\lambda_1}^{(+)}(M_1)}{D_1} \frac{\Delta_{\lambda_2}^{(-)}(M_2)}{D_2}. \quad (42)$$

Here two of the amplitudes are taken at lowest order, whereas the remaining one contains all possible one-loop contributions, including the W wave-function factors that appear in Eq. (5). In this way the well-known on-shell RC to the production and decay of pairs of W bosons [12]–[15] appear as basic building blocks of the factorizable corrections.⁵ In the semi-soft limit the virtual factorizable corrections to the production stage, contained in Π , will cancel against the corresponding real-photon corrections. Non-vanishing contributions from Π occur as soon as the k^2 terms in the propagators cannot be neglected anymore. An example of this is the factorizable correction from the Coulomb graph, given in Eq. (37). For the on-shell (factorizable) part of the Coulomb effect photons with momenta $k_0 = \mathcal{O}(\Delta E)$ and $|\vec{k}| = \mathcal{O}(\sqrt{M_W \Delta E})$ are important [11], i.e. k^2 cannot be neglected in the propagators of the unstable particles. Since we stay well away from the W -pair threshold ($\Delta E \gg \Gamma_W$), this situation occurs outside the realm of the semi-soft photons. This fits nicely into the picture of the production stage being a “hard” subprocess, governed by relatively short time scales as compared with the much longer time scales required for the non-factorizable corrections, which interconnect the different subprocesses.

5.2 Real-photon radiation

In this subsection we discuss the aspects of real-photon radiation in the DPA. To this end we consider the process

$$e^+(q_1) e^-(q_2) \rightarrow W^+(p_1) W^-(p_2) [\gamma(k)] \rightarrow \bar{f}_1(k_1) f'_1(k'_1) f_2(k_2) \bar{f}'_2(k'_2) \gamma(k), \quad (43)$$

where in the intermediate state there may or may not be a photon. We will show how to extract the gauge-invariant double-pole residues in different situations. The exact cross-section for process (43) can be written in the following form

$$d\sigma = \frac{1}{2s} |\mathcal{M}_\gamma|^2 d\Gamma_{4f\gamma} = \frac{1}{2s} \left[2\text{Re} \left(\mathcal{M}_0 \mathcal{M}_+^* + \mathcal{M}_0 \mathcal{M}_-^* + \mathcal{M}_+ \mathcal{M}_-^* \right) + |\mathcal{M}_0|^2 + |\mathcal{M}_+|^2 + |\mathcal{M}_-|^2 \right] d\Gamma_{4f\gamma}, \quad (44)$$

where $d\Gamma_{4f\gamma}$ indicates the complete five-particle phase-space factor, and the matrix elements \mathcal{M}_0 and \mathcal{M}_\pm correspond to the diagrams where the photon is attached to the production or decay stage of the three W -pair diagrams, respectively. This split-up can be achieved with the help of the real-photon version of the partial-fraction decomposition (36). Each contribution

⁵Note that the complete density matrix is required in this case, in contrast to the pure on-shell calculation which involves the trace of the density matrix only.

to the cross-section can be written in terms of polarization density matrices, which originate from the amplitudes

$$\mathcal{M}_0 = \Pi_\gamma(M_1, M_2) \frac{\Delta^{(+)}(M_1)}{D_1} \frac{\Delta^{(-)}(M_2)}{D_2}, \quad (45)$$

$$\mathcal{M}_+ = \Pi(M_{1\gamma}, M_2) \frac{\Delta_\gamma^{(+)}(M_{1\gamma})}{D_{1\gamma}} \frac{\Delta^{(-)}(M_2)}{D_2}, \quad (46)$$

$$\mathcal{M}_- = \Pi(M_1, M_{2\gamma}) \frac{\Delta^{(+)}(M_1)}{D_1} \frac{\Delta_\gamma^{(-)}(M_{2\gamma})}{D_{2\gamma}}, \quad (47)$$

where all polarization indices for the W bosons and the photon have been suppressed, and

$$D_{i\gamma} = D_i + 2kk_i + 2kk'_i, \quad M_{i\gamma}^2 = M_i^2 + 2kk_i + 2kk'_i, \quad M_i^2 = (k_i + k'_i)^2. \quad (48)$$

The matrix elements Π_γ and $\Delta_\gamma^{(\pm)}$ describe the production and decay of the W bosons accompanied by the radiation of a photon. The matrix elements without subscript γ have been introduced in Eq. (12).

In the calculation of the Born matrix element and virtual corrections only two poles could be identified in the amplitudes, originating from the Breit–Wigner propagators $1/D_i$. The pole-scheme expansion was performed around these two poles. In contrast, the bremsstrahlung matrix element has four in general different poles, originating from the four Breit–Wigner propagators $1/D_i$ and $1/D_{i\gamma}$. As mentioned above, the matrix element can be rewritten as a sum of three matrix elements ($\mathcal{M}_0, \mathcal{M}_+, \mathcal{M}_-$), each of which only contain two Breit–Wigner propagators. For these three individual matrix elements the pole-scheme expansion is fixed, as before, to an expansion around the corresponding two poles. However, when calculating cross-sections [see Eq. (44)] the mapping of the five-particle phase space introduces a new type of ambiguity. The interference terms in Eq. (44) involve two different double-pole expansions simultaneously. As such there is no natural choice for the phase-space mapping in those cases. The resulting ambiguity (implementation dependence) might have important repercussions on the quality of the DPA calculation and therefore deserves some special attention. In this context the three earlier-defined regimes for the photon energy play a role:

- for hard photons [$E_\gamma \gg \Gamma_W$] the Breit–Wigner poles of the W -boson resonances before and after photon radiation are well separated in phase space (see $M_{i\gamma}^2$ and M_i^2 defined above). As a result, the interference terms in Eq. (44) can be neglected. This leads to three *distinct* regions of on-shell contributions, where the photon can be assigned unambiguously to the W -pair-production subprocess or to one of the two decays. This assignment is determined by the pair of invariant masses (out of M_i^2 and $M_{i\gamma}^2$) that is in the M_W^2 region. Therefore, the double-pole residue can be expressed as the sum of the three on-shell contributions without increasing the intrinsic error of the DPA. Note that in the same way it is also possible to experimentally assign the photon to one of the subprocesses, since misassignment errors are suppressed, assuming for convenience that all final-state momenta can ideally be measured.

- for semi-soft photons [$E_\gamma = \mathcal{O}(\Gamma_W)$] the Breit–Wigner poles are relatively close together in phase space, resulting in a substantial overlap of the line shapes. The assignment of the photon is now subject to larger errors. Moreover, since the interference terms in Eq. (44) cannot be neglected, the issue of the phase-space mapping has to be addressed. In the following we give a proper prescription for calculating the DPA residues and discuss their quality.
- for soft photons [$E_\gamma \ll \Gamma_W$] the Breit–Wigner poles are on top of each other, resulting in a pole-scheme expansion that is identical to the one without the photon.

5.2.1 Hard photons

Let us first consider the hard-photon regime in more detail. Due to the fact that the poles are well separated in the hard-photon regime, it is clear that the interference terms are suppressed and can be neglected:

$$d\sigma = \frac{1}{2s} \left[|\mathcal{M}_0|^2 + |\mathcal{M}_+|^2 + |\mathcal{M}_-|^2 \right] d\Gamma_{4f\gamma}. \quad (49)$$

Note that each of the three terms has two poles, originating from two resonant propagators. However, these poles are different for different terms. The phase-space factor can be rewritten in three equivalent ways. The first is

$$d\Gamma_{4f\gamma} = d\Gamma_0^\gamma = d\Gamma_{\text{pr}}^\gamma \cdot d\Gamma_{\text{dec}}^+ \cdot d\Gamma_{\text{dec}}^- \cdot \frac{dM_1^2}{2\pi} \cdot \frac{dM_2^2}{2\pi}, \quad (50)$$

with

$$d\Gamma_{\text{pr}}^\gamma = \frac{1}{(2\pi)^2} \delta(q_1 + q_2 - p_1 - p_2 - k) \frac{d\vec{p}_1}{2p_{10}} \frac{d\vec{p}_2}{2p_{20}} \frac{d\vec{k}}{(2\pi)^3 2k_0}. \quad (51)$$

The two others are

$$d\Gamma_{4f\gamma} = d\Gamma_+^\gamma = d\Gamma_{\text{pr}} \cdot d\Gamma_{\text{dec}}^{+\gamma} \cdot d\Gamma_{\text{dec}}^- \cdot \frac{dM_{1\gamma}^2}{2\pi} \cdot \frac{dM_2^2}{2\pi}, \quad (52)$$

with

$$d\Gamma_{\text{dec}}^{+\gamma} = \frac{1}{(2\pi)^2} \delta(p_1 - k_1 - k'_1 - k) \frac{d\vec{k}_1}{2k_{10}} \frac{d\vec{k}'_1}{2k'_{10}} \frac{d\vec{k}}{(2\pi)^3 2k_0}, \quad (53)$$

and a similar expression for $d\Gamma_-^\gamma$. The phase-space factors $d\Gamma_{\text{pr}}$ and $d\Gamma_{\text{dec}}^\pm$ are just the lowest-order ones. The cross-section can then be written in the following equivalent form

$$d\sigma = \frac{1}{2s} \left[|\mathcal{M}_0|^2 d\Gamma_0^\gamma + |\mathcal{M}_+|^2 d\Gamma_+^\gamma + |\mathcal{M}_-|^2 d\Gamma_-^\gamma \right]. \quad (54)$$

In order to extract gauge-invariant quantities, the DPA limit should be taken. This amounts to taking the limit $p_{1,2}^2 \rightarrow M_W^2$, using a prescription that resembles the one presented in Sect. 3. Note however that $p_{1,2}$ can be different according to the δ -functions in the decay parts of the different phase-space factors. To be specific, the production term $|\mathcal{M}_0|^2$ has poles at

$p_i^2 = M_i^2 = M_W^2$, $|\mathcal{M}_+|^2$ has poles at $p_1^2 = M_{1\gamma}^2 = M_W^2$ and $p_2^2 = M_2^2 = M_W^2$, and $|\mathcal{M}_-|^2$ has poles at $p_1^2 = M_1^2 = M_W^2$ and $p_2^2 = M_{2\gamma}^2 = M_W^2$. Again we fix solid angles in the mapping, including the solid angle of the photon. Since the energy range of the photon in the on-shell kinematics of the W bosons is different from the off-shell case, it may happen that the energy of the photon in an off-shell four-fermion–one-photon event with certain solid angles lies outside the on-shell phase space with the same solid angles. A possible procedure is to assign a zero cross-section to those events. Since the events are anyhow rare, being close to the edge of the off-shell phase space, this procedure constitutes an acceptable and simple solution. An alternative way to avoid unphysical on-shell phase-space points would be to write the photon energy as a fraction of the maximum attainable photon energy for given invariant masses $\sqrt{p_i^2}$ of the resonant W bosons and given solid angles:

$$E_\gamma = x_\gamma E_\gamma^{\max}(\sqrt{p_1^2}, \sqrt{p_2^2}, \text{angles}). \quad (55)$$

In this way the photon energy is projected on the interval $[0, 1]$. The maximum photon energy E_γ^{\max} depends on the specific term in Eq. (54). Subsequently the fraction x_γ and the aforementioned solid angles are kept fixed during the mapping from off- to on-shell events. Then E_γ for the on-shell case is found from Eq. (55), where p_i^2 are replaced by M_W^2 .

It should be stressed that in the on-shell phase space there is no ambiguity concerning the treatment of the photon. One obtains in the DPA limit three gauge-invariant on-shell contributions to Eq. (54). The calculation of the corresponding matrix elements is presented in App. B.

5.2.2 Semi-soft and soft photons

We complete our survey of the different photon-energy regimes by considering semi-soft and soft photons. The split-up of factorizable and non-factorizable real-photon corrections proceeds in the same way as described in the previous subsection for virtual corrections. The result reads in semi-soft approximation

$$d\sigma = \frac{1}{2s} |\mathcal{M}_\gamma|^2 d\Gamma_{4f\gamma} \approx -d\sigma_{\text{DPA}}^0 \frac{d\vec{k}}{(2\pi)^3 2k_0} \left[2\text{Re} \left(\mathcal{I}_0^\mu \mathcal{I}_{+, \mu}^* + \mathcal{I}_0^\mu \mathcal{I}_{-, \mu}^* + \mathcal{I}_+^\mu \mathcal{I}_{-, \mu}^* \right) + |\mathcal{I}_0^2| + |\mathcal{I}_+^2| + |\mathcal{I}_-^2| \right]. \quad (56)$$

The gauge-invariant currents \mathcal{I}_0 and \mathcal{I}_\pm are given by

$$\begin{aligned} \mathcal{I}_0^\mu &= e \left[\frac{p_1^\mu}{kp_1} - \frac{p_2^\mu}{kp_2} - \frac{q_1^\mu}{kq_1} + \frac{q_2^\mu}{kq_2} \right], \\ \mathcal{I}_+^\mu &= -e \left[\frac{p_1^\mu}{kp_1} + Q_{f_1} \frac{k_1^\mu}{kk_1} - Q_{f'_1} \frac{k'_1{}^\mu}{kk'_1} \right] \frac{D_1}{D_1 + 2kp_1}, \\ \mathcal{I}_-^\mu &= +e \left[\frac{p_2^\mu}{kp_2} + Q_{f_2} \frac{k_2^\mu}{kk_2} - Q_{f'_2} \frac{k'_2{}^\mu}{kk'_2} \right] \frac{D_2}{D_2 + 2kp_2}. \end{aligned} \quad (57)$$

The first three interference terms in Eq. (56) correspond to the real non-factorizable corrections. The last three squared terms in Eq. (56) belong to the factorizable real-photon corrections.

They constitute the semi-soft limit of Eq. (54). Note also that the currents are the same for both possible expressions for p_i , i.e. it does not matter whether $p_i = k_i + k'_i$ or $p_i = k_i + k'_i + k$.

As mentioned before, the DPA residues have to be defined properly in the presence of overlapping Breit–Wigner resonances in the semi-soft regime. The above equation (56) specifies such a procedure: the Born cross-section for a four-particle phase space is factored out and does not depend on the photon momentum. The factor between the square brackets is the usual soft-photon factor, except that the rapid variation of the Breit–Wigner resonances has been kept, leading to the ratios $D_i/D_{i\gamma}$ which take into account the shift in the Breit–Wigner distributions due to the photon. In the vicinity of the M_i^2 resonance these ratios are negligible for hard photons, unity for soft photons, and of $\mathcal{O}(1)$ for semi-soft photons.

This prescription is by no means unique. In principle one could have chosen any of the two Breit–Wigner resonances, $1/D_i$ or $1/D_{i\gamma}$, to define the phase-space mapping for the interference terms. Or in other words, both on-shell phase-space limits, $M_i^2 = M_W^2$ or $M_{i\gamma}^2 = M_W^2$, constitute equally plausible DPA mappings. The differences between both phase-space mappings are of $\mathcal{O}(k)$. Since the interference terms are only non-negligible in the semi-soft regime, it is conceivable that the implementation dependence associated with these different on-shell limits remains of $\mathcal{O}(\Gamma_W/M_W)$. Let us, for instance, consider the M_i^2 distribution in the vicinity of the resonance. Any $\mathcal{O}(k)$ shift in the factor multiplying $1/D_i$ would result in additional terms of $\mathcal{O}(k/M_W)$, i.e. at worst $\mathcal{O}(\Gamma_W/M_W)$ in the semi-soft limit. A similar shift in the factor belonging to $1/D_{i\gamma}$ results in additional contributions to the DPA residues that are suppressed by $\mathcal{O}(\Gamma_W/E)$ for *all* values of the photon energy, as is explained in App. C. Therefore one can conclude that overlapping Breit–Wigner resonances do not necessarily imply a reduced quality of the DPA.

Based on this observation, we have the freedom to choose a suitable procedure for semi-soft photons. The fact whether hard-photon contributions are suppressed or not will serve as our guideline for fixing the choice. Whenever the hard-photon effects yield vanishing contributions to certain observables, we will use the semi-soft currents of Eqs. (56) and (57). As a consequence, the non-factorizable corrections are always calculated with the help of the semi-soft interference terms. In order to specify our approach, we indicate in the following how the above-defined matrix elements and currents are used in the various distributions of experimental interest.

5.2.3 Real-photon contributions to various distributions

As in all RC, the role of the bremsstrahlung process is twofold. In the first place the off-shell W -pair process (3) has at lowest-order level all kinds of distributions to which one would like to calculate $\mathcal{O}(\alpha)$ RC. These RC consist of virtual and real-photon contributions. An integration over all allowed photon energies should be carried out, i.e. the radiated photon should be treated inclusively.

The second application of the bremsstrahlung process involves the evaluation of exclusive photon distributions. Since the photon has to be detected it should be sufficiently hard. How hard depends on the experimental resolution. An example of such an exclusive photon distri-

photon energy	contributions to $d\sigma/dM_1^2 dM_2^2$			
	prod. + γ	W^+ decay + γ	W^- decay + γ	non-factorizable
hard	$ \mathcal{M}_0 ^2$ (54)	$\rightarrow 0$	$\rightarrow 0$	$\rightarrow 0$
semi-soft	$ \mathcal{M}_0 ^2$ (54)	$ \mathcal{I}_+^2 $ (56)	$ \mathcal{I}_-^2 $ (56)	interference (56)
soft	$ \mathcal{I}_0^2 $ (56)	$ \mathcal{I}_+^2 _{\text{soft}}$ (56)	$ \mathcal{I}_-^2 _{\text{soft}}$ (56)	soft interference (56)

Table 1: Formulae for the bremsstrahlung matrix elements for the distribution $d\sigma/dM_1^2 dM_2^2$.

bution is the photon-energy spectrum $d\sigma/dE_\gamma$. This distribution receives contributions from the three hard-photon terms in Eq. (54) as well as from the semi-soft interference terms of Eq. (56). The latter terms of course only contribute for photon energies that are not too hard.

In the next section results will be given for various distributions. For exclusive photons we present the photon-energy spectrum $d\sigma/dE_\gamma$. For the inclusive photon distributions we discuss in the following how the bremsstrahlung part is treated. Depending on the distribution, different approximations can be made.

As indicated above, the calculation of RC to distributions of the off-shell W -pair process (3) involves an integration over the photon phase space that is left available when fixing other kinematic variables. This means that the photon phase space for hard, semi-soft, and soft photons will in general be integrated over. The soft-photon part is standard and should be combined with the virtual corrections. How the non-soft part should be treated depends on the distribution one likes to study. In general one considers distributions of the form $d\sigma_{\text{DPA}}/dX$, where dX stands for $dM_1^2 dM_2^2$ and a product of solid angles for W -boson production and decay. For the following discussion it does not matter whether these solid angles are kept or integrated out. However, it does matter whether one wants a double distribution in M_1^2 and M_2^2 , a single distribution in M_1^2 , or no distribution in M_i^2 at all. In other words, the treatment differs depending on whether one integrates over M_i^2 or not.

Let us first discuss the procedure for the real-photon corrections to the double Breit–Wigner distribution $d\sigma/dM_1^2 dM_2^2$ in the vicinity of the peak, i.e. one is not interested in the tails of this peaked distribution. In Table 1 we specify which expressions are used in the different regimes for the photon energy. For this specification we use the positions of the Breit–Wigner poles as listed below Eq. (54).

The entries of Table 1 can be explained as follows. The real-photon corrections to the distribution $d\sigma/dM_1^2 dM_2^2$ come in the first place from the production part, where the hard-photon matrix element squared $|\mathcal{M}_0|^2$ contains the overall Breit–Wigner line shapes in M_1^2 and M_2^2 . This term should be taken from Eq. (54) and should be integrated over the photon phase space. In the soft-photon limit the usual soft-photon factorization in terms of $|\mathcal{I}_0^2|$ is obtained. This explains the second column in Table 1, where the usual RC to stable W -pair production appear, except that one now calculates the full density matrices rather than merely the trace.

photon energy	contributions to $d\sigma/dM_1^2$			
	prod. + γ	W^+ decay + γ	W^- decay + γ	non-factorizable
hard	$ \mathcal{M}_0 ^2$ (54)	$\rightarrow 0$	$ \mathcal{M}_- ^2$ (54)	$\rightarrow 0$
semi-soft	$ \mathcal{M}_0 ^2$ (54)	$ \mathcal{I}_+^2 $ (56)	$ \mathcal{M}_- ^2$ (54)	interference (56)
soft	$ \mathcal{I}_0^2 $ (56)	$ \mathcal{I}_+^2 _{\text{soft}}$ (56)	$ \mathcal{I}_-^2 _{\text{soft}}$ (56)	soft interference (56)

Table 2: Formulae for the bremsstrahlung matrix elements for the distribution $d\sigma/dM_1^2$.

The second type of contribution involves the W -boson decays with additional photon. When the photon is hard these contributions tend to zero as Γ_W^2/k_0^2 (see App. C), since they do not contain a double Breit–Wigner distribution in both M_1^2 and M_2^2 according to the list below Eq. (54). For (semi)soft photons, however, one gets overlapping Breit–Wigner resonances and the $|\mathcal{I}_\pm^2|$ terms of Eq. (56) can be used. These (semi)soft-photon factors have to be integrated while keeping D_i fixed, i.e. we keep the variables M_i^2 fixed. The corresponding integrals can be found in App. C. The integration over the semi-soft photon momenta leads to contributions from $M_{i\gamma}^2$ values that are higher than M_i^2 , resulting in a distortion of the original M_i^2 Breit–Wigner distribution. This final-state-radiation effect has been discussed recently in the literature and turns out to be quite sizeable [7]. The reason why the distortion is so large lies in the fact that the final-state collinear singularities [$\propto \frac{\alpha}{\pi} Q_f^2 \log(m_f^2/M_W^2)$] do not vanish, even not for fully inclusive photons. After all, a fixed value of M_i^2 makes it impossible to sum over all degenerate final states by a mere integration over the photon momentum.⁶ On top of that the IR poles $\propto 1/k$ induce a further enhancement of the collinear logarithms by a factor $\log(D_i/M_W^2)$.

So far we have included all factorizable corrections. To this one should add the non-factorizable corrections. Again effectively only the (semi)soft region is relevant. For more information on these non-factorizable corrections we refer to the detailed discussion in the literature [9, 10, 22].

As the next relevant distribution we discuss the real-photon corrections to the single Breit–Wigner distribution $d\sigma/dM_1^2$, obtained from the previous case by integrating over M_2^2 . To this end we make a similar table (Table 2) and discuss the necessary changes. Based on the discussion below Eq. (54), it is clear that a Breit–Wigner distribution in M_1^2 is present explicitly in $|\mathcal{M}_0|^2$ and $|\mathcal{M}_-|^2$, both for hard and semi-soft photons. These two terms should be taken from Eq. (54) and should be integrated over the photon phase space and M_2^2 . The $|\mathcal{M}_+|^2$ term does not have a Breit–Wigner distribution in M_1^2 as long as the photon is hard. Therefore it effectively only contributes in the (semi)soft regime, like in the previous case. Therefore the $|\mathcal{I}_+^2|$ term in Eq. (56) is used and the photon integration is performed while keeping M_1^2 fixed. The non-factorizable corrections contribute in the same way as described for the previous case.

We conclude by considering pure angular distributions. In this case the picture is simple.

⁶The usual cancellation of final-state collinear singularities is achieved only if also M_i^2 is integrated over.

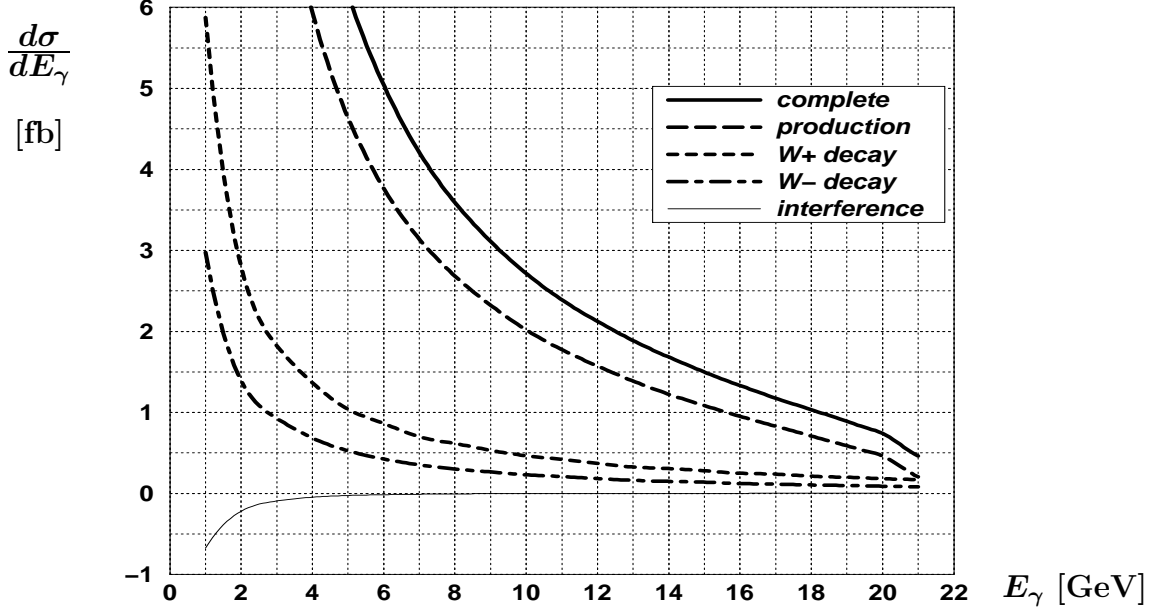


Figure 6: The photon-energy distribution $d\sigma/dE_\gamma$ for the $\mu^+\nu_\mu\tau^-\bar{\nu}_\tau\gamma$ final state at $2E = 184$ GeV. In addition the separate production and decay contributions are given.

All contributions should be taken from Eq. (54) and should be integrated over the photon phase space and the invariant masses M_i^2 . The non-factorizable corrections vanish in this situation, which is typical for these interference effects [21].

6 Numerical results

All the corrections discussed in the previous sections were combined into a Fortran program. In this section we present some numerical results. In particular we study the implications of the RC on various distributions. For the numerical evaluations we use the G_μ -parametrization (see Sect. 4) and the input parameters listed in Eqs. (31)–(35).

6.1 One-dimensional distributions

We start off by considering various one-dimensional distributions. Where applicable both the lowest-order distribution ($d\sigma_{\text{DPA}}^0$) and the corrected one ($d\sigma_{\text{DPA}}$) will be presented, followed by a separate plot for the relative correction factor δ_{DPA} [see Eq. (9)].

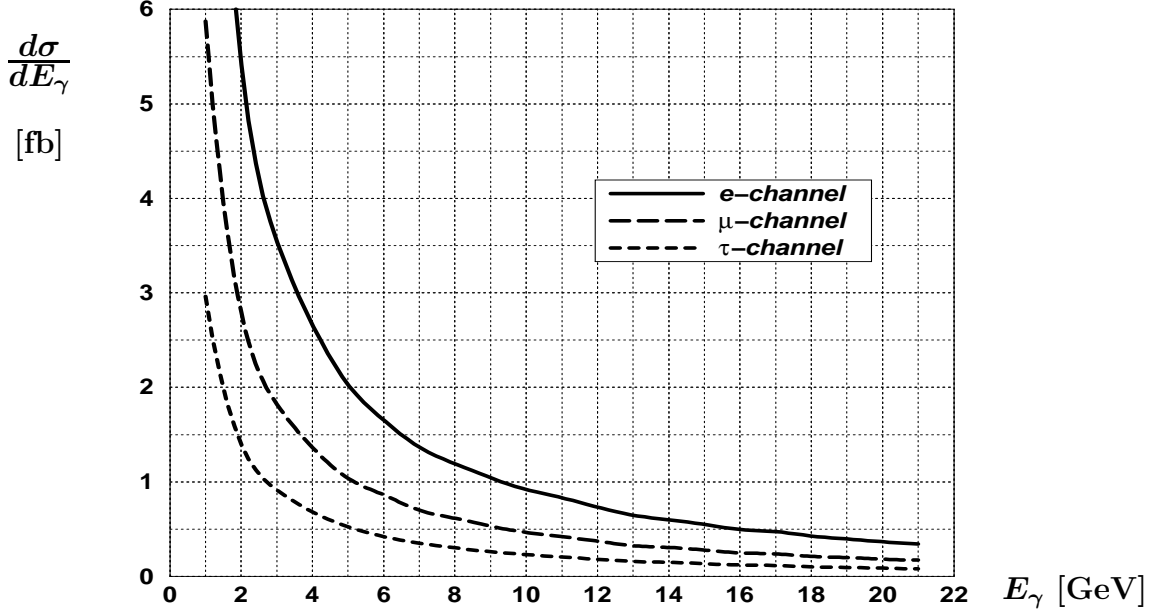


Figure 7: Decay contributions to the photon spectrum from different leptonic W decays.

6.1.1 The photon-energy spectrum

Since real-photon bremsstrahlung contributes to the RC to various distributions, it is useful to evaluate the photon-energy spectrum $d\sigma/dE_\gamma$ separately as well. In DPA it gets contributions from the three terms in Eq. (54) and the semi-soft interference terms of Eq. (56). The photon spectrum originating from the production stage is the same for all final states, but the spectra from the decay stages depend on the specific final state. In Fig. 6 the DPA photon-energy distribution $d\sigma/dE_\gamma$ is shown for the $\mu^+\nu_\mu\tau^-\bar{\nu}_\tau\gamma$ final state at $2E = 184$ GeV, together with the production and decay parts of the spectrum. In Fig. 7 we separately list the three possible leptonic radiative-decay contributions, originating from $W \rightarrow \ell\nu_\ell\gamma$ ($\ell = e, \mu, \tau$). The substantial differences are caused by the explicit fermion-mass dependence for collinear photon radiation (see App. B.4).

6.1.2 The total cross-section as a function of energy

In Fig. 8 we compare the total cross-section with and without RC for the $\mu^+\nu_\mu\tau^-\bar{\nu}_\tau$ final state. The corresponding relative correction factor δ is given in Fig. 9. As a check of our calculation we have verified that the corrected cross-section coincides within the integration errors with the corrected cross-section for stable W bosons multiplied by the corrected branching ratio $(\Gamma_{W \rightarrow \ell\nu_\ell}/\Gamma_W)^2$.

The observed RC are large and negative, especially close to the W -pair threshold. This is mainly caused by real-photon ISR, which effectively lowers the available W -pair energy,

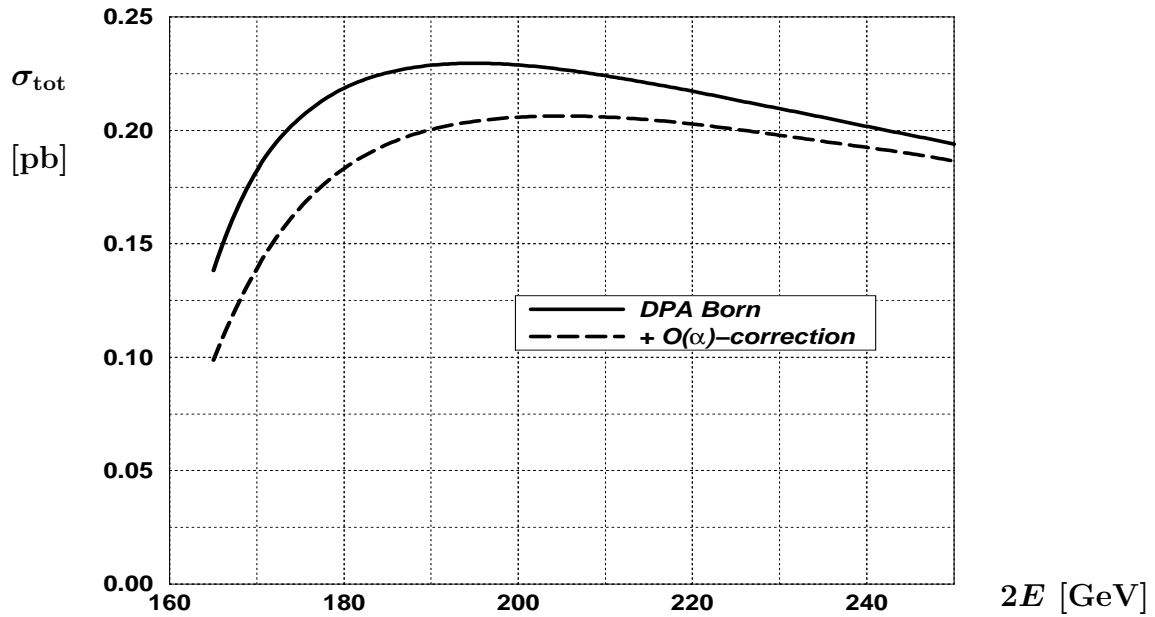


Figure 8: The energy dependence of the total cross-section σ_{tot} for the $\mu^+\nu_\mu\tau^-\bar{\nu}_\tau$ final state.

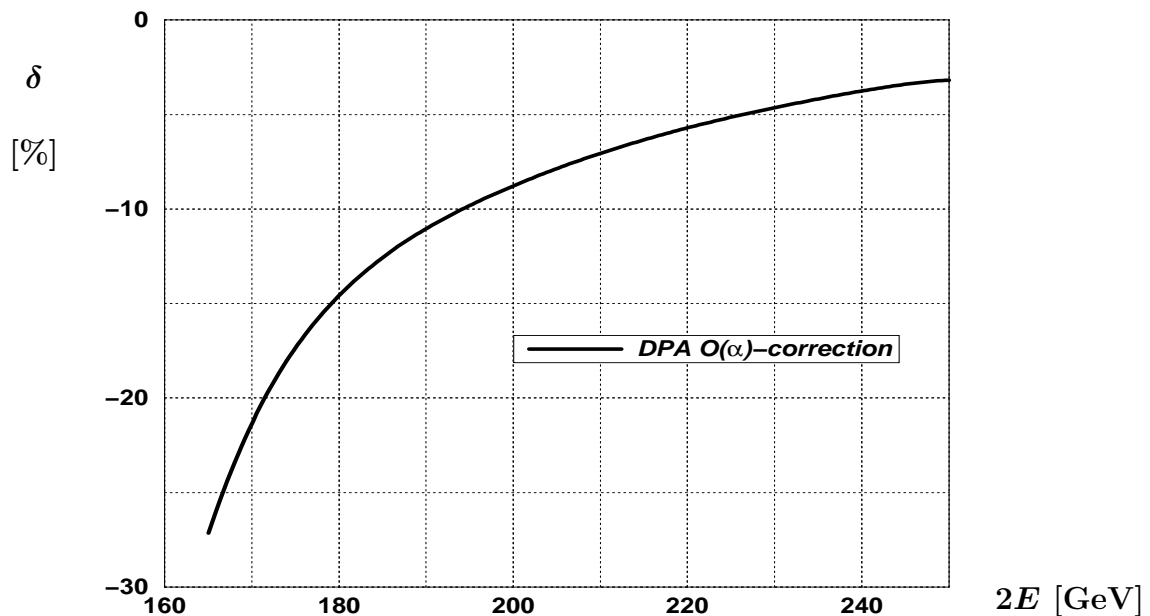


Figure 9: The relative correction factor corresponding to Fig. 8.

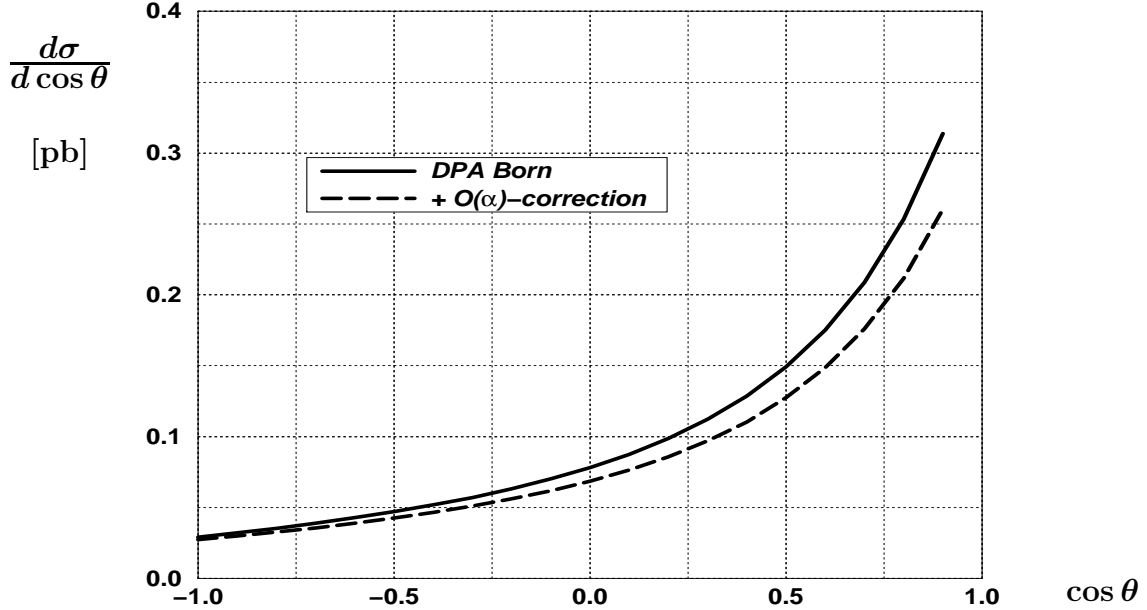


Figure 10: The production-angle distribution $d\sigma/d\cos\theta$ for the $\mu^+\nu_\mu\tau^-\bar{\nu}_\tau$ final state at $2E = 184$ GeV.

combined with the fact that near the W -pair threshold the cross-section is rapidly decreasing with decreasing energy.

6.1.3 Production-angle distribution

In Fig. 10 we plot the production-angle distribution $d\sigma/d\cos\theta$ for the $\mu^+\nu_\mu\tau^-\bar{\nu}_\tau$ final state at $2E = 184$ GeV. The relative correction factor displayed in Fig. 11 differs substantially from the -12.8% normalization effect that was observed for the total cross-section. In the forward direction it is slightly more negative, whereas in the backward direction it is substantially less negative. A proper understanding of this distortion is quite important, since non-standard triple gauge-boson couplings might lead to exactly this type of signature. The origin of the distortion can be traced back to hard-photon ISR. Such hard-photon emissions boost the centre-of-mass (CM) system of the W bosons, causing a migration of events to take place from regions with large cross-sections in the CM system (forward direction) to regions with small cross-sections in the LAB system (backward direction). The more peaked the distribution is, the stronger the boost effects will be.

6.1.4 Invariant-mass distribution

In Fig. 12 we compare the Breit–Wigner line shape $d\sigma/dM_1^2$ with and without RC for the $\mu^+\nu_\mu\tau^-\bar{\nu}_\tau$ final state at $2E = 184$ GeV. Since the corrected line shape receives completely different contributions from the production and decay stages, these parts are displayed separately.

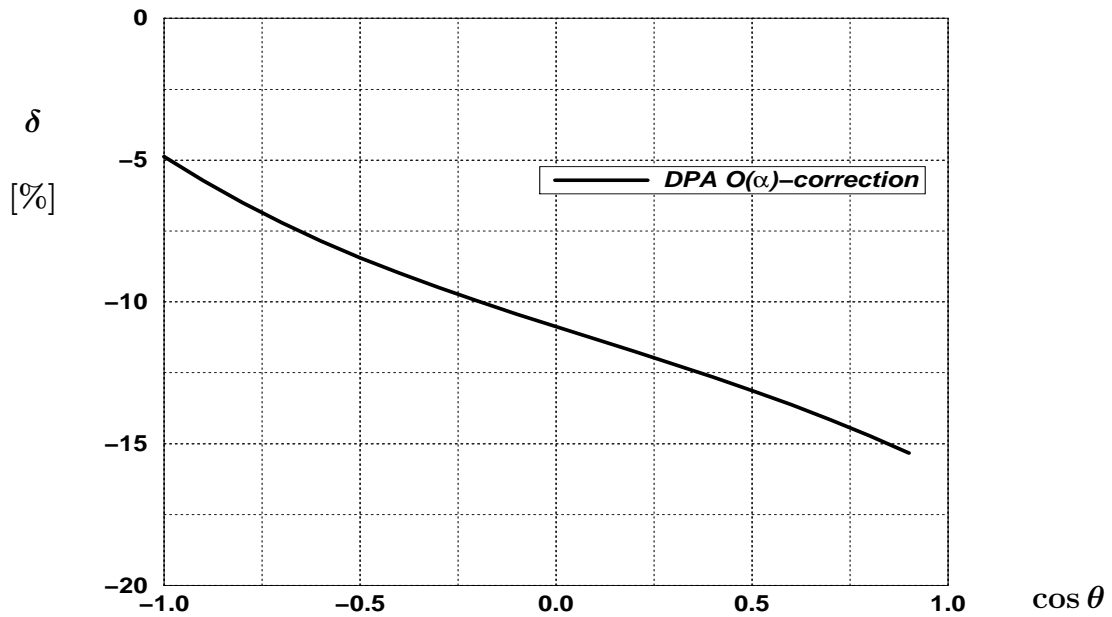


Figure 11: The relative correction factor corresponding to Fig. 10.

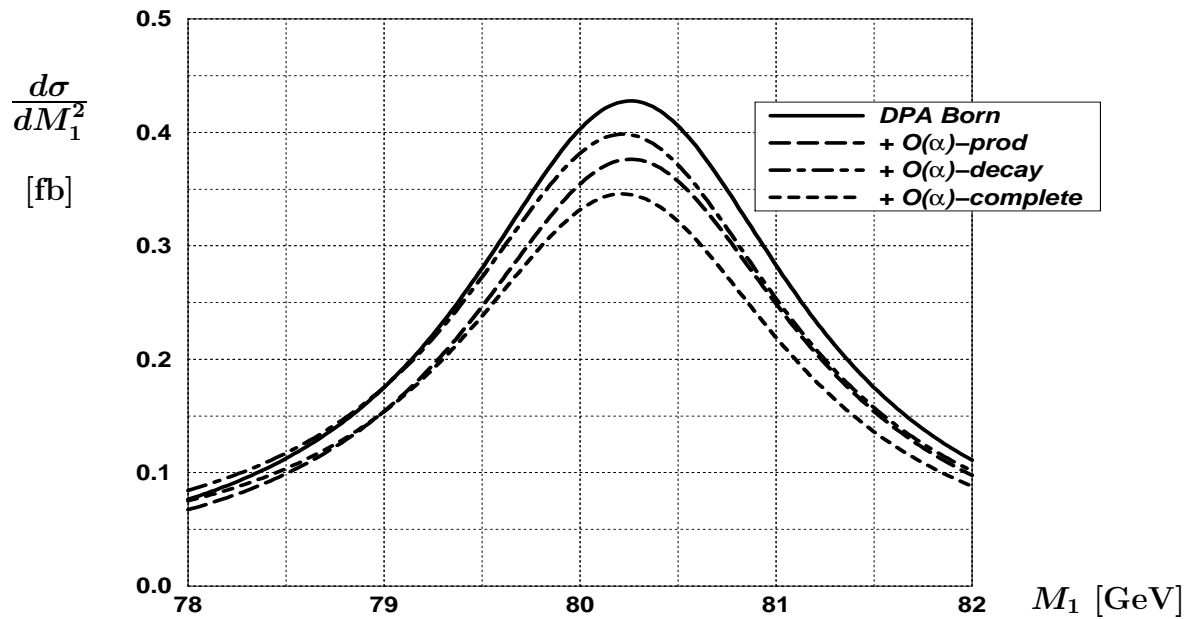


Figure 12: The invariant-mass distribution $d\sigma/dM_1^2$ for the $\mu^+\nu_\mu\tau^-\bar{\nu}_\tau$ final state at $2E = 184$ GeV.

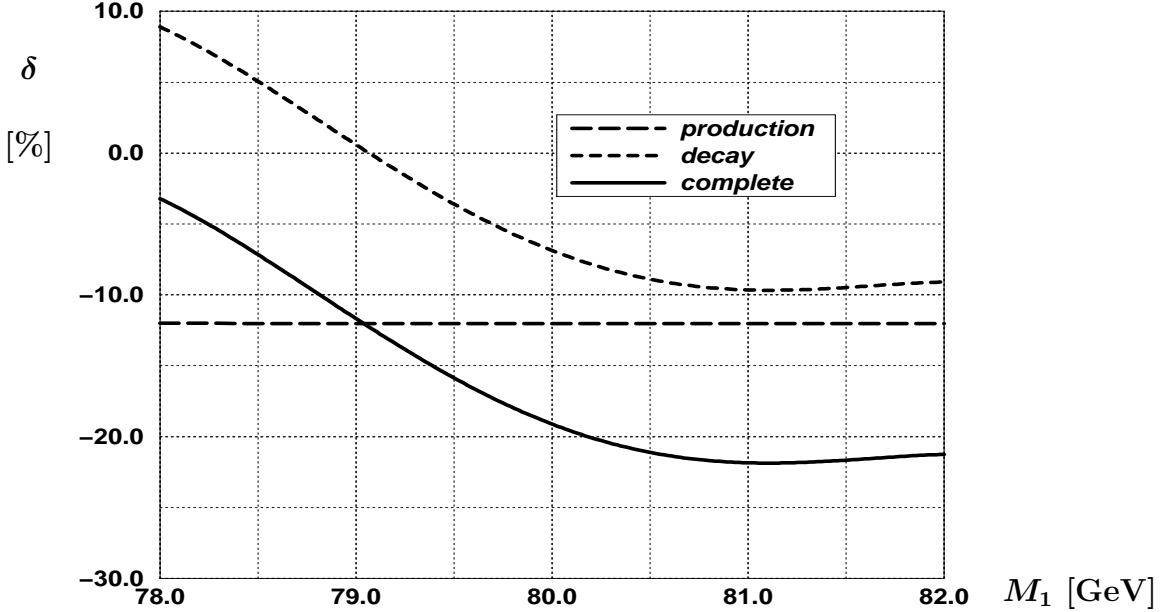


Figure 13: The relative correction factors δ corresponding to Fig. 12.

The corresponding relative correction factors are presented in Fig. 13.

The correction to the production stage leads to a constant reduction of the Breit–Wigner line shape. The corrections to the decay stages comprise the factorizable decay corrections (columns 3 and 4 in Table 2) and the non-factorizable corrections (column 5 in Table 2). The latter are very small [9, 10]. We see that also the decay corrections reduce the Breit–Wigner line shape. The amount of reduction depends on the particular final state, as can be seen from Figs. 14 and 15, where we consider different leptonic final states. The differences are caused by the explicit fermion-mass dependence for collinear photon radiation (see Apps. B.4 and C). For other final states, involving quarks, the reduction is determined by the masses and charges of the decay products of the W^+ boson (see App. C). Besides the reduction, the decay corrections also distort the resonance shape, as is clear from Fig. 13. This final-state-dependent FSR distortion effect has recently been discussed in the literature [7]. It can be quantified in terms of the shift in the peak position of the Breit–Wigner line shape, which we find to be -20 , -39 , and -77 MeV for W^+ -boson decays into $\tau^+\nu_\tau$, $\mu^+\nu_\mu$, and $e^+\nu_e$, respectively. This is in agreement with the (leading) shifts predicted by the W -boson version of Eq. (19) in Ref. [7], taking into account the fact that the correction to the production stage reduces the line shape by 12.0%. The observed shifts differ by -5 MeV to -10 MeV from these predictions as a result of the non-leading terms that are present in our full DPA calculation.

It should be stressed that theoretically the large distortion is a genuine effect. It would also be as relevant in practice if the invariant mass of the fermions could be measured. For various reasons this is problematic. One reason is the almost unavoidable inclusion of a collinear photon in the measured invariant mass. Such an inclusion would effectively decrease the leading logarithm $[\log(M_W^2/m_f^2)]$ that dominates the effect. What remains of the distortion in practice

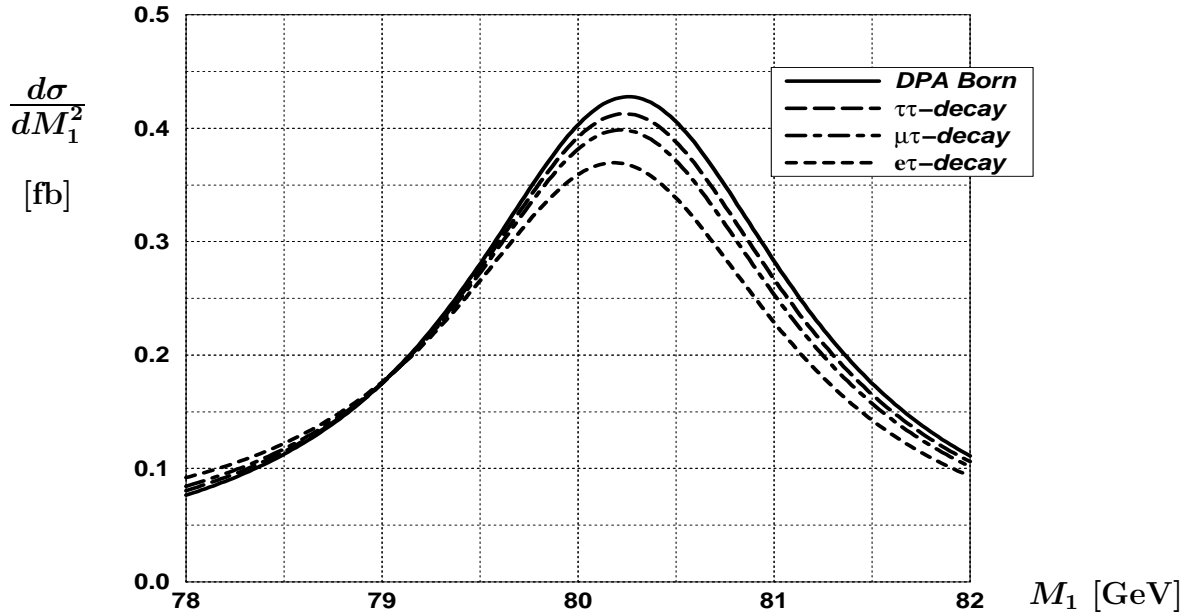


Figure 14: Distortion of the invariant-mass distribution $d\sigma/dM_1^2$ at $2E = 184$ GeV due to the decay corrections. Three leptonic final states are considered: $\tau^+\nu_\tau\tau^-\bar{\nu}_\tau$ ($\tau\tau$ -decay), $\mu^+\nu_\mu\tau^-\bar{\nu}_\tau$ ($\mu\tau$ -decay), and $e^+\nu_e\tau^-\bar{\nu}_\tau$ ($e\tau$ -decay).

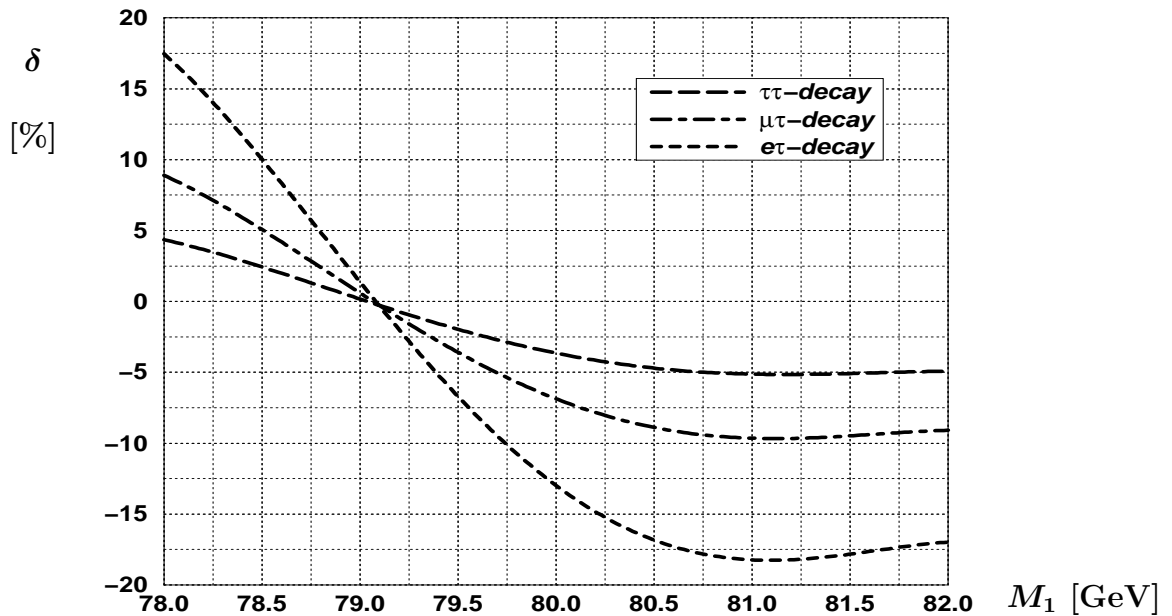


Figure 15: The relative correction factors δ corresponding to Fig. 14

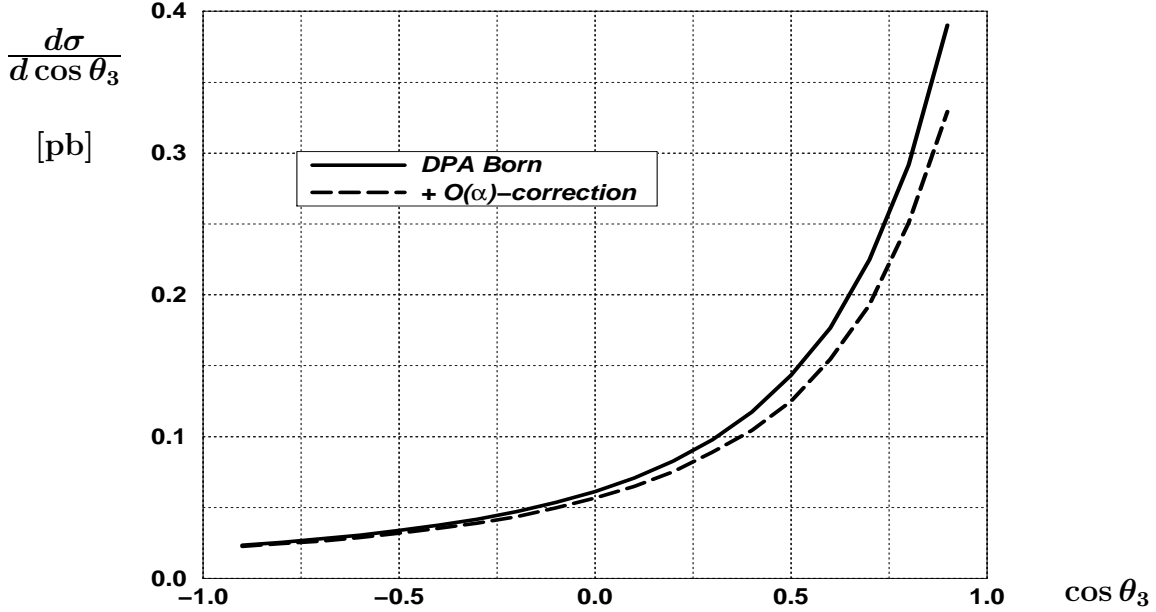


Figure 16: The decay-angle distribution $d\sigma/d\cos\theta_3$ for the $\mu^+\nu_\mu\tau^-\bar{\nu}_\tau$ final state at $2E = 184$ GeV. Here $\theta_3 = \angle(\mu^+, W^+)$ in the LAB frame.

should be studied with an event generator, which simulates the actual measurement.

6.1.5 Decay-angle distribution

In Figs. 16 and 17 the results are shown for the decay-angle distribution $d\sigma/d\cos\theta_3$ for the $\mu^+\nu_\mu\tau^-\bar{\nu}_\tau$ final state at $2E = 184$ GeV. Here θ_3 is the angle between the μ^+ and the W^+ boson in the LAB frame [see Eq. (22)]. The correction is negative and becomes more negative for forward angles. The shape of the relative correction factor is again the result of hard-photon boost effects.

6.2 Double invariant-mass distribution

Finally we consider the two-dimensional distribution $d\sigma/dM_1^2 dM_2^2$ at $2E = 184$ GeV, evaluated using the contributions specified in Table 1. Instead of plotting the absolute distributions, only the relative correction factors δ are presented. We do this for two specific leptonic final states. In Fig. 18 the $e^+\nu_e e^-\bar{\nu}_e$ final state is considered. This final state has the largest correction. Keeping one M_i^2 fixed, the correction to the other distribution is qualitatively the same as the correction to the one-dimensional distribution in Fig. 15. For the $e^+\nu_e\tau^-\bar{\nu}_\tau$ final state (Fig. 19) the correction is clearly not symmetric in the M_i^2 . This was to be expected, since the decay corrections for $e^+\nu_e$ and $\tau^-\bar{\nu}_\tau$ differ appreciably.

In Tables 3 and 4 we present some explicit values for the relative correction factor, split up

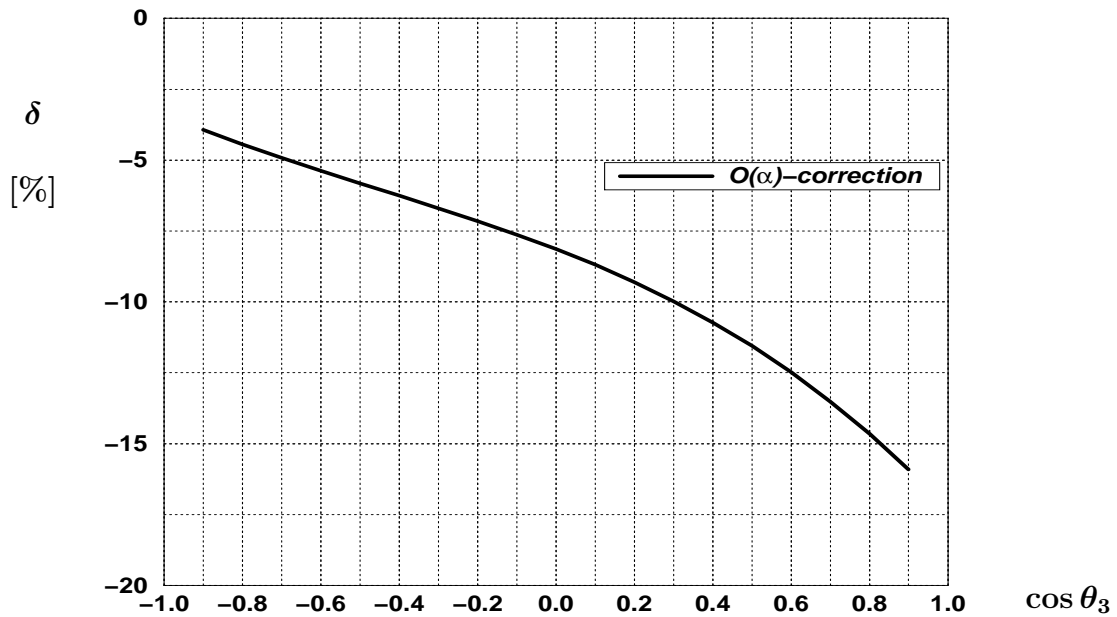


Figure 17: The relative correction factor δ corresponding to Fig. 16.

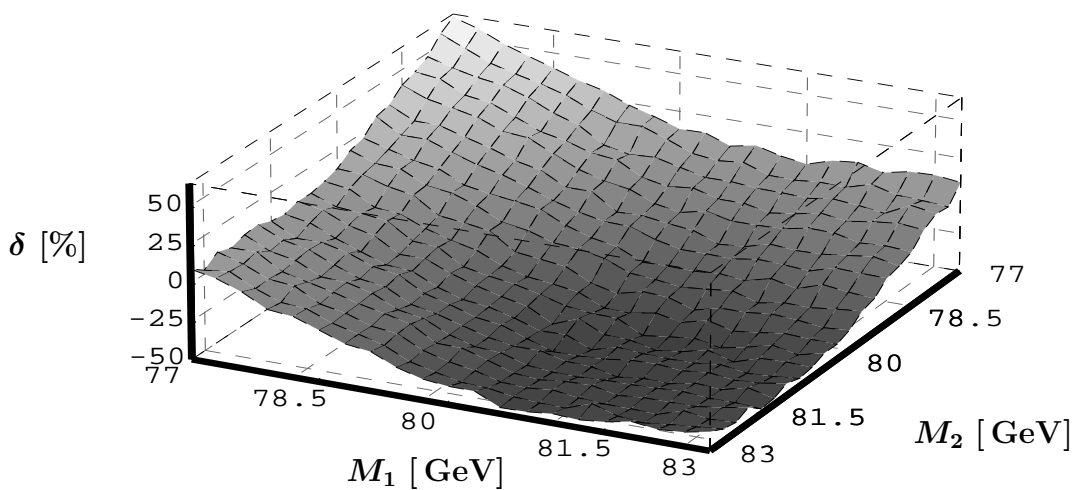


Figure 18: Correction to the double invariant-mass distribution $d\sigma/dM_1^2 dM_2^2$ for the $e^+ \nu_e e^- \bar{\nu}_e$ final state at $2E = 184$ GeV.

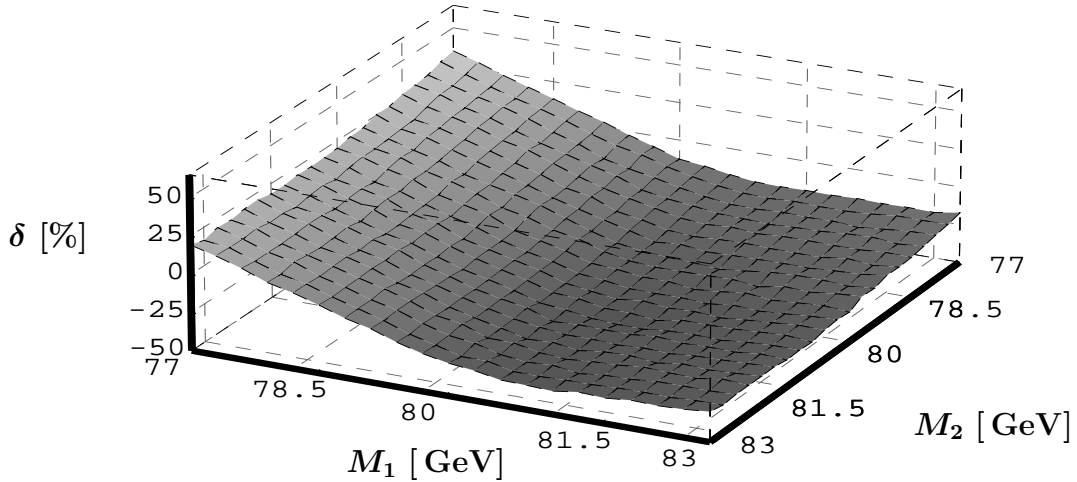


Figure 19: Correction to the double invariant-mass distribution $d\sigma/dM_1^2 dM_2^2$ for the $e^+\nu_e\tau^-\bar{\nu}_\tau$ final state at $2E = 184$ GeV.

Δ_1	decay channel			Δ_2
	$e^+\nu_e$	$\mu^+\nu_\mu$	$\tau^+\nu_\tau$	
-1/2	-1.4	-0.8	-0.5	-1/2
0	-15.0	-7.8	-4.0	0
1/2	-17.3	-9.0	-4.6	1/2

Δ_1	Δ_2		
	-1/2	0	1/2
-1/2	+0.5	+0.2	-0.1
0	+0.2	+0.0	-0.2
1/2	-0.1	-0.2	-0.4

$$\delta_{\text{dec}}^+(M_1)$$

$$\delta_{\text{nf}}(M_1, M_2)$$

Table 3: Relative correction factors [in %] for the double invariant-mass distribution $d\sigma/dM_1^2 dM_2^2$ at $2E = 184$ GeV. Left: the corrections from the W^+ -boson decay stage $\delta_{\text{dec}}^+(M_1)$ for different leptonic decay channels and three near-resonant invariant masses. Right: the non-factorizable corrections $\delta_{\text{nf}}(M_1, M_2)$.

Δ_1	Δ_2		
	-1/2	0	1/2
-1/2	-14.3	-28.2	-30.8
0	-28.2	-42.0	-44.5
1/2	-30.8	-44.5	-47.0

$e^+\nu_e e^-\bar{\nu}_e$ final state

Δ_1	Δ_2		
	-1/2	0	1/2
-1/2	-13.4	-17.2	-18.1
0	-27.3	-31.0	-31.8
1/2	-29.9	-33.5	-34.3

$e^+\nu_e \tau^-\bar{\nu}_\tau$ final state

Table 4: Relative correction factors [in %] for the double invariant-mass distribution $d\sigma/dM_1^2 dM_2^2$ at $2E = 184$ GeV. Left: the $e^+\nu_e e^-\bar{\nu}_e$ final state. Right: the $e^+\nu_e \tau^-\bar{\nu}_\tau$ final state.

into the separate contributions according to

$$\delta_{\text{DPA}}(M_1, M_2) = \delta_{\text{pr}} + \delta_{\text{dec}}^+(M_1) + \delta_{\text{dec}}^-(M_2) + \delta_{\text{nf}}(M_1, M_2).$$

The correction from the production stage is constant as a function of the invariant masses, $\delta_{\text{pr}} = -12.0\%$. The non-factorizable contribution $\delta_{\text{nf}}(M_1, M_2)$ is given in Table 3 for three near-resonant values for the invariant masses M_i . We indicate these three values by $\Delta_i = (M_i - M_W)/\Gamma_W = -1/2, 0, 1/2$. The non-factorizable corrections do not depend on the particular leptonic final state. The corrections $\delta_{\text{dec}}^\pm(M_i)$ from the decay stages do depend on the particular leptonic final state as explained before. In Table 3 we present these corrections for the three leptonic decay modes and the three near-resonant values for the invariant mass.

7 Discussion and conclusions

In this paper $\mathcal{O}(\alpha)$ radiative corrections (RC) to four-fermion production in e^+e^- collisions have been studied. The energy region chosen is that of LEP2, where the four-fermion final state is predominantly formed through intermediate W -pair production.

Since a complete $\mathcal{O}(\alpha)$ RC calculation for a two-particle to four-particle process is beyond present possibilities, a sensible approximation scheme has to be used. The smallness of Γ_W/M_W offers the possibility to use the double-pole approximation (DPA). In practice it means that we calculate $\mathcal{O}(\alpha)$ and $\mathcal{O}(\Gamma_W/M_W)$ corrections but neglect $\mathcal{O}(\alpha\Gamma_W/M_W)$ corrections. Although this approximation has been advocated in the literature for quite some time, so far no complete $\mathcal{O}(\alpha)$ results have been given. As far as we know, the study that has come closest to achieving a complete DPA calculation for an actual process involves the factorizable QCD corrections to the process $e^+e^- \rightarrow t\bar{t}$ [23]. Many of the issues discussed in the present paper have, however, not been addressed in Ref. [23].

We have applied the method to W -pair-mediated four-fermion production for a number of reasons. There is the methodological aspect of dealing with unstable particles in DPA, involving

issues like gauge invariance, interactions between different stages of the reaction, RC to density matrices, and the phase-space mappings. All of these issues play a role in the W -pair-mediated four-fermion production process. There is also the practical aspect of assessing how large $\mathcal{O}(\alpha)$ corrections can be for certain distributions. This is of importance for W -pair studies at LEP2.

On the methodological side, we have succeeded in finding a consistent prescription for applying the idea of the DPA. The kinematics for calculating the poles of the matrix elements is necessarily on-shell kinematics. Also the phase-space factor in the cross-section is treated in on-shell kinematics. The off-shell invariant masses occur only in the Breit–Wigner factors. All of this is well defined both for the radiative and non-radiative parts of the cross-section and therefore our calculation itself is unambiguous.

An unavoidable problem is the relation between off-shell four-fermion events and the on-shell calculated events. This question arises when one likes to connect experimental cross-sections to the calculated DPA cross-sections. Also here recipes are chosen both for the radiative and non-radiative phase-space points. For the latter the mapping is natural if one chooses the invariant masses $M_{1,2}$ and angles as variables. All off-shell points can be mapped onto on-shell points. For the radiative events in an off-shell phase space, the photon variables have to be added. A natural choice is the photon energy and angles. If the mapping is chosen such that the photon variables remain the same, one sometimes maps outside the on-shell phase space. Different remedies for this problem are possible. One can choose a procedure that assigns zero cross-sections to those points. On the other hand, the photon energy in the off-shell four-fermion–one-photon phase space may be rescaled in order to obtain a physical point in the on-shell phase space. In general, there will be a dependence on the chosen mapping between off-shell and on-shell phase spaces. However, the induced numerical differences remain within the accuracy of the calculation, i.e. $\mathcal{O}(\alpha\Gamma_W/M_W)$. At high energies, say above 2 TeV, when peaks in the cross-section become much more pronounced, a more sizeable implementation dependence may occur. The present calculation is primarily meant for LEP2 energies and slightly above, say up to 500 GeV.

On the practical side, the results give an insight in the size of RC for off-shell W -pair production. Within the claimed accuracy it is a complete calculation. It should be stated that imaginary parts of loop diagrams have been neglected in the expectation that they only induce small effects. Moreover, such terms are characterized by an explicit $\sin\phi_3$ and/or $\sin\phi_4$ dependence in the cross-section, since they select the antisymmetric parts of the \mathcal{D} -matrices. Integration over these azimuthal angles removes the imaginary parts of loop diagrams from the cross-section. So they do not contribute to the distributions of Sect. 6. It should also be stated that some large corrections (ISR, FSR), which usually require the inclusion of higher-order terms, are considered purely in first order here. The corresponding higher-order terms can be determined in a straightforward way within our approach, using the usual exponentiation/factorization techniques.

We have presented the results for leptonic final states. The reason is that those states are theoretically well defined. In exactly the same way also quark final states can be treated as long as one assumes certain masses for the quarks. It is this mass assignment which gives

some arbitrariness in the actual numbers. The RC presented are corrections to ideal theoretical situations, which cannot be realized experimentally in the same way. For that purpose the calculation should be implemented in an event generator. In principle this is possible. Events can be generated in the on-shell phase space with a radiatively corrected weight. The outside Breit–Wigner distributions can then generate the invariant masses and consequently off-shell events could be constructed from the on-shell ones (with certain angles kept fixed). Event generators offer the possibility to include realistic experimental cuts and therefore to study effects like the line-shape deformation in practical cases. The actual numbers presented here should give the reader an indication of the size of RC in ideal cases, of which remnants survive in practical situations.

For some questions the present study could already be useful in its present form. An example of this would be the comparison of a DPA Born cross-section with CP -conserving anomalous triple gauge-boson couplings and a normal DPA cross-section with RC. The question of how RC mimic anomalous couplings could be studied in this way, but goes beyond the size and scope of the present paper.

In conclusion, the DPA method for unstable-particle production has been shown to give reasonable results. It could also be applied to other unstable-particle production processes that undergo electroweak or QCD radiative corrections.

A Helicity amplitudes for the virtual factorizable corrections

In this appendix we give the basic ingredients for the calculation of the virtual factorizable corrections. The one-loop RC to on-shell W -pair production have been carried out in the literature in terms of helicity amplitudes with a particular choice for the decomposition into basic matrix elements and invariant functions [12]. This calculation serves as our basis for obtaining the RC to the production density matrix $\mathcal{P}_{[\lambda_1 \lambda_2][\lambda'_1 \lambda'_2]}(M_W, M_W)$, defined in Eq. (15). Therefore we will set up our conventions in close analogy to what has been used in the numerical routines of Ref. [12]. Once we have fixed the choice of polarization basis in the production stage, the same choice should be applied to the decay stages as well, i.e to $\mathcal{D}_{\lambda_i \lambda'_i}(M_W)$ in Eq. (16).

A.1 Virtual corrections to the production stage

The amplitude $\Pi_{\lambda_1 \lambda_2}(M_W, M_W)$ for on-shell W -pair production depends on the spinors of the initial-state e^\pm and on the polarization vectors $\varepsilon_i^\mu(p_i, \lambda_i)$ of the W bosons. In order to define the latter we first introduce

$$\begin{aligned} \varepsilon_{1,2}^\mu(p_{1,2}, ||) &= \frac{q_{1,2}^\mu(M_W^2 + u) - q_{2,1}^\mu(M_W^2 + t) + p_{1,2}^\mu(t - u)}{\sqrt{ut - M_W^4} \sqrt{s - 4M_W^2}}, \\ \varepsilon_i^\mu(p_i, \perp) &= -2 \frac{\epsilon^{\mu\nu\rho\tau} q_{2\nu} q_{1\rho} p_{i\tau}}{\sqrt{s(ut - M_W^4)}}, \\ \varepsilon_i^\mu(p_i, L) &= \frac{sp_i^\mu - 2M_W^2(q_1 + q_2)^\mu}{M_W \sqrt{s(s - 4M_W^2)}}, \end{aligned} \quad (58)$$

using the conventions defined in Sect. 3 and $\epsilon^{0123} = -1$. The helicity states, defined in the LAB frame, can be expressed in terms of the energy E and velocity $\beta = p/E = \sqrt{1 - M_W^2/E^2}$ of the W bosons in the following way:

$$\begin{aligned} \varepsilon_1^\mu(p_1, \pm 1) &= \frac{1}{\sqrt{2}} \left[\varepsilon_1^\mu(p_1, ||) \pm i \varepsilon_1^\mu(p_1, \perp) \right] = \frac{1}{\sqrt{2}} (0, -1, \pm i, 0), \\ \varepsilon_1^\mu(p_1, 0) &= \varepsilon_1^\mu(p_1, L) = \frac{E}{M_W} (\beta, 0, 0, 1), \\ \varepsilon_2^\mu(p_2, \pm 1) &= \frac{1}{\sqrt{2}} \left[\varepsilon_2^\mu(p_2, ||) \mp i \varepsilon_2^\mu(p_2, \perp) \right] = \frac{1}{\sqrt{2}} (0, 1, \pm i, 0), \\ \varepsilon_2^\mu(p_2, 0) &= \varepsilon_2^\mu(p_2, L) = \frac{E}{M_W} (\beta, 0, 0, -1). \end{aligned} \quad (59)$$

This polarization basis satisfies the usual identities

$$p_i^\mu \varepsilon_{i,\mu}(p_i, \lambda_i) = 0, \quad \varepsilon_i^\mu(p_i, \lambda_i) \varepsilon_{i,\mu}^*(p_i, \lambda'_i) = -\delta_{\lambda_i \lambda'_i}. \quad (60)$$

In its most general form, the amplitude $\Pi_{\lambda_1\lambda_2}(M_W, M_W)$ can be written as a sum of invariant functions $\mathcal{C}_j(\sigma)$ multiplied by Lorentz-invariant basic matrix elements $\mathcal{M}_j^\sigma(\lambda_1, \lambda_2)$. The basic matrix elements are simple, purely kinematical objects and contain the complete dependence on the W -boson polarizations. The invariant functions contain the dynamical information, i.e. details of the model, but are independent of the W -boson polarizations. Both parts depend on the helicity of the electron, $\lambda_{e^-} \equiv \sigma/2$ ($\sigma = \pm 1$). In view of our massless treatment of the e^\pm , the helicity of the positron is fixed to $\lambda_{e^+} = -\lambda_{e^-}$ in the virtual corrections. For a specific helicity of the electron the decomposition of the helicity amplitudes reads

$$\Pi_{\sigma;\lambda_1\lambda_2}(M_W, M_W) = \sum_{j=1}^9 \mathcal{C}_j(\sigma) \mathcal{M}_j^\sigma(\lambda_1, \lambda_2), \quad (61)$$

with

$$\begin{aligned} \mathcal{M}_1^\sigma(\lambda_1, \lambda_2) &= \left[\bar{v}(q_1) \not{p}_1 \omega_\sigma u(q_2) \right] (\varepsilon_1 \varepsilon_2), \\ \mathcal{M}_2^\sigma(\lambda_1, \lambda_2) &= \left[\bar{v}(q_1) \not{p}_1 \omega_\sigma u(q_2) \right] (p_1 \varepsilon_2) (p_2 \varepsilon_1), \\ \mathcal{M}_3^\sigma(\lambda_1, \lambda_2) &= \bar{v}(q_1) \left[\not{p}_1 (p_1 \varepsilon_2) - \not{p}_2 (p_2 \varepsilon_1) \right] \omega_\sigma u(q_2), \\ \mathcal{M}_4^\sigma(\lambda_1, \lambda_2) &= \bar{v}(q_1) \not{p}_1 (\not{p}_1 - \not{p}_2) \not{p}_2 \omega_\sigma u(q_2), \\ \mathcal{M}_5^\sigma(\lambda_1, \lambda_2) &= \bar{v}(q_1) \left[\not{p}_1 (q_1 \varepsilon_2) - \not{p}_2 (q_2 \varepsilon_1) \right] \omega_\sigma u(q_2), \\ \mathcal{M}_6^\sigma(\lambda_1, \lambda_2) &= \left[\bar{v}(q_1) \not{p}_1 \omega_\sigma u(q_2) \right] (q_1 \varepsilon_2) (q_2 \varepsilon_1), \\ \mathcal{M}_7^\sigma(\lambda_1, \lambda_2) &= \left[\bar{v}(q_1) \not{p}_1 \omega_\sigma u(q_2) \right] [(p_1 \varepsilon_2) (q_2 \varepsilon_1) + (p_2 \varepsilon_1) (q_1 \varepsilon_2)], \\ \mathcal{M}_8^\sigma(\lambda_1, \lambda_2) &= i \left[\bar{v}(q_1) \gamma^\mu \omega_\sigma u(q_2) \right] \epsilon_{\mu\nu\rho\tau} \varepsilon_2^\nu \varepsilon_1^\rho (p_1 - p_2)^\tau, \\ \mathcal{M}_9^\sigma(\lambda_1, \lambda_2) &= i \left[\bar{v}(q_1) \gamma^\mu \omega_\sigma u(q_2) \right] \epsilon_{\mu\nu\rho\tau} p_2^\nu p_1^\rho [\varepsilon_1^\tau (p_1 \varepsilon_2) - \varepsilon_2^\tau (p_2 \varepsilon_1)]. \end{aligned} \quad (62)$$

The helicity projectors

$$\omega_\sigma = \frac{1 + \sigma \gamma_5}{2}, \quad (63)$$

with $\gamma_5 = i\gamma^0\gamma^1\gamma^2\gamma^3$, project on right- and left-handed massless fermions. Note that our set of 18 basic matrix elements \mathcal{M}_j^σ is overcomplete. Because of the massless treatment of the fermions, CP invariance implies the relation⁷

$$\mathcal{M}_j^\sigma(\lambda_1, \lambda_2) = \mathcal{M}_j^\sigma(-\lambda_2, -\lambda_1), \quad (64)$$

resulting in only 12 independent matrix elements. The last three pairs, $\mathcal{M}_{7,8,9}^\sigma$, have been kept for convenience and can be expressed in terms of the others according to

$$\mathcal{M}_7^\sigma = \frac{s}{4} \sigma \mathcal{M}_8^\sigma + \mathcal{M}_2^\sigma + \frac{t-u}{4} \mathcal{M}_3^\sigma, \quad \mathcal{M}_9^\sigma = -\frac{s}{2} \mathcal{M}_8^\sigma, \quad \sigma \mathcal{M}_8^\sigma = 2(\mathcal{M}_1^\sigma + \mathcal{M}_4^\sigma + \mathcal{M}_5^\sigma) - 3\mathcal{M}_3^\sigma. \quad (65)$$

⁷We have fixed the overall phase of the matrix elements such that this relation holds. The density matrix will of course not be affected by this choice.

For the lowest-order matrix element only a few of these basic matrix elements are relevant:

$$\Pi_{\sigma; \lambda_1 \lambda_2}^0(M_W, M_W) = \delta_{(\sigma, -1)} G_1(t) \mathcal{M}_4^\sigma(\lambda_1, \lambda_2) + 2 G_2(s, \sigma) [\mathcal{M}_3^\sigma(\lambda_1, \lambda_2) - \mathcal{M}_1^\sigma(\lambda_1, \lambda_2)], \quad (66)$$

where the coefficients $G_{1,2}$ are defined as

$$G_1(t) = -\frac{ie^2}{2s_W^2} \frac{1}{t}, \quad G_2(s, \sigma) = ie^2 \left(\frac{Q_e}{s} + \frac{c_W}{s_W} \frac{g_e(\sigma)}{s - M_Z^2} \right). \quad (67)$$

Here s_W and c_W are the sine and cosine of the weak mixing angle θ_W :

$$c_W = \cos \theta_W = \frac{M_W}{M_Z}, \quad s_W = \sin \theta_W = \sqrt{1 - c_W^2}, \quad (68)$$

and $g_e(\sigma)$ denotes the coupling between the Z boson and electrons:

$$g_e(+1) = -\frac{s_W}{c_W} Q_e, \quad g_e(-1) = -\frac{1 + 2Q_e s_W^2}{2s_W c_W}, \quad (69)$$

where $Q_e = -1$ is the charge of the electron.

For the virtual corrections to on-shell W -pair production we need the complete list of basic matrix elements \mathcal{M}_j^σ . For the W -boson helicity states (59) the non-vanishing matrix elements read:

$$\begin{aligned} \mathcal{M}_4^\sigma(\pm 1, \mp 1) &= 2E^2(\cos \theta \mp \sigma) \sin \theta \\ \mathcal{M}_5^\sigma(\pm 1, \mp 1) &= -2E^2(\cos \theta \mp \sigma) \sin \theta \\ \mathcal{M}_6^\sigma(\pm 1, \mp 1) &= E^4 \beta \sin^3 \theta \end{aligned} \quad (70)$$

$$\begin{aligned} \mathcal{M}_1^\sigma(\pm 1, \pm 1) &= 2E^2 \beta \sin \theta \\ \mathcal{M}_4^\sigma(\pm 1, \pm 1) &= 2E^2(\cos \theta - \beta) \sin \theta \\ \mathcal{M}_5^\sigma(\pm 1, \pm 1) &= -2E^2 \cos \theta \sin \theta \\ \mathcal{M}_6^\sigma(\pm 1, \pm 1) &= E^4 \beta \sin^3 \theta \end{aligned} \quad (71)$$

$$\begin{aligned} \mathcal{M}_3^\sigma(\pm 1, 0) &= \mathcal{M}_3^\sigma(0, \mp 1) = \frac{\sqrt{2}E}{M_W} 2E^2 \beta (\cos \theta \mp \sigma) \\ \mathcal{M}_4^\sigma(\pm 1, 0) &= \mathcal{M}_4^\sigma(0, \mp 1) = \frac{\sqrt{2}E}{M_W} E^2 [2\beta - 2 \cos \theta \mp \sigma(1 - \beta^2)] (\cos \theta \mp \sigma) \\ \mathcal{M}_5^\sigma(\pm 1, 0) &= \mathcal{M}_5^\sigma(0, \mp 1) = \frac{\sqrt{2}E}{M_W} E^2 (\beta + 2 \cos \theta \pm \sigma) (\cos \theta \mp \sigma) \\ \mathcal{M}_6^\sigma(\pm 1, 0) &= \mathcal{M}_6^\sigma(0, \mp 1) = -\frac{\sqrt{2}E}{M_W} E^4 \beta (\beta + \cos \theta) \sin^2 \theta \\ \mathcal{M}_7^\sigma(\pm 1, 0) &= \mathcal{M}_7^\sigma(0, \mp 1) = -\frac{\sqrt{2}E}{M_W} 2E^4 \beta^2 \sin^2 \theta \\ \mathcal{M}_8^\sigma(\pm 1, 0) &= \mathcal{M}_8^\sigma(0, \mp 1) = \pm \frac{\sqrt{2}E}{M_W} 2E^2 \beta^2 (\cos \theta \mp \sigma) \end{aligned}$$

$$\mathcal{M}_9^\sigma(\pm 1, 0) = \mathcal{M}_9^\sigma(0, \mp 1) = \mp \frac{\sqrt{2}E}{M_W} 4E^4\beta^2(\cos\theta \mp \sigma) \quad (72)$$

$$\begin{aligned} \mathcal{M}_1^\sigma(0, 0) &= \frac{E^2}{M_W^2} 2E^2\beta(1 + \beta^2)\sin\theta \\ \mathcal{M}_2^\sigma(0, 0) &= \frac{E^2}{M_W^2} 8E^4\beta^3\sin\theta \\ \mathcal{M}_3^\sigma(0, 0) &= \frac{E^2}{M_W^2} 8E^2\beta\sin\theta \\ \mathcal{M}_4^\sigma(0, 0) &= \frac{E^2}{M_W^2} 2E^2[3\beta - \beta^3 - 2\cos\theta]\sin\theta \\ \mathcal{M}_5^\sigma(0, 0) &= \frac{E^2}{M_W^2} 4E^2(\beta + \cos\theta)\sin\theta \\ \mathcal{M}_6^\sigma(0, 0) &= \frac{E^2}{M_W^2} 2E^4\beta(\beta + \cos\theta)^2\sin\theta \\ \mathcal{M}_7^\sigma(0, 0) &= \frac{E^2}{M_W^2} 8E^4\beta^2(\beta + \cos\theta)\sin\theta. \end{aligned} \quad (73)$$

From this list and the invariant functions of Ref. [12] the density matrix $\mathcal{P}_{[\lambda_1\lambda_2][\lambda'_1\lambda'_2]}(M_W, M_W)$ follows in a straightforward way.

A.2 Virtual corrections to the decay stages

Since we have chosen a specific polarization basis for the calculation of the production stage, both at lowest order and at virtual one-loop order, the same basis has to be used for describing the on-shell W -boson decays. All results presented in this subsection are therefore given in the LAB frame, rather than the often used rest frame of the decaying W boson.

Like in the on-shell W -pair-production case, we again write the decay matrix element as a sum of invariant functions $\mathcal{E}_j^{(\pm)}$ multiplied by Lorentz-invariant basic matrix elements $\mathcal{M}_j^{(\pm)}(\lambda_i)$:

$$\Delta_{\lambda_1}^{(+)}(M_W) = \sum_j \mathcal{E}_j^{(+)} \mathcal{M}_j^{(+)}(\lambda_1), \quad \Delta_{\lambda_2}^{(-)}(M_W) = \sum_j \mathcal{E}_j^{(-)} \mathcal{M}_j^{(-)}(\lambda_2). \quad (74)$$

In the most general case of the decay of a W boson into massive quarks, there are four basic matrix elements [15]. For the decay of the W^- boson, $W^-(p_2) \rightarrow f_2(k_2)\bar{f}'_2(k'_2)$, they are given by

$$\begin{aligned} \mathcal{M}_0^{(-)}(\lambda_2) &= \bar{u}(k_2) \not{\epsilon}_2^* \omega_- v(k'_2), \\ \mathcal{M}_1^{(-)}(\lambda_2) &= \bar{u}(k_2) \not{\epsilon}_2^* \omega_+ v(k'_2), \\ \mathcal{M}_2^{(-)}(\lambda_2) &= [\bar{u}(k_2) \omega_- v(k'_2)](\varepsilon_2^* k_2), \\ \mathcal{M}_3^{(-)}(\lambda_2) &= [\bar{u}(k_2) \omega_+ v(k'_2)](\varepsilon_2^* k_2), \end{aligned} \quad (75)$$

with similar expressions for the decay of the W^+ boson. For massless particles in the final state only $\mathcal{M}_0^{(\pm)}$ occurs. At lowest-order we then obtain

$$\Delta_{\lambda_i}^0(M_W) = \frac{ieV_{f'_i f_i}}{\sqrt{2}s_W} \mathcal{M}_0^{(\pm)}(\lambda_i), \quad (76)$$

with $V_{f' f}$ the quark mixing matrix.

For the decay density matrix $\mathcal{D}_{\lambda_i \lambda'_i}(M_W)$ it is useful to have the expressions for

$$\mathcal{M}_{00}^{(\pm)}(\lambda_i, \lambda'_i) = \sum_{\text{fermion helicities}} \mathcal{M}_0^{(\pm)}(\lambda_i) \mathcal{M}_0^{(\pm)*}(\lambda'_i). \quad (77)$$

For the decay of the W^- boson one finds

$$\begin{aligned} \mathcal{M}_{00}^{(-)}(0, 0) &= \frac{M_W^4}{E^2} \frac{\sin^2 \theta_4}{(1 - \beta \cos \theta_4)^2}, \\ \mathcal{M}_{00}^{(-)}(\pm 1, \pm 1) &= \frac{M_W^2}{2} (1 \pm \beta)^2 \frac{(1 \mp \cos \theta_4)^2}{(1 - \beta \cos \theta_4)^2}, \\ \mathcal{M}_{00}^{(-)}(\pm 1, 0) &= \pm \frac{M_W^3}{\sqrt{2}E} (1 \pm \beta) e^{\mp i\phi_4} \frac{(1 \mp \cos \theta_4) \sin \theta_4}{(1 - \beta \cos \theta_4)^2}, \\ \mathcal{M}_{00}^{(-)}(0, \pm 1) &= \pm \frac{M_W^3}{\sqrt{2}E} (1 \pm \beta) e^{\pm i\phi_4} \frac{(1 \mp \cos \theta_4) \sin \theta_4}{(1 - \beta \cos \theta_4)^2}, \\ \mathcal{M}_{00}^{(-)}(\pm 1, \mp 1) &= - \frac{M_W^4}{2E^2} e^{\mp 2i\phi_4} \frac{\sin^2 \theta_4}{(1 - \beta \cos \theta_4)^2}. \end{aligned} \quad (78)$$

The expressions for the charge-conjugate process, describing the decay of the W^+ boson, can be obtained through the simple relation

$$\mathcal{M}_{00}^{(+)}(\lambda_1, \lambda'_1) = \mathcal{M}_{00}^{(-)}(-\lambda_1, -\lambda'_1), \quad \text{with } \phi_4 \rightarrow \phi_3, \cos \theta_4 \rightarrow \cos \theta_3, \sin \theta_4 \rightarrow -\sin \theta_3. \quad (79)$$

These expressions can be combined with the invariant functions from Ref. [15] to obtain the decay density matrices including virtual RC. It can be seen from Eq. (78) that the matrices $\mathcal{M}_{00}^{(\pm)}(\lambda_i, \lambda'_i)$ contain asymmetric imaginary parts proportional to $\sin \phi_{3,4}$. These terms will be responsible for picking up imaginary loop effects present in the invariant functions, which do not depend on $\phi_{3,4}$. The symmetric parts of $\mathcal{M}_{00}^{(\pm)}(\lambda_i, \lambda'_i)$ are real and depend on $\cos \phi_{3,4}$. Upon integration over the azimuthal angles $\phi_{3,4}$ the matrices $\mathcal{M}_{00}^{(\pm)}(\lambda_i, \lambda'_i)$ become real and diagonal, and the same holds for the corresponding decay density matrices.

B The Weyl–van der Waerden formalism for the real-photon factorizable corrections

Like in the case of the virtual factorizable corrections, also for the real-photon factorizable corrections our choice for the polarization basis and the calculational scheme is guided by existing

calculations in the literature. As mentioned in Sect. 3, there is no objection against having different choices for the polarization basis in different contributions to the RC, provided that the contribution to the density matrix is calculated consistently within the chosen approach. We adopt the conventions of Ref. [14] and calculate the real-photon RC in the Weyl–van der Waerden formalism.

B.1 The Weyl–van der Waerden formalism for massive gauge bosons

Before giving the results for the various matrix elements, we first give a few essential details of the Weyl–van der Waerden formalism for massive gauge bosons. We follow the conventions of Ref. [14] and define the two-dimensional Weyl spinor for a massless particle with light-like momentum q as

$$q_A = \begin{pmatrix} \sqrt{q_0 - q_3} \\ -(q_1 + iq_2)/\sqrt{q_0 - q_3} \end{pmatrix}, \quad q_{\dot{A}} = (q_A)^*. \quad (80)$$

The indices can be raised and lowered by the spinor metric

$$\epsilon^{AB} = \begin{pmatrix} 0 & 1 \\ -1 & 0 \end{pmatrix} = \epsilon_{AB} = \epsilon^{\dot{A}\dot{B}} = \epsilon_{\dot{A}\dot{B}} \quad (81)$$

according to

$$q^A = q_B \epsilon^{BA}, \quad q_A = \epsilon_{AB} q^B. \quad (82)$$

The spinor products

$$\langle qk \rangle = q_A k^A = -q^A k_A, \quad \langle qk \rangle^* = q_{\dot{A}} k^{\dot{A}} = -q^{\dot{A}} k_{\dot{A}} \quad (83)$$

are hence antisymmetric. In the Weyl representation for the γ -matrices we obtain the following set of translation rules into two-dimensional spinor language:

$$\begin{aligned} u(q, +) &= v(q, -) = \begin{pmatrix} q_A \\ 0 \end{pmatrix}, \\ u(q, -) &= v(q, +) = \begin{pmatrix} 0 \\ q^{\dot{A}} \end{pmatrix}, \\ \gamma^\mu &= \begin{pmatrix} 0 & \sigma_{\dot{B}A}^\mu \\ \sigma^{\mu\dot{A}B} & 0 \end{pmatrix}, \\ Q_\mu \sigma_{\dot{A}B}^\mu &= Q_{\dot{A}B} \quad \Rightarrow \quad 2QK = Q^{\dot{A}B} K_{\dot{A}B}, \\ q_\mu \sigma_{\dot{A}B}^\mu &= q_{\dot{A}B} = q_{\dot{A}} q_B \quad \Rightarrow \quad 2qk = |\langle qk \rangle|^2, \end{aligned} \quad (84)$$

with Q, K arbitrary Lorentz vectors and q, k light-like ones. The Dirac spinors $u(q, \pm)$ denote right-handed (+) and left-handed (−) states. The matrices $\sigma^{\mu\dot{A}B} = (\sigma^0, \vec{\sigma})$ consist of the 2×2 unit matrix σ^0 and the standard Pauli matrices σ^i ($i = 1, 2, 3$).

For a photon with momentum k we use the polarization vectors describing the two helicity eigenstates

$$\varepsilon_{\gamma}^{\dot{A}B}(+1) = \sqrt{2} \frac{k^{\dot{A}} b^B}{\langle kb \rangle}, \quad \varepsilon_{\gamma}^{\dot{A}B}(-1) = \sqrt{2} \frac{b^{\dot{A}} k^B}{\langle kb \rangle^*} = \varepsilon_{\gamma}^{\dagger \dot{A}B}(+1). \quad (85)$$

To handle the massive W^{\pm} bosons we first decompose their massive momenta $p_{1,2}$ into a sum of two light-like momenta:

$$p_{1,2}^{\mu} = p_{3,4}^{\mu} + c_{1,2} m_{3,4}^{\mu}, \quad c_1 (2p_3 m_3) = c_2 (2p_4 m_4) = M_W^2. \quad (86)$$

Note that the so-defined light-like vectors $m_{3,4}$ can be chosen freely. An orthogonal basis for the three physical polarizations of the massive W^{\pm} bosons is now given by

$$\begin{aligned} \varepsilon_1^{\dot{A}B}(+1) &= \sqrt{2} \frac{p_3^{\dot{A}} m_3^B}{\langle p_3 m_3 \rangle}, & \varepsilon_1^{\dot{A}B}(-1) &= \sqrt{2} \frac{m_3^{\dot{A}} p_3^B}{\langle p_3 m_3 \rangle^*}, & \varepsilon_1^{\dot{A}B}(0) &= \frac{1}{M_W} (p_3 - c_1 m_3)^{\dot{A}B}, \\ \varepsilon_2^{\dot{A}B}(+1) &= \sqrt{2} \frac{p_4^{\dot{A}} m_4^B}{\langle p_4 m_4 \rangle}, & \varepsilon_2^{\dot{A}B}(-1) &= \sqrt{2} \frac{m_4^{\dot{A}} p_4^B}{\langle p_4 m_4 \rangle^*}, & \varepsilon_2^{\dot{A}B}(0) &= \frac{1}{M_W} (p_4 - c_2 m_4)^{\dot{A}B}, \end{aligned} \quad (87)$$

with $\varepsilon_i^{\dot{A}B}(-1) = \varepsilon_i^{\dagger \dot{A}B}(+1)$. It should be stressed that the so-obtained polarization basis does not correspond to the helicity eigenstates. However, the corresponding states transform like helicity eigenstates under a parity transformation, which is very useful for practical calculations.

B.1.1 An example: lowest-order on-shell W-pair production

As an example we apply the above method to the lowest-order on-shell production stage. To this end we choose $m_{3,4} = p_{4,3}$ in Eqs. (86) and (87), and write $c_1 = c_2 = M_W^2 / (2p_3 p_4) \equiv c$.

The complete Born amplitude of the process is of the form

$$\Pi_{\sigma; \lambda_1 \lambda_2}^0(M_W, M_W) = G_1(t) \mathcal{M}_t(\sigma, \lambda_1, \lambda_2) + G_2(s, \sigma) \mathcal{M}_s(\sigma, \lambda_1, \lambda_2), \quad (88)$$

where the coefficients $G_{1,2}$ are defined in Eq. (67), and

$$\begin{aligned} \mathcal{M}_t(\sigma, \lambda_1, \lambda_2) &= \bar{v}(q_1) \not{v}_1 (\not{q}_2 - \not{p}_2) \not{v}_2 \omega_- u(q_2), \\ \mathcal{M}_s(\sigma, \lambda_1, \lambda_2) &= \bar{v}(q_1) \not{V}(p_1, \varepsilon_1, p_2, \varepsilon_2) \omega_{\sigma} u(q_2), \end{aligned} \quad (89)$$

where

$$V^{\mu}(p_1, \varepsilon_1, p_2, \varepsilon_2) = 2\varepsilon_1^{\mu}(\varepsilon_2 p_1) - 2\varepsilon_2^{\mu}(\varepsilon_1 p_2) + (p_2^{\mu} - p_1^{\mu})(\varepsilon_1 \varepsilon_2). \quad (90)$$

These matrix elements can be translated into two-dimensional representation, e.g. for $\sigma = -1$ one obtains

$$\begin{aligned} \mathcal{M}_t(\sigma = -1, \lambda_1, \lambda_2) &= q_1^A \varepsilon_{1 \dot{B}A} (q_2 - p_2)^{\dot{B}C} \varepsilon_{2 \dot{D}C} q_2^{\dot{D}}, \\ \mathcal{M}_s(\sigma = -1, \lambda_1, \lambda_2) &= q_1^A V_{\dot{B}A}(p_1, \varepsilon_1, p_2, \varepsilon_2) q_2^{\dot{B}}. \end{aligned} \quad (91)$$

For $\sigma = +1$ we can make use of the relations

$$\mathcal{M}_t(\sigma = +1, \lambda_1, \lambda_2) = 0, \quad \mathcal{M}_s(\sigma = +1, \lambda_1, \lambda_2) = \mathcal{M}_s^*(\sigma = -1, -\lambda_1, -\lambda_2), \quad (92)$$

where the last identity is the result of parity conservation of the s -channel matrix element \mathcal{M}_s , since all parity violation is contained in the coefficient $G_2(s, \sigma)$. From CP invariance one obtains two more relations:

$$\mathcal{M}_{s,t}(q_1, -\sigma, q_2, \sigma, p_1, \lambda_1, p_2, \lambda_2) = -\mathcal{M}_{s,t}^*(q_2, -\sigma, q_1, \sigma, p_2, -\lambda_2, p_1, -\lambda_1), \quad (93)$$

so only 6 independent polarization states remain. The independent matrix elements read:

$$\begin{aligned} \mathcal{M}_t(-1, +1, +1) &= \frac{2}{\langle p_3 p_4 \rangle^2} \langle q_1 p_4 \rangle \langle q_2 p_4 \rangle^* [2q_1 p_3 - M_W^2], \\ \mathcal{M}_t(-1, +1, -1) &= -\frac{\langle q_1 p_4 \rangle \langle q_2 p_4 \rangle \langle q_2 p_3 \rangle^{*2}}{p_3 p_4}, \\ \mathcal{M}_t(-1, -1, +1) &= \frac{\langle q_1 p_3 \rangle^2 \langle q_1 p_4 \rangle^* \langle q_2 p_4 \rangle^*}{p_3 p_4}, \\ \mathcal{M}_t(-1, +1, 0) &= \frac{\sqrt{2} \langle q_1 p_4 \rangle \langle q_2 p_3 \rangle^*}{M_W \langle p_3 p_4 \rangle} [2q_2 p_4 - 2c q_2 p_3 + M_W^2], \\ \mathcal{M}_t(-1, -1, 0) &= \frac{\sqrt{2} \langle q_1 p_3 \rangle \langle q_2 p_4 \rangle^*}{M_W \langle p_3 p_4 \rangle^*} [2q_2 p_4 - 2c q_2 p_3 - M_W^2], \\ \mathcal{M}_t(-1, 0, 0) &= \langle q_1 p_3 \rangle \langle q_2 p_3 \rangle^* \left\{ 1 - c + \frac{2}{M_W^2} (1 + c) [q_2 p_4 - c q_2 p_3] \right\} \end{aligned} \quad (94)$$

for the t -channel matrix elements, and

$$\begin{aligned} \mathcal{M}_s(-1, +1, +1) &= -2 \langle q_1 p_3 \rangle \langle q_2 p_3 \rangle^* \frac{\langle p_3 p_4 \rangle^*}{\langle p_3 p_4 \rangle} (1 - c), \\ \mathcal{M}_s(-1, +1, -1) &= \mathcal{M}_s(-1, -1, +1) = 0, \\ \mathcal{M}_s(-1, +1, 0) &= \frac{\sqrt{2}}{M_W} \langle q_1 p_4 \rangle \langle q_2 p_3 \rangle^* \langle p_3 p_4 \rangle^* (1 - c^2), \\ \mathcal{M}_s(-1, -1, 0) &= \frac{\sqrt{2}}{M_W} \langle q_1 p_3 \rangle \langle p_3 p_4 \rangle \langle q_2 p_4 \rangle^* (1 - c^2), \\ \mathcal{M}_s(-1, 0, 0) &= \langle q_1 p_3 \rangle \langle q_2 p_3 \rangle^* \left(\frac{1}{c} + 3 - 3c - c^2 \right) \end{aligned} \quad (95)$$

for the s -channel matrix elements.

B.2 Non-collinear photon radiation from the production stage

Using the above example as guideline, we now address the process of non-collinear real-photon radiation from the production stage:

$$e^+(q_1, \sigma_1) e^-(q_2, \sigma_2) \rightarrow W^+(p_1, \lambda_1) W^-(p_2, \lambda_2) \gamma(k, \lambda). \quad (96)$$

Since we are dealing with non-collinear radiation and massless initial-state electrons and positrons, we can ignore the possibility of helicity flip in the initial state. Therefore again the condition $\sigma_1 = -\sigma_2 = -\sigma$ applies. As a first step we extend the list of kinematical invariants of Sect. 3:

$$\begin{aligned} s &= (q_1 + q_2)^2, & t &= (q_1 - p_1)^2, & u &= (q_1 - p_2)^2, \\ s' &= (p_1 + p_2)^2, & t' &= (q_2 - p_2)^2, & u' &= (q_2 - p_1)^2. \end{aligned} \quad (97)$$

The complete matrix element can now be written in the form

$$\Pi_\gamma(M_W, M_W) = -e \left[G_1(t') \mathcal{M}_1^\gamma + G_1(t) \mathcal{M}_2^\gamma + G_2(s', \sigma) \mathcal{M}_3^\gamma + G_2(s, \sigma) \mathcal{M}_4^\gamma \right], \quad (98)$$

where the functions $G_{1,2}$ are the same as the ones defined in Eq. (67). The basic matrix elements \mathcal{M}_j^γ are invariant under gauge transformations of the radiated photon. They are given by

$$\begin{aligned} \mathcal{M}_1^\gamma &= \bar{v}(q_1) \left\{ \not{\epsilon}_\gamma \frac{\not{q}_1 - \not{k}}{2q_1 k} \not{\epsilon}_1 (\not{q}_2 - \not{p}_2) \not{\epsilon}_2 + \left[-2\not{\epsilon}_1(\epsilon_\gamma p_1) + 2\not{\epsilon}_\gamma(\epsilon_1 k) - 2\not{k}(\epsilon_\gamma \epsilon_1) \right] \frac{\not{q}_2 - \not{p}_2}{2p_1 k} \not{\epsilon}_2 \right\} \omega_- u(q_2), \\ \mathcal{M}_2^\gamma &= \bar{v}(q_1) \left\{ \not{\epsilon}_1 (\not{q}_1 - \not{p}_1) \not{\epsilon}_2 \frac{\not{q}_2 - \not{k}}{2q_2 k} \not{\epsilon}_\gamma + \not{\epsilon}_1 \frac{\not{p}_1 - \not{q}_1}{2p_2 k} \left[2\not{\epsilon}_2(\epsilon_\gamma p_2) - 2\not{\epsilon}_\gamma(\epsilon_2 k) + 2\not{k}(\epsilon_\gamma \epsilon_2) \right] \right\} \omega_- u(q_2), \\ \mathcal{M}_3^\gamma &= \bar{v}(q_1) \left\{ \not{\epsilon}_\gamma \frac{\not{q}_1 - \not{k}}{2q_1 k} V(p_1, \epsilon_1, p_2, \epsilon_2) - V(p_1, \epsilon_1, p_2, \epsilon_2) \frac{\not{q}_2 - \not{k}}{2q_2 k} \not{\epsilon}_\gamma \right\} \omega_\sigma u(q_2), \\ \mathcal{M}_4^\gamma &= \bar{v}(q_1) \left\{ -2\not{\epsilon}_\gamma(\epsilon_1 \epsilon_2) + V_b(p_1, \epsilon_1, p_2, \epsilon_2) + V_b(p_2, \epsilon_2, p_1, \epsilon_1) \right\} \omega_\sigma u(q_2), \end{aligned} \quad (99)$$

where we introduced the shorthand notation

$$\begin{aligned} \frac{p_1 k}{2} V_b^\mu(p_1, \epsilon_1, p_2, \epsilon_2) &= -\frac{\epsilon_\gamma p_1}{2} V^\mu(p_1 + k, \epsilon_1, p_2, \epsilon_2) + \left[p_1^\mu(\epsilon_1 \epsilon_\gamma) + \epsilon_\gamma^\mu(\epsilon_1 k) \right] (\epsilon_2 p_1 + \epsilon_2 k) \\ &\quad + \epsilon_2^\mu \left[(\epsilon_1 \epsilon_\gamma)(kp_1 + kp_2) - (\epsilon_1 k)(\epsilon_\gamma p_2) \right] + p_2^\mu \left[(\epsilon_2 \epsilon_\gamma)(\epsilon_1 k) + (\epsilon_1 \epsilon_\gamma)(\epsilon_2 p_1) \right]. \end{aligned} \quad (100)$$

The vertex function V can be taken from Eq. (90). Note that the term $-2\not{k}(\epsilon_\gamma \epsilon_1)$ between the square brackets of \mathcal{M}_1^γ originally had the form $(\not{p}_1 - \not{k})(\epsilon_\gamma \epsilon_1)$. The difference $(\not{p}_1 + \not{k})(\epsilon_\gamma \epsilon_1)$ cancels against similar terms in \mathcal{M}_4^γ . This cancellation is a consequence of the lowest-order Ward identity of the W^+ boson. In the same way also the Ward identity of the W^- boson has been used to simplify \mathcal{M}_2^γ .

For the calculation in the Weyl–van der Waerden formalism we choose $m_{3,4} = k$ in Eqs. (86) and (87). Furthermore we choose the free gauge parameter b in Eq. (85) to be equal to q_1 . Like in the case without photon radiation, we can exploit some symmetry relations. First of all CP invariance implies the relations

$$\begin{aligned} \mathcal{M}_1^\gamma(q_1, -\sigma, q_2, \sigma, p_1, \lambda_1, p_2, \lambda_2, k, \lambda) &= \mathcal{M}_2^\gamma{}^*(q_2, -\sigma, q_1, \sigma, p_2, -\lambda_2, p_1, -\lambda_1, k, -\lambda), \\ \mathcal{M}_{3,4}^\gamma(q_1, -\sigma, q_2, \sigma, p_1, \lambda_1, p_2, \lambda_2, k, \lambda) &= \mathcal{M}_{3,4}^\gamma{}^*(q_2, -\sigma, q_1, \sigma, p_2, -\lambda_2, p_1, -\lambda_1, k, -\lambda). \end{aligned} \quad (101)$$

The matrix elements for right-handed electrons are again completely determined:

$$\begin{aligned} \mathcal{M}_1^\gamma(\sigma = +1) &= \mathcal{M}_2^\gamma(\sigma = +1) = 0, \\ \mathcal{M}_{3,4}^\gamma(\sigma = +1, \lambda_1, \lambda_2, \lambda) &= \mathcal{M}_{3,4}^\gamma{}^*(\sigma = -1, -\lambda_1, -\lambda_2, -\lambda), \end{aligned} \quad (102)$$

where the last identity is the result of parity conservation of the s -channel matrix elements $\mathcal{M}_{3,4}^\gamma$. Due to the symmetry (antisymmetry) property of the quartic (triple) gauge boson vertex under the exchange of the W^+ and W^- bosons, one can derive two more relations:

$$\begin{aligned}\mathcal{M}_3^\gamma(p_1, \lambda_1, p_2, \lambda_2, k, \lambda) &= -\mathcal{M}_3^\gamma(p_2, \lambda_2, p_1, \lambda_1, k, \lambda), \\ \mathcal{M}_4^\gamma(p_1, \lambda_1, p_2, \lambda_2, k, \lambda) &= +\mathcal{M}_4^\gamma(p_2, \lambda_2, p_1, \lambda_1, k, \lambda).\end{aligned}\quad (103)$$

After all these preparations we now list the independent matrix elements for $\sigma = -1$. In order to keep the results as compact as possible we use the shorthand notations $\langle r_i r_j \rangle = \langle ij \rangle$ and $\langle r_i r_j \rangle = (ij)$, with $r_i = (q_1, q_2, p_3, p_4, k)$ for $i = (1, 2, 3, 4, 5)$. For the amplitude $\mathcal{M}_1^\gamma(\lambda_1, \lambda_2, \lambda)$ we find:

$$\begin{aligned}\mathcal{M}_1^\gamma(+1, +1, +1) &= -4\sqrt{2} \frac{\langle 15 \rangle \langle 24 \rangle^*}{\langle 35 \rangle^2 \langle 45 \rangle} \left[(35) - (13) - (15) \right], \\ \mathcal{M}_1^\gamma(+1, -1, +1) &= -2\sqrt{2} \frac{\langle 25 \rangle^*}{\langle 35 \rangle^2 \langle 45 \rangle^*} \left[\langle 24 \rangle \left(\langle 13 \rangle \langle 23 \rangle^* + \langle 15 \rangle \langle 25 \rangle^* \right) - c_2 \langle 13 \rangle \langle 45 \rangle \langle 35 \rangle^* \right], \\ \mathcal{M}_1^\gamma(-1, +1, +1) &= -2\sqrt{2} \frac{\langle 13 \rangle^2 \langle 24 \rangle^*}{\langle 15 \rangle \langle 45 \rangle} \left[1 - \frac{\langle 15 \rangle}{\langle 35 \rangle} \right], \\ \mathcal{M}_1^\gamma(-1, -1, +1) &= -\sqrt{2} \frac{\langle 13 \rangle^2 \langle 24 \rangle \langle 25 \rangle^{*2}}{\langle 15 \rangle \langle 45 \rangle^* \langle 35 \rangle}, \\ \mathcal{M}_1^\gamma(+1, 0, +1) &= -\frac{2}{\langle 35 \rangle^2 M_W} \left\{ \left[\langle 13 \rangle \langle 23 \rangle^* + \langle 15 \rangle \langle 25 \rangle^* \right] \left[t' + 4(24) \right] \right. \\ &\quad \left. - 2c_2 \langle 13 \rangle \langle 45 \rangle \langle 24 \rangle^* \langle 35 \rangle^* \right\}, \\ \mathcal{M}_1^\gamma(-1, 0, +1) &= -\frac{\langle 13 \rangle^2 \langle 25 \rangle^*}{\langle 15 \rangle \langle 35 \rangle M_W} \left[t' + 4(24) \right], \\ \mathcal{M}_1^\gamma(0, +1, +1) &= -4 \frac{\langle 13 \rangle \langle 24 \rangle^*}{\langle 35 \rangle \langle 45 \rangle M_W} \left\{ -(13) + (1 - c_1) \left[(35) - (15) \right] \right\}, \\ \mathcal{M}_1^\gamma(0, -1, +1) &= -2 \frac{\langle 13 \rangle \langle 25 \rangle^*}{\langle 35 \rangle \langle 45 \rangle^* M_W} \left[\frac{\langle 13 \rangle}{\langle 15 \rangle} \left(\langle 24 \rangle \langle 23 \rangle^* - c_2 \langle 45 \rangle \langle 35 \rangle^* \right) + (1 - c_1) \langle 24 \rangle \langle 25 \rangle^* \right], \\ \mathcal{M}_1^\gamma(0, 0, +1) &= -\frac{\sqrt{2} \langle 13 \rangle}{\langle 35 \rangle M_W^2} \left[-2c_2 \frac{\langle 13 \rangle}{\langle 15 \rangle} \langle 45 \rangle \langle 24 \rangle^* \langle 35 \rangle^* \right. \\ &\quad \left. + \left[t' + 4(24) \right] \left(\frac{\langle 13 \rangle}{\langle 15 \rangle} \langle 23 \rangle^* + (1 - c_1) \langle 25 \rangle^* \right) \right], \\ \mathcal{M}_1^\gamma(+1, +1, -1) &= \sqrt{2} \frac{\langle 15 \rangle^2 \langle 13 \rangle^{*2} \langle 24 \rangle^*}{\langle 45 \rangle \langle 15 \rangle^* \langle 35 \rangle}, \\ \mathcal{M}_1^\gamma(+1, -1, -1) &= -\sqrt{2} \frac{\langle 15 \rangle \langle 13 \rangle^* \langle 25 \rangle^*}{\langle 15 \rangle^* \langle 45 \rangle^* \langle 35 \rangle} \left[\langle 24 \rangle \langle 23 \rangle^* - c_2 \langle 45 \rangle \langle 35 \rangle^* \right], \\ \mathcal{M}_1^\gamma(-1, +1, -1) &= -\frac{8\sqrt{2} \langle 24 \rangle^*}{\langle 45 \rangle \langle 15 \rangle^* \langle 35 \rangle^{*2}} \left[(15) - (35) \right] \left[(35) - (13) - (15) \right], \\ \mathcal{M}_1^\gamma(-1, -1, -1) &= \frac{4\sqrt{2} \langle 24 \rangle \langle 25 \rangle^{*2}}{\langle 35 \rangle^{*2} \langle 45 \rangle^* \langle 15 \rangle^*} \left[(35) - (13) - (15) \right],\end{aligned}$$

$$\begin{aligned}
\mathcal{M}_1^\gamma(+1, 0, -1) &= -\frac{\langle 15 \rangle \langle 13 \rangle^*}{\langle 15 \rangle^* \langle 35 \rangle M_W} \left\{ -2c_2 \langle 45 \rangle \langle 24 \rangle^* \langle 35 \rangle^* + \langle 23 \rangle^* [t' + 4(24)] \right\}, \\
\mathcal{M}_1^\gamma(-1, 0, -1) &= \frac{4 \langle 25 \rangle^*}{\langle 15 \rangle^* \langle 35 \rangle^* M_W} [t' + 4(24)] [(35) - (13) - (15)], \\
\mathcal{M}_1^\gamma(0, +1, -1) &= -\frac{4 \langle 15 \rangle \langle 13 \rangle^* \langle 24 \rangle^*}{\langle 45 \rangle \langle 15 \rangle^* \langle 35 \rangle^* M_W} \left\{ c_1 [(15) - (35)] - (13) - (15) + (35) \right\}, \\
\mathcal{M}_1^\gamma(0, -1, -1) &= \frac{2 \langle 25 \rangle^*}{\langle 15 \rangle^* \langle 35 \rangle^* \langle 45 \rangle^* M_W} \left\{ c_1 \langle 15 \rangle \langle 24 \rangle \langle 13 \rangle^* \langle 25 \rangle^* \right. \\
&\quad \left. + 2(\langle 24 \rangle \langle 23 \rangle^* - c_2 \langle 45 \rangle \langle 35 \rangle^*) [(35) - (13) - (15)] \right\}, \\
\mathcal{M}_1^\gamma(0, 0, -1) &= \frac{\sqrt{2}}{\langle 15 \rangle^* \langle 35 \rangle^* M_W^2} \left\{ -4c_2 \langle 24 \rangle^* \langle 35 \rangle^* \langle 45 \rangle [(35) - (13) - (15)] \right. \\
&\quad \left. + [t' + 4(24)] (c_1 \langle 15 \rangle \langle 13 \rangle^* \langle 25 \rangle^* + 2 \langle 23 \rangle^* [(35) - (13) - (15)]) \right\}. \quad (104)
\end{aligned}$$

The independent matrix elements $\mathcal{M}_3^\gamma(\lambda_1, \lambda_2, \lambda)$ read:

$$\begin{aligned}
\mathcal{M}_3^\gamma(+1, +1, +1) &= -\frac{4\sqrt{2} \langle 15 \rangle \langle 34 \rangle^*}{\langle 25 \rangle \langle 35 \rangle \langle 45 \rangle} [-(12) + (35) + (45)], \\
\mathcal{M}_3^\gamma(+1, -1, +1) &= \frac{2\sqrt{2}}{\langle 25 \rangle \langle 35 \rangle \langle 45 \rangle^*} \left\{ 2 \frac{\langle 12 \rangle}{\langle 15 \rangle} \langle 45 \rangle \langle 14 \rangle \langle 23 \rangle^* + c_2 \langle 12 \rangle \langle 45 \rangle \langle 25 \rangle^* \langle 35 \rangle^* \right. \\
&\quad \left. - \langle 35 \rangle^* [\langle 34 \rangle (\langle 12 \rangle \langle 23 \rangle^* + \langle 15 \rangle \langle 35 \rangle^*) - 2 \langle 45 \rangle \langle 14 \rangle] \right\}, \\
\mathcal{M}_3^\gamma(-1, -1, +1) &= -\frac{2\sqrt{2} \langle 12 \rangle^2 \langle 34 \rangle \langle 25 \rangle^{*2}}{\langle 15 \rangle \langle 25 \rangle \langle 35 \rangle^* \langle 45 \rangle^*}, \\
\mathcal{M}_3^\gamma(+1, 0, +1) &= \frac{-4}{\langle 25 \rangle \langle 35 \rangle M_W} \left\{ -c_2 \langle 12 \rangle \langle 45 \rangle \langle 25 \rangle^* \langle 34 \rangle^* \right. \\
&\quad \left. + [\langle 12 \rangle \langle 23 \rangle^* + \langle 15 \rangle \langle 35 \rangle^*] [(34) + c_1(45) - c_2(35)] \right\}, \\
\mathcal{M}_3^\gamma(-1, 0, +1) &= -\frac{4 \langle 12 \rangle \langle 25 \rangle^*}{\langle 15 \rangle \langle 25 \rangle \langle 35 \rangle^* M_W} \left\{ -c_2 \langle 15 \rangle \langle 34 \rangle \langle 45 \rangle^* + \langle 13 \rangle [(34) + c_1(45) - c_2(35)] \right\}, \\
\mathcal{M}_3^\gamma(0, 0, +1) &= -\frac{\sqrt{2}}{\langle 25 \rangle M_W^2} \left\{ -2 \frac{\langle 13 \rangle}{\langle 15 \rangle} \langle 14 \rangle \langle 34 \rangle^* [(34) + c_2(35) + c_1(45)] \right. \\
&\quad \left. + \langle 13 \rangle \langle 35 \rangle^* [2c_2^2(35) - 4c_1^2(45) + (2c_2 - 4c_1)(34) - (3c_1 - 2c_2)M_W^2] \right. \\
&\quad \left. - \langle 14 \rangle \langle 45 \rangle^* [2c_1^2(45) - 4c_2^2(35) + (2c_1 - 4c_2)(34) - (3c_2 - 2c_1)M_W^2] \right\}. \quad (105)
\end{aligned}$$

For $\mathcal{M}_4^\gamma(\lambda_1, \lambda_2, \lambda)$ we obtain:

$$\mathcal{M}_4^\gamma(+1, +1, +1) = -4\sqrt{2} \frac{\langle 15 \rangle^2 \langle 12 \rangle^*}{\langle 35 \rangle^2 \langle 45 \rangle^2} [(34) + (35) + (45)],$$

$$\begin{aligned}
\mathcal{M}_4^\gamma(+1, -1, +1) &= \frac{2\sqrt{2}}{\langle 35 \rangle^2 \langle 45 \rangle^*} \left\{ c_1 \langle 15 \rangle \langle 34 \rangle \langle 25 \rangle^* \langle 35 \rangle^* + 2 \frac{\langle 14 \rangle}{\langle 45 \rangle} \langle 34 \rangle \langle 23 \rangle^* \langle 35 \rangle \right. \\
&\quad \left. + 2 \langle 14 \rangle \langle 25 \rangle^* \left[(34) + (45) \right] \right\}, \\
\mathcal{M}_4^\gamma(-1, -1, +1) &= \frac{\sqrt{2}}{2} \frac{\langle 12 \rangle \langle 34 \rangle^2 \langle 25 \rangle^{*2}}{\langle 35 \rangle \langle 45 \rangle}, \\
\mathcal{M}_4^\gamma(+1, 0, +1) &= \frac{4}{M_W \langle 35 \rangle^2} \left\{ \frac{\langle 15 \rangle}{\langle 45 \rangle} \langle 34 \rangle \langle 23 \rangle^* \left[(34) + (35)(1 - c_2) + (45)(1 + c_1) \right] \right. \\
&\quad \left. - \langle 15 \rangle \langle 25 \rangle^* \left[(34)(1 + 2c_2) + (35)(1 + c_2) + (45)(1 + c_1) + M_W^2 \right] \right\}, \\
\mathcal{M}_4^\gamma(-1, 0, +1) &= \frac{2 \langle 25 \rangle^*}{M_W \langle 45 \rangle \langle 35 \rangle} \left\{ -c_2 \langle 14 \rangle \langle 35 \rangle \langle 34 \rangle \langle 45 \rangle^* \right. \\
&\quad \left. + \langle 13 \rangle \langle 34 \rangle \left[(34) + (35)(1 - c_2) + (45)(1 + c_1 + 2c_2) \right] \right\}, \\
\mathcal{M}_4^\gamma(0, 0, +1) &= \frac{2\sqrt{2} \langle 34 \rangle \langle 15 \rangle \langle 25 \rangle^*}{M_W^2 \langle 35 \rangle \langle 45 \rangle} \left[-2c_1(1 + c_1)(45) + c_2(1 + c_2)(35) \right. \\
&\quad \left. + (c_2 - 2c_1)(34) + \left(c_2 - \frac{3}{2}c_1 - \frac{1}{2} \right) M_W^2 \right] \\
&\quad - \frac{2\sqrt{2} \langle 14 \rangle}{M_W^2 \langle 45 \rangle} \left[\langle 25 \rangle^* + \langle 24 \rangle^* \frac{\langle 34 \rangle}{\langle 35 \rangle} \right] \left[(34) + (35)(1 + c_2) + (45)(1 + c_1) \right]. \tag{106}
\end{aligned}$$

B.2.1 Lowest-order decay of the W bosons

Having fixed the polarization choice for the real-photon factorizable corrections to the production stage, we now calculate the lowest-order decay parts accordingly, since they are needed for obtaining the DPA limit of the full matrix element \mathcal{M}_0 in Eq. (45). The matrix elements for the W -boson decays are given by

$$\Delta_{\lambda_i}^0(M_W) = \frac{ieV_{f_i' f_i}}{\sqrt{2} s_W} \mathcal{M}_0^{(\pm)}(\lambda_i). \tag{107}$$

Using again $m_{3,4} = k$ in Eqs. (86) and (87), one ends up with

$$\begin{aligned}
\mathcal{M}_0^{(+)}(+1) &= \sqrt{2} \frac{\langle k'_1 p_3 \rangle \langle k_1 k \rangle^*}{\langle p_3 k \rangle^*}, & \mathcal{M}_0^{(+)}(-1) &= \sqrt{2} \frac{\langle k'_1 k \rangle \langle k_1 p_3 \rangle^*}{\langle p_3 k \rangle}, \\
\mathcal{M}_0^{(+)}(0) &= \frac{1}{M_W} \left(\langle k'_1 p_3 \rangle \langle k_1 p_3 \rangle^* - c_1 \langle k'_1 k \rangle \langle k_1 k \rangle^* \right) \tag{108}
\end{aligned}$$

for the W^+ boson, and

$$\mathcal{M}_0^{(-)}(+1) = \sqrt{2} \frac{\langle k_2 p_4 \rangle \langle k'_2 k \rangle^*}{\langle p_4 k \rangle^*}, \quad \mathcal{M}_0^{(-)}(-1) = \sqrt{2} \frac{\langle k_2 k \rangle \langle k'_2 p_4 \rangle^*}{\langle p_4 k \rangle},$$

$$\mathcal{M}_0^{(-)}(0) = \frac{1}{M_W} \left(\langle k_2 p_4 \rangle \langle k'_2 p_4 \rangle^* - c_2 \langle k_2 k \rangle \langle k'_2 k \rangle^* \right) \quad (109)$$

for the W^- boson.

B.3 Non-collinear photon radiation from the decay stages

Next we address the process of non-collinear real-photon radiation from the decay stages. We start off with the decay of the W^+ boson:

$$W^+(p_1, \lambda_1) \rightarrow \bar{f}_1(k_1) f'_1(k'_1) \gamma(k, \lambda). \quad (110)$$

We do not explicitly write the helicities of the final-state fermions. The final-state fermions are treated as being massless, hence for non-collinear radiation their helicities are fixed by the left-handed interaction with the W bosons: $\lambda_{f_1} = -\lambda_{f'_1} = +1$. The matrix element for process (110) can be written as

$$\Delta_\gamma^{(+)}(M_W) = \frac{ie^2 V_{f'_1 f_1}}{\sqrt{2} s_W} \left[-Q_{f_1} \mathcal{M}_1^{\gamma(+)} + Q_{f'_1} \mathcal{M}_2^{\gamma(+)} + \mathcal{M}_3^{\gamma(+)} \right], \quad (111)$$

with

$$\begin{aligned} \mathcal{M}_1^{\gamma(+)} &= \bar{u}(k'_1) \not{d}_1^* \omega_- \frac{\not{k}_1 + \not{k}}{2k_1 k} \not{d}_\gamma v(k_1) = k'_1{}^A \varepsilon_{1 \dot{B} A}^\dagger \frac{(k_1 + k)^{\dot{B} C}}{2k_1 k} \varepsilon_{\gamma \dot{D} C} k_1^{\dot{D}}, \\ \mathcal{M}_2^{\gamma(+)} &= \bar{u}(k'_1) \not{d}_\gamma \frac{\not{k}'_1 + \not{k}}{2k'_1 k} \not{d}_1^* \omega_- v(k_1) = k'_1{}^A \varepsilon_{\gamma \dot{B} A} \frac{(k'_1 + k)^{\dot{B} C}}{2k'_1 k} \varepsilon_{1 \dot{D} C}^\dagger k_1^{\dot{D}}, \\ \mathcal{M}_3^{\gamma(+)} &= \bar{u}(k'_1) \frac{\mathcal{V}(-p_1, \varepsilon_1^*, k, \varepsilon_\gamma)}{2p_1 k} \omega_- v(k_1) = k'_1{}^A \frac{V(-p_1, \varepsilon_1^*, k, \varepsilon_\gamma)_{\dot{B} A}}{2p_1 k} k_1^{\dot{B}}. \end{aligned} \quad (112)$$

Here the vertex function V can be taken from Eq. (90), but $(\not{k} + \not{p}_1)$ can be replaced by $2\not{k}$ as a result of the lowest-order Ward identity of the W^+ boson.

For the calculation in the Weyl–van der Waerden formalism we choose the same polarization basis as adopted for the on-shell W -pair example in Sect. B.1.1, i.e. $m_{3,4} = p_{4,3}$. For the definition of the photon polarizations we choose the free gauge parameter b in Eq. (85) to be equal to k_1 . A straightforward calculation gives the following results for the amplitudes $\mathcal{M}_1^{\gamma(+)}(\lambda_1, \lambda)$:

$$\begin{aligned} \mathcal{M}_1^{\gamma(+)}(+1, +1) &= -2 \frac{\langle k'_1 p_3 \rangle \langle p_4 k \rangle^*}{\langle k_1 k \rangle \langle p_3 p_4 \rangle^*}, \\ \mathcal{M}_1^{\gamma(+)}(+1, -1) &= \mathcal{M}_1^{\gamma(+)}(-1, -1) = \mathcal{M}_1^{\gamma(+)}(0, -1) = 0, \\ \mathcal{M}_1^{\gamma(+)}(-1, +1) &= -2 \frac{\langle k'_1 p_4 \rangle \langle p_3 k \rangle^*}{\langle k_1 k \rangle \langle p_3 p_4 \rangle^*}, \\ \mathcal{M}_1^{\gamma(+)}(0, +1) &= \frac{\sqrt{2}}{\langle k_1 k \rangle M_W} \left[c \langle k'_1 p_4 \rangle \langle p_4 k \rangle^* - \langle k'_1 p_3 \rangle \langle p_3 k \rangle^* \right]. \end{aligned} \quad (113)$$

The corresponding expressions for $\mathcal{M}_{2,3}^{\gamma(+)}(\lambda_1, \lambda)$ read:

$$\begin{aligned}
\mathcal{M}_2^{\gamma(+)}(+1, +1) &= 2 \frac{\langle k_1 k'_1 \rangle \langle k'_1 p_3 \rangle \langle k_1 p_4 \rangle^*}{\langle k_1 k \rangle \langle k'_1 k \rangle \langle p_3 p_4 \rangle^*}, \\
\mathcal{M}_2^{\gamma(+)}(+1, -1) &= -2 \frac{c \langle p_3 p_4 \rangle \langle k_1 p_4 \rangle^{*2}}{\langle k_1 k \rangle^* \langle k'_1 k \rangle^* \langle p_3 p_4 \rangle^*}, \\
\mathcal{M}_2^{\gamma(+)}(-1, +1) &= 2 \frac{\langle k_1 k'_1 \rangle \langle k'_1 p_4 \rangle \langle k_1 p_3 \rangle^*}{\langle k_1 k \rangle \langle k'_1 k \rangle \langle p_3 p_4 \rangle}, \\
\mathcal{M}_2^{\gamma(+)}(-1, -1) &= 2 \frac{\langle k_1 p_3 \rangle^{*2}}{\langle k_1 k \rangle^* \langle k'_1 k \rangle^*}, \\
\mathcal{M}_2^{\gamma(+)}(0, +1) &= \frac{\sqrt{2} \langle k_1 k'_1 \rangle}{M_W \langle k_1 k \rangle \langle k'_1 k \rangle} \left[\langle k'_1 p_3 \rangle \langle k_1 p_3 \rangle^* - c \langle k'_1 p_4 \rangle \langle k_1 p_4 \rangle^* \right], \\
\mathcal{M}_2^{\gamma(+)}(0, -1) &= -2\sqrt{2}c \frac{\langle p_3 p_4 \rangle \langle k_1 p_3 \rangle^* \langle k_1 p_4 \rangle^*}{M_W \langle k_1 k \rangle^* \langle k'_1 k \rangle^*}, \tag{114}
\end{aligned}$$

and

$$\begin{aligned}
2p_1 k \mathcal{M}_3^{\gamma(+)}(+1, +1) &= -\frac{2 \langle k'_1 p_3 \rangle}{\langle k_1 k \rangle \langle p_3 p_4 \rangle^*} \left[\langle k_1 k'_1 \rangle \langle k_1 p_4 \rangle^* \langle k'_1 k \rangle^* - 2k_1 k \langle p_4 k \rangle^* \right], \\
2p_1 k \mathcal{M}_3^{\gamma(+)}(+1, -1) &= 2c \frac{\langle k'_1 k \rangle \langle p_3 p_4 \rangle \langle k_1 p_4 \rangle^{*2}}{\langle k_1 k \rangle^* \langle p_3 p_4 \rangle^*}, \\
2p_1 k \mathcal{M}_3^{\gamma(+)}(-1, +1) &= -\frac{2 \langle k'_1 p_4 \rangle}{\langle k_1 k \rangle \langle p_3 p_4 \rangle} \left[\langle k_1 k'_1 \rangle \langle k_1 p_3 \rangle^* \langle k'_1 k \rangle^* - 2k_1 k \langle p_3 k \rangle^* \right], \\
2p_1 k \mathcal{M}_3^{\gamma(+)}(-1, -1) &= -2 \frac{\langle k'_1 k \rangle \langle k_1 p_3 \rangle^{*2}}{\langle k_1 k \rangle^*}, \\
2p_1 k \mathcal{M}_3^{\gamma(+)}(0, +1) &= -\frac{\sqrt{2}}{\langle k_1 k \rangle M_W} \left[\langle k_1 k'_1 \rangle \langle k'_1 k \rangle^* \left(\langle k'_1 p_3 \rangle \langle k_1 p_3 \rangle^* - c \langle k'_1 p_4 \rangle \langle k_1 p_4 \rangle^* \right) \right. \\
&\quad \left. - 2k_1 k \left(\langle k'_1 p_3 \rangle \langle p_3 k \rangle^* - c \langle k'_1 p_4 \rangle \langle p_4 k \rangle^* \right) \right], \\
2p_1 k \mathcal{M}_3^{\gamma(+)}(0, -1) &= 2\sqrt{2}c \frac{\langle k'_1 k \rangle \langle p_3 p_4 \rangle \langle k_1 p_3 \rangle^* \langle k_1 p_4 \rangle^*}{M_W \langle k_1 k \rangle^*}. \tag{115}
\end{aligned}$$

The expressions for the charge-conjugate process, describing the decay of the W^- boson, can be obtained as follows:

$$\Delta_{\gamma}^{(-)}(M_W) = -\frac{ie^2 V_{f'_2 f_2}}{\sqrt{2} s_W} \left[-Q_{f_2} \mathcal{M}_1^{\gamma(-)} + Q_{f'_2} \mathcal{M}_2^{\gamma(-)} + \mathcal{M}_3^{\gamma(-)} \right], \tag{116}$$

where

$$\mathcal{M}_j^{\gamma(-)}(\lambda_2, \lambda) = \left[\mathcal{M}_j^{\gamma(+)}(-\lambda_2, -\lambda) \right]^*, \quad \text{with} \quad (k_1, k'_1, p_3, p_4) \rightarrow (k_2, k'_2, p_4, p_3). \tag{117}$$

When the above matrix elements for real-photon radiation from the decay stages are combined with the lowest-order matrix element for the production stage, presented in App. B.1.1, one obtains the DPA limit of the full matrix elements \mathcal{M}_{\pm} in Eqs. (46) and (47).

B.4 Radiation of collinear photons

Up to now we have only discussed the case of non-collinear photon radiation, which allowed us to neglect the fermion masses and the possibility of spin-flip in the initial state. The picture changes, however, if the radiated photons are sufficiently collinear with one of the external fermions. In such cases factorization takes place, i.e. the matrix element squared including collinear radiation can be approximately written in terms of the lowest-order matrix element squared and collinear factors.

Let us first consider collinear photon radiation in the direction of one of the light fermions in the production stage of the process, e.g. the positron. In that case the matrix element squared can be written in the following form [6]:

$$\sum_{\lambda} |\mathcal{M}_{\text{coll}, e^+}(q_1, \sigma_1, q_2, \sigma_2, k, \lambda)|^2 \approx e^2 f_{\text{coll}}^{(\sigma_2)}(q_1, \sigma_1, k) |\mathcal{M}_{\text{DPA}}^0(x_1 q_1, -\sigma_2, q_2, \sigma_2)|^2, \quad (118)$$

where $x_1 = (E - k_0)/E$ is the ratio of the positron energy after and before photon radiation, $\sigma_{1,2}$ are the helicities of the e^{\pm} , and

$$f_{\text{coll}}^{(\sigma_2)}(q_1, \sigma_1, k) = \delta_{(\sigma_1, -\sigma_2)} \left[\frac{1 + x_1^2}{x_1(1 - x_1)} \frac{1}{q_1 k} - \frac{1 + x_1^2}{2x_1} \frac{m_e^2}{(q_1 k)^2} \right] + \delta_{(\sigma_1, \sigma_2)} \frac{(1 - x_1)^2}{2x_1} \frac{m_e^2}{(q_1 k)^2}. \quad (119)$$

The last term in this collinear factor gives rise to the so-called spin-flip, which allows the positron to have the same helicity as the electron. Note that we have only indicated the momenta and helicities of the relevant particles (e^{\pm}, γ) and that the photon helicities are summed over, as the photon cannot be detected anyway. Collinear radiation in the direction of the initial-state electron can be obtained in the same way, with the role of the e^+ and e^- interchanged. If the initial-state particles are not polarized, as is the case at LEP2, the collinear factor takes on the well known form

$$\sum_{\sigma_1} f_{\text{coll}}^{(\sigma_2)}(q_1, \sigma_1, k) = \frac{1 + x_1^2}{x_1(1 - x_1)} \frac{1}{q_1 k} - \frac{m_e^2}{(q_1 k)^2}. \quad (120)$$

When the photon angles are integrated out, the terms $\propto 1/q_1 k$ yield contributions of the large-logarithmic type [$\propto \log(s/m_e^2)$], whereas the term $\propto m_e^2/(q_1 k)^2$ gives rise to additional $\mathcal{O}(1)$ contributions, which would have been neglected in a massless treatment of the initial state.

In the case of collinear photon radiation in the direction of one of the final-state fermions, say the fermion f_2 from the W^- decay, the factorization reads

$$\sum |\mathcal{M}_{\text{coll}, f_2}(k_1, k'_1, k_2, k'_2, k)|^2 \approx e^2 Q_{f_2}^2 \left[\frac{1 + y_2^2}{1 - y_2} \frac{1}{k_2 k} - \frac{m_{f_2}^2}{(k_2 k)^2} \right] |\mathcal{M}_{\text{DPA}}^0(k_1, k'_1, k_2/y_2, k'_2)|^2, \quad (121)$$

where the summation is performed over all final-state helicities and $y_2 = E_4/(E_4 + k_0)$ is the ratio of the f_2 energy after and before photon radiation. The other final-state collinear factors can be obtained in the same way.

C Special integrals for semi-soft photon radiation

In this appendix we have a closer look at the inclusive treatment of the photon in shifted Breit–Wigner resonances $1/[D_i + 2kp_i]$ in the vicinity of the M_i^2 resonance (see Sect. 5). We start off with factorizable real-photon radiation, involving the ratios

$$\frac{|D_i|^2}{|D_i + 2kp_i|^2} = \left[\frac{1}{D_i^* + 2kp_i} - \frac{1}{D_i + 2kp_i} \right] \frac{|D_i|^2}{2iM_W\Gamma_W} = \frac{|D_i|^2}{M_W\Gamma_W} \operatorname{Re} \frac{i}{D_i + 2kp_i}. \quad (122)$$

In order to study the phenomenon of hard-photon suppression we consider the generic integrals

$$I_n = \frac{|D_i|^2}{M_W\Gamma_W} \operatorname{Re} \left\{ \int_{\lambda_s < k_0 < \Lambda} \frac{d\vec{k}}{(2\pi)^3 2k_0} \frac{M_W^{n-2}}{k_0^n} \frac{i}{D_i + 2kp_i} \right\} \quad (123)$$

for $n = 1$ or 2 . The integration is performed over the photon angles and the photon-energy range $\lambda_s < k_0 < \Lambda$, where λ_s is a soft-photon cut-off ($\lambda_s \ll \Gamma_W$). For $n = 2$ this integral quantifies the influence of the shifted resonance on the M_i^2 distribution in the vicinity of the pole $M_i^2 = M_W^2$. For $n = 1$ it quantifies the effect of $\mathcal{O}(k)$ shifts in the definition of the DPA residues. In the latter case we find

$$I_1 = - \frac{|D_i|^2}{16\pi^2 E \beta M_W^2 \Gamma_W} \operatorname{Im} \left\{ \operatorname{Li}_2 \left(\frac{-1 + \beta}{z} \right) - \operatorname{Li}_2 \left(\frac{-1 - \beta}{z} \right) \right\}, \quad (124)$$

with $z = D_i/(2E\Lambda)$ and Li_2 the usual dilogarithm. One can immediately read off that I_1 is suppressed by $\mathcal{O}(\Gamma_W/E)$, irrespective of the precise value for Λ . For $n = 2$ the integral reads

$$I_2 = - \frac{1}{4\pi^2} \operatorname{Im} \left\{ \frac{D_i^*}{M_W\Gamma_W} \left[1 + \log \left(\frac{D_i}{2E\lambda_s} \right) + \frac{z+1-\beta}{2\beta} \log(z+1-\beta) - \frac{z+1+\beta}{2\beta} \log(z+1+\beta) \right] \right\}. \quad (125)$$

This type of integral will lead to an $\mathcal{O}(1)$ contribution. The dependence on the cut-off Λ , however, is suppressed by $\mathcal{O}(\Gamma_W^2/\Lambda^2)$. So, the more energetic the photon is the more suppressed its contribution will be. Hence, as soon as Λ is taken to be much larger than Γ_W it can safely be replaced by infinity.

Based on the latter observation, we can now list the relevant integrals needed for the inclusive treatment of final-state radiation effects involving shifted Breit–Wigner resonances (see columns 3,4 of Table 1 and column 3 of Table 2). For the radiation from the W^+ -boson decay stage the following four integrals are required:

$$\begin{aligned} \int_{k_0 > \lambda_s} \frac{d\vec{k}}{(2\pi)^3 2k_0} \frac{1}{(2kk_1)^2 [D_1 + 2kp_1]} &= \frac{1}{16\pi^2 m_{f_1}^2 D_1} \log \left(\frac{D_1 E_3}{\lambda_s M_W^2} \right), \\ \int_{k_0 > \lambda_s} \frac{d\vec{k}}{(2\pi)^3 2k_0} \frac{1}{(2kk_1)(2kp_1) [D_1 + 2kp_1]} &= - \frac{1}{16\pi^2 M_W^2 D_1} \left[\log \left(\frac{\lambda_s M_W^2}{D_1 E_3} \right) \log \left(\frac{M_W^2}{m_{f_1}^2} \right) \right. \\ &\quad \left. + \operatorname{Li}_2 \left(1 - \frac{1-\beta}{2} \frac{E}{E_3} \right) + \operatorname{Li}_2 \left(1 - \frac{1+\beta}{2} \frac{E}{E_3} \right) \right], \end{aligned}$$

$$\begin{aligned}
\int_{k_0 > \lambda_s} \frac{d\vec{k}}{(2\pi)^3 2k_0} \frac{1}{(2kp_1)^2 [D_1 + 2kp_1]} &= -\frac{1}{16\pi^2 M_W^2 D_1} \left[\log\left(\frac{2\lambda_s M_W}{D_1}\right) + 1 + \frac{1}{2\beta} \log\left(\frac{1-\beta}{1+\beta}\right) \right], \\
\int_{k_0 > \lambda_s} \frac{d\vec{k}}{(2\pi)^3 2k_0} \frac{1}{(2kk_1)(2kk'_1) [D_1 + 2kp_1]} &= \int_{k_0 > \lambda_s} \frac{d\vec{k}}{(2\pi)^3 2k_0} \frac{1}{(2kp_1) [D_1 + 2kp_1]} \left[\frac{1}{2kk_1} + \frac{1}{2kk'_1} \right].
\end{aligned} \tag{126}$$

From these integrals one can determine the correction factor corresponding to the $|\mathcal{I}_+^2|$ term in Eq. (56):

$$\begin{aligned}
-\int_{k_0 > \lambda_s} \frac{d\vec{k}}{(2\pi)^3 2k_0} |\mathcal{I}_+^2| &= -\frac{\alpha}{\pi} \operatorname{Re} \left\{ \frac{iD_1^*}{M_W \Gamma_W} \left[-\log\left(\frac{2\lambda_s M_W}{D_1}\right) - 1 - \frac{1}{2\beta} \log\left(\frac{1-\beta}{1+\beta}\right) \right. \right. \\
&\quad + Q_{f_1}^2 \left\{ \log\left(\frac{\lambda_s M_W^2}{D_1 E_3}\right) \left[\log\left(\frac{M_W^2}{m_{f_1}^2}\right) - 1 \right] + \operatorname{Li}_2\left(1 - \frac{1-\beta}{2} \frac{E}{E_3}\right) + \operatorname{Li}_2\left(1 - \frac{1+\beta}{2} \frac{E}{E_3}\right) \right\} \\
&\quad \left. \left. + Q_{f'_1}^2 \left\{ \log\left(\frac{\lambda_s M_W^2}{D_1 E'_3}\right) \left[\log\left(\frac{M_W^2}{m_{f'_1}^2}\right) - 1 \right] + \operatorname{Li}_2\left(1 - \frac{1-\beta}{2} \frac{E}{E'_3}\right) + \operatorname{Li}_2\left(1 - \frac{1+\beta}{2} \frac{E}{E'_3}\right) \right\} \right] \right\}.
\end{aligned} \tag{127}$$

Here E'_3 denotes the energy of f'_1 , i.e. $E'_3 = E - E_3$. The correction factor corresponding to the $|\mathcal{I}_-^2|$ term in Eq. (56) is obtained by replacing $(D_1, f_1, f'_1, E_3, E'_3)$ by $(D_2, f_2, f'_2, E_4, E'_4)$.

Finally we study the hard-photon suppression for the non-factorizable corrections. To this end we consider the integrals

$$J_n = \operatorname{Re} \left\{ \int_{\lambda_s < k_0 < \Lambda} \frac{d\vec{k}}{(2\pi)^3 2k_0} \frac{M_W^{n-2}}{k_0^n} \frac{D_i}{D_i + 2kp_i} \right\} \tag{128}$$

for $n = 1$ and 2 . From the results for $I_{1,2}$ one straightforwardly obtains

$$J_1 = \frac{1}{16\pi^2 E \beta M_W} \operatorname{Re} \left\{ D_i \left[\operatorname{Li}_2\left(\frac{-1+\beta}{z}\right) - \operatorname{Li}_2\left(\frac{-1-\beta}{z}\right) \right] \right\} \tag{129}$$

and

$$J_2 = \frac{1}{4\pi^2} \operatorname{Re} \left\{ 1 + \log\left(\frac{D_i}{2E\lambda_s}\right) + \frac{z+1-\beta}{2\beta} \log(z+1-\beta) - \frac{z+1+\beta}{2\beta} \log(z+1+\beta) \right\}. \tag{130}$$

Again a suppression of $\mathcal{O}(\Gamma_W/E)$ is observed for $n = 1$, whereas for $n = 2$ the dependence on the cut-off Λ is suppressed by $\mathcal{O}(M_W \Gamma_W/[E\Lambda])$. So, again Λ can be replaced by infinity if it is sufficiently large. For explicit expressions for the non-factorizable corrections we refer to the literature [9, 10].

References

- [1] The LEP Collaborations ALEPH, DELPHI, L3, OPAL, the LEP Electroweak Working Group and the SLD Heavy Flavour Working Group, CERN-PPE/97-154 (1997).
- [2] D. Bardin *et al.*, in *Reports of the working group on precision calculations for the Z resonance*, eds. D. Bardin, W. Hollik and G. Passarino, (CERN-95-03, Genève, 1995) p. 7, *hep-ph/9709229*.
- [3] G. Gounaris *et al.*, in *Physics at LEP2*, eds. G. Altarelli, T. Sjöstrand and F. Zwirner, (CERN 96-01, Genève, 1996) Vol. 1, p. 525, *hep-ph/9601233*.
- [4] W. Beenakker *et al.*, in *Physics at LEP2*, eds. G. Altarelli, T. Sjöstrand and F. Zwirner, (CERN 96-01, Genève, 1996) Vol. 1, p. 79, *hep-ph/9602351*;
R.L. Sekulin, *Journal of Physics* **G24** (1998) 297;
F.A. Berends *et al.*, *ibid.* 405.
- [5] D. Bardin, *et al.*, in *Physics at LEP2*, eds. G. Altarelli, T. Sjöstrand and F. Zwirner, (CERN 96-01, Genève, 1996) Vol. 2, p. 3, *hep-ph/9709270*.
- [6] W. Beenakker and A. Denner, *Int. J. Mod. Phys.* **A9** (1994) 4837.
- [7] W. Beenakker, F.A. Berends and A.P. Chapovsky, *Phys. Lett.* **B435** (1998) 233.
- [8] K. Melnikov and O. Yakovlev, *Nucl. Phys.* **B471** (1996) 90.
- [9] W. Beenakker, A.P. Chapovsky and F.A. Berends, *Phys. Lett.* **B411** (1997) 203 and *Nucl. Phys.* **B508** (1997) 17.
- [10] A. Denner, S. Dittmaier and M. Roth, *Nucl. Phys.* **B519** (1998) 39 and *Phys. Lett.* **B429** (1998) 145.
- [11] V.S. Fadin and V.A. Khoze, *Sov. J. Nucl. Phys.* **48** (1988) 309;
V.S. Fadin, V.A. Khoze and A.D. Martin, *Phys. Lett.* **B311** (1993) 311;
D. Bardin, W. Beenakker and A. Denner, *Phys. Lett.* **B317** (1993) 213;
V.S. Fadin *et al.*, *Phys. Rev.* **D52** (1995) 1377.
- [12] M. Böhm *et al.*, *Nucl. Phys.* **B304** (1988) 463;
W. Beenakker, K. Kołodziej and T. Sack, *Phys. Lett.* **B258** (1991) 469.
- [13] J. Fleischer, F. Jegerlehner and M. Zrałek, *Z. Phys.* **C42** (1989) 409;
K. Kołodziej and M. Zrałek, *Phys. Rev.* **D43** (1991) 3619;
J. Fleischer, F. Jegerlehner and K. Kołodziej, *Phys. Rev.* **D47** (1993) 830.
- [14] W. Beenakker, F.A. Berends and T. Sack, *Nucl. Phys.* **B367** (1991) 287.
- [15] A. Denner and T. Sack, *Z. Phys.* **C46** (1990) 653 and papers quoted therein.
- [16] F.A. Berends and G.B. West, *Phys. Rev.* **D1** (1970) 122.

- [17] E.N. Argyres *et al.*, *Phys. Lett.* **B358** (1995) 339.
- [18] W. Beenakker *et al.*, *Nucl. Phys.* **B500** (1997) 255.
- [19] R.G. Stuart, *Phys. Lett.* **B262** (1991) 113;
A. Aeppli, G.J. van Oldenborgh and D. Wyler, *Nucl. Phys.* **B428** (1994) 126.
- [20] M. Böhm, A. Denner and S. Dittmaier, *Nucl. Phys.* **B376** (1992) 29;
W. Beenakker *et al.*, *Nucl. Phys.* **B410** (1993) 245 and *Phys. Lett.* **B317** (1993) 622;
M. Kuroda and D. Schildknecht, *hep-ph/9807250*.
- [21] K. Melnikov and O. Yakovlev, *Phys. Lett.* **B324** (1994) 217;
V.S. Fadin, V.A. Khoze and A.D. Martin, *Phys. Rev.* **D49** (1994) 2247.
- [22] W. Beenakker and A. Denner, to appear in Proceedings of the Zeuthen Workshop on Elementary Particle Theory: Loops and Legs in Gauge Theories, Rheinsberg, Germany, April 19-24, 1998, *hep-ph/9806475*.
- [23] C.R. Schmidt, *Phys. Rev.* **D54** (1996) 3250.